University of Tennessee, Knoxville

TRACE: Tennessee Research and Creative Exchange

Doctoral Dissertations

Graduate School

5-2017

Design-Structure-Property Relationships of Purine-Based Copolymers and Chromophores

Graham Smith Collier
University of Tennessee, Knoxville, gcollie1@vols.utk.edu

Follow this and additional works at: https://trace.tennessee.edu/utk_graddiss

Part of the Materials Chemistry Commons, Organic Chemistry Commons, and the Polymer Chemistry Commons

Recommended Citation

Collier, Graham Smith, "Design-Structure-Property Relationships of Purine-Based Copolymers and Chromophores. " PhD diss., University of Tennessee, 2017.
https://trace.tennessee.edu/utk_graddiss/4451

This Dissertation is brought to you for free and open access by the Graduate School at TRACE: Tennessee Research and Creative Exchange. It has been accepted for inclusion in Doctoral Dissertations by an authorized administrator of TRACE: Tennessee Research and Creative Exchange. For more information, please contact trace@utk.edu.

To the Graduate Council:

I am submitting herewith a dissertation written by Graham Smith Collier entitled "Design-Structure-Property Relationships of Purine-Based Copolymers and Chromophores." I have examined the final electronic copy of this dissertation for form and content and recommend that it be accepted in partial fulfillment of the requirements for the degree of Doctor of Philosophy, with a major in Chemistry.

Sydney M. Kilbey, Major Professor

We have read this dissertation and recommend its acceptance:

Brian K. Long, Eric T. Boder, Michael D. Best

Accepted for the Council:

Dixie L. Thompson

Vice Provost and Dean of the Graduate School

(Original signatures are on file with official student records.)

Design-Structure-Property Relationships of Purine-Based Copolymers and Chromophores

A Dissertation Presented for the
Doctor of Philosophy
Degree
The University of Tennessee, Knoxville

Graham Smith Collier
May 2017

Copyright © 2017 by Graham Smith Collier
All rights reserved.

DEDICATION

This dissertation is dedicated to my Ma, Peggy Collier, for always encouraging me to strive for academic excellence.

"Where there's a will, there's an A."

ACKNOWLEDGEMENTS

Firstly, I would like to thank my advisor Prof. S. Michael Kilbey II, for his guidance, encouragement, and investment in my education. I feel I have grown as a scientist and a professional by following his example of professionalism and desire to clearly communicate ideas and results. Dr. Kilbey also exemplifies what it means to be a "family-man" and I hope I can mimic his commitment to family and work in the future. My years in Dr. Kilbey's lab have been an exceptional learning environment, filled with laughter and fostering life-long friendships with my group members and Dr. Kilbey. I will forever be grateful to Dr. Kilbey for his mentorship and friendship as I continue to develop my career.

I would like to express my deepest appreciation for my family and friends who have given support and encouragement through my years of graduate school. I thank my parents, Mark and Margaret Collier and Allison and Lance DeLong. I would not be the person I am today without their guidance, encouragement, and support. The values they instilled in me have helped me through the toughest times of graduate school and life. I also acknowledge my dear friend Luke Raynor, who has always been willing to lend an ear when I need advice and always finds a way to make me laugh. Finally, I sincerely acknowledge my fiancé, Liz Coggin. While we have had our ups and downs, you have always been encouraging and supportive. Your support while I wrote this dissertation is appreciated more than you can ever imagine.

I also would like to express my gratitude to collaborators who were instrumental for my studies. Firstly, Lauren Brown and Dr. Brian Long: Their willingness to invest in

my research has taught me valuable lessons as a scientist and motivated me to understand all aspects of my chemistry. The valuable advice and assistance they provided through my tenure here at the University of Tennessee will serve me well for the rest of my life. Secondly, I must acknowledge the assistance and mentorship from Dr. Michael Walter of the University of North Carolina at Charlotte, who advised by M.S. thesis work. As my first graduate advisor, he motivated me to study conjugated polymers and small molecules and he continues to support my growth as a scientist. Certain measurements described in this dissertation would not have been possible without his willingness to help me study my materials. Lastly, I express my sincere gratitude to the rest of my graduate committee, Dr. Michael D. Best and Dr. Eric T. Boder. The feedback I have received through my seminars and meetings has helped me address many hurdles in my research.

Finally, I must thank the members of the Kilbey research group that have given feedback and friendships over the years: Zach Seibers, Bethany Aden, Dayton Street, Jesse Davis, Rachel Ramirez, Kamlesh Bornani, Sina Sabury, Evan Boone, and Ben Hopkins. I am thankful to join a group that forms such strong friendships as we all traverse the struggles of graduate school. I look forward to years of laughter while sharing memories with you all.

ABSTRACT

Understanding the relationship between monomer design and polymer properties is imperative for developing polymeric systems that can find applicability in targeted technologies. Purines have been extensively studied across many scientific disciplines and are useful due to the diverse properties they possess, which is due in part to the broad scope of precise synthetic transformations that are used to tailor their properties. The overarching goal of my dissertation involves developing the synthesis of "poly(purine)s" and investigating the effect of purine monomer design on polymer properties. In this vein, poly(purine)s and purine-based donor-acceptor small-molecules are synthesized via Stille cross-coupling reactions with a key variation being the nature of the π-conjugated comonomers and substitution pattern of the purine monomer. Investigations of thermal and photophysical properties reveal a dependence on purinyl monomer design and comonomer type on properties such as glass transition temperature (thermal behavior) and charge-transfer character (photophysical properties). The work described herein presents the first example of poly(purine)s in which a purine is directly incorporated into a polymer backbone, systematic design of donor-acceptor purine-based chromophores with tunable thermal and photophysical properties, and the first example of the synthesis of fully conjugated donor-acceptor poly(purine)s. My findings demonstrate the viability of purines in metal-catalyzed reactions and the potential to tailor optoelectronic properties of purine-based polymers and small molecules. This work lays the foundation for further development of purine-based π-conjugated systems, including poly(purine)s suitable for high performance organic electronic devices.

TABLE OF CONTENTS

Chapter 1: Introduction 1

1.1 Motivation 2

1.2 Synthesis of Poly(purine)s 5

1.2.1 Purines and Palladium Catalyzed Reactions 5

1.2.2 Stille Cross-Coupling Mechanism and Step-Growth Polymerizations 7

1.2.3 N-9 Protection of Purines: For Monomers and/or Solubilizing Groups 9

1.2.4 Design of Donor-Acceptor Chromophores and Copolymers 10

1.3 Characterization of Physical Properties 12

1.4 Optoelectronic Characterization of Chromophores 13

1.4.1 Photophysical Characterization of Chromophores in Solution 13

1.4.2 Photophysical Characterization of Chromophores as Thin Films 18

1.5 Research Objectives 20

Chapter 2: Synthesis of Main Chain Purine-Based Copolymers and Effects of Monomer Design on Thermal and Optical Properties 24

2.1 Abstract 25

2.2 Introduction 26

2.3 Synthesis and Characterization 29

2.3.1 Materials and Methods 29

2.3.2 Synthesis of 6-bromo-(4-bromobenzyl)-9H-purine (M1) using the Mitsunobu Reaction 30

2.3.3 Synthesis of 6-bromo-(4-bromobenzyl)-9H-purine (M1) by alkylation 32

2.3.4 Synthesis of 6-bromo-(3-bromobenzyl)-9H-purine (M2) using the Mitsunobu Reaction 33

2.3.5 General Procedure for the Synthesis of Polymers (P1-P4) using Conventional Heating 34

2.3.6 General Procedure for the Synthesis of Polymers (P1-P4) using Microwave Heating 35

2.4 Results and Discussion 36

2.5 Conclusions 52

Chapter 3: Synthesis of Donor-Acceptor Purine-Based Chromophores and an Investigation of Thermal, Photophysical, and Electrochemical Properties 53

3.1 Abstract 54

3.2 Introduction 54

3.3 Experimental 57

3.3.1 Materials and Methods 57

3.3.2 Synthesis of 6-Bromo-9-ethylhexylpurine 58

3.3.3 General Stille Cross-Coupling Procedure 59

3.4 Results and Discussion 61

3.5 Conclusions 74

Chapter 4: Synthesis of Purine-Based Donor-Acceptor Conjugated Polymers and the Effect of Incorporating Purines on Photophysical Properties 76

4.1 Abstract 77

4.2 Introduction 78

4.3 Experimental 81

4.3.1 Materials and Methods 81

4.3.2 Organic Photovoltaic Device Fabrication 83

4.3.3 Synthesis of Dibromo-P-BDT-P (Br_2PBDTP) 84

4.3.4 General Polymerization Procedure 85

4.4 Results and Discussion 87

4.5 Conclusions 109

Chapter 5: Summary, Future Works, and Conclusion 111

5.1 Summary 112

5.2 Future Work 114

5.2.1 Purines as Monomer Building Blocks for π-Conjugated Polymers 115

5.2.2 Purines in Small-Molecule π-Conjugated Systems 118

5.3 Conclusion 120

References 121

Appendices 139

Appendix A-Chapter 2: Synthesis of Main Chain Purine-Based Copolymers and Effects of Monomer Design on Thermal and Optical Properties 140

Appendix B-Chapter 3: Synthesis of Donor-Acceptor Purine-Based Chromophores and an Investgation of Thermal, Photophysical, and Electrochemical Properties 148

Appendix C-Chapter 4: Synthesis of Purine-Based Donor-Acceptor Conjugated Polymers and the Effect of Incorporating Purines on Photophysical Properties 162

Appendix D-Synthesis of Various Purine Building Blocks and Chromophores 166

Vita 173

LIST OF TABLES

Table 2.1. Molecular weight data from the synthesis of P1 using conventional heating methods 41

Table 2.2. Polymerization data for P1-P4 synthesized via conventional heating methods ... 43

Table 2.3. Absorbance and emission maximums of P1-P4 measured in chloroform 49

Table 3.1. Photophysical properties of purine chromophores 67

Table 3.2. Molecular orbital data obtained via CV measurements 72

Table 4.1. UV-Vis and photoluminescence properties of conjugated poly(purine)s in chloroform solutions 96

Table 4.2. Absorbance onset data for conjugated poly(purine)s in solution and as thin films 100

Table 4.3. Photophysical properties of conjugated poly(purine)s as thin films 102

Table 4.4. Oxidation and reduction potentials measured with cyclic voltammetry and the resulting HOMO and LUMO levels for PPBDTPBT 104

Table 4.5. Data for OPV devices made using PPBDTPBT as the donor-type polymer 107

Table A.1. Molecular weight characterization of poly(purine)s synthesized using microwave-assisted polymerizations 145

LIST OF FIGURES

Figure 1.1. The purine scaffold with the corresponding numbering scheme of each position of the fused heterocyclic system. Motivation for this figure comes from References 1 and 2 3

Figure 1.2. Chemical structures of purine-functionalized conjugated polymers from (a) Reference 24 and (b) Reference 25 4

Figure 1.3. Illustration of orbital mixing of the donor and acceptor substituents of a donor-acceptor conjugated polymer. Inspiration for this illustration was gained from Reference 36 11

Figure 1.4. Jablonksi diagram illustrating photophysical processes. (1) represents the absorbance of photons from the singlet ground electronic state (S_0) to the first (S_1) and second (S_2) singlet electronic excited state by photons (hv) of arbitrary energy, process (2) is the emission of photons ($hv_F \neq hv_{abs}$) through fluorescence from the lowest vibrational energy state following internal conversion (vibrational relaxation), and (3) represents emission of photons through phosphorescence (hv_P) following intersystem crossing from the sinlget excited state to the triplet excited state. Solid black lines represent non-radiative relaxation pathways from the excited state to the ground state. Dashed black lines represent non-radiative relaxation pathways in the excited state 14

Figure 1.5. Absorbance spectra of P-BDT-P at various concentrations (left) and the corresponding Beer's Law plot (right), which is used to calculate the molar absorptivity ... 15

Figure 1.6 Integrated fluorescence intensity versus absorbance plot of Rhodamine 101 (black) and the purine chromophore P-TBTT-P (red) used for calculating the fluorescence quantum yield with the comparative method 18

Figure 1.7. Chemical structures of (a) poly(p-phenyleneethynylene) and (b) pentiptycene substituted poly(p-phenyleneethynylene) from Reference 71 20

Figure 2.1. Chemical structures of purine inspired functional materials. (a) To template the synthesis of conjugated polymers from Reference 17, (b) push-pull purines for blue emitting OLEDs from References 8 and 9, and (c) donor-acceptor purine π–conjugated chromophores from Reference 70 27

Figure 2.2. Comparision of ^{1}H spectra of M1 (top) and a mono-substituted thienyl-purine (bottom) that shows a shift in the purine protons from 8.73 ppm and 8.11 ppm to 8.92 ppm and 8.07 ppm upon thiophene substitution at C-6 position of the purine ring 44

Figure 2.3. HMBC of M1 (top) and a mono-substituted thienyl-purine (bottom). The red box highlights the unchanged shifts of the *ortho* protons on the phenyl pendant while the blue box shows the correlation between the proton located at the 3-position of the thienyl ring and the C-6 position of the purine ring 45

Figure 2.4. Thermal characterization of poly(purine)s P1-P4. Data shown are (a) thermogravimetric analysis of P1-P4 (20 °C to 800 °C), with T_d values given in the legend, and (b) differential scanning calorimetry traces for P1-P4 (second heating cycle), with T_g values listed adjacent to each trace 47

Figure 2.5. (a) Normalized UV-Vis spectra for P1-P4 at 0.01 mg/mL in chloroform and (b) normalized fluorescence spectra for P1-P4 at 0.0025 mg/mL in chloroform.....49

Figure 2.6. Possible repeat unit confirmations of regiorandom poly(purine)s.....50

Figure 2.7. UV-Vis spectra of the soluble fraction of P1 in DMF measured after sequential additions of a 0.1 M LiBr solution (in DMF) to investigate the possibility of hydrogen-bonding.....51

Figure 3.1. Thermogravimetric analysis of P-BDT-P, P-Th-P, and P-TBTT-P (20-800 °C) 63

Figure 3.2 Differential scanning calorimetry traces of P-BDT-P, P-Th-P, and P-TBTT-P showing the heating (a) and cooling (b) cycles.....64

Figure 3.3 ^{1}H NMR spectra of the aromatic regions of the three purine chromophores. The R-groups are representative of the ethylhexyl solubilizing chains.....65

Figure 3.4. (a) UV-Vis and (b) photoluminescence spectra of P-BDT-P, P-Th-P, and P-TBTT-P in chloroform 66

Figure 3.5 Normalized photoluminescence spectra of (a) P-BDT-P and (b) P-TBTT-P in solvents of varying polarity 69

Figure 3.6. Time-resolved photoluminescence profiles of P-BDT-P, P-Th-P, and P-TBTT-P in $CHCl_3$.....70

Figure 3.7. (a) Overlay of cyclic voltammetry traces illustrating redox potentials of P-BDT-P, P-Th-P, and P-TBTT-P and (b) HOMO/LUMO level diagrams of P-BDT-P, P-Th-P, and P-TBTT-P obtained via cyclic voltammetry.....73

Figure 4.1. Thermal stability of PPBDTPBDT, PPBDTPTh, and PPBDTPBT measured using TGA (25 °C to 800 °C) 90

Figure 4.2. DSC traces for PPBDTPBDT, PPBDTPTh, and PPBDTPBT on the second heating cycle 90

Figure 4.3. (a) UV-Vis and (b) photoluminescence spectra of conjugated poly(purine)s in chloroform 92

Figure 4.4. Chemical structures of PPBDTPBDT and O-PBDT. Absorbance onsets of the two polymers are 545 nm (poly(purine)) and O-PBDT 560 nm, Reference 112 93

Figure 4.5. Chemical structures of PPBDTPTh and BDTT. Absorbance onsets of the two polymers are 545 nm (poly(purine)) and BDTT ~575 nm. Reference 115 94

Figure 4.6. Chemical structures of PPBDTPBT, PBDTDTBT from Reference 114, and polymer Z3 from Reference 113 highlight the dependence of thiophene substitution on the onset of absorbance 95

Figure 4.7. Time-resolved photoluminescence profiles of PPBDTPBDT (3.24 ns), PPBDTPTh (1.80 ns), and PPBDTPBT (1.49 ns) in $CHCl_3$ 97

Figure 4.8. (a) UV-Vis and (b) photoluminescence spectra of PPBDTPBDT, PPBDTPTh, and PPBDTPBT as thin films made by spin-coating from chloroform solutions of 5 mg/mL 98

Figure 4.9. Comparison of normalized UV-Vis spectra of conjugated poly(purine)s in chloroform and as thin films 101

Figure 4.10. (a) Cyclic voltammetry trace of PPBDTPBT in DCM illustrating redox behavior with potentials reported relative to the Fc/Fc^+ redox couple and (b) HOMO and LUMO levels of PPBDTPBT calculated from oxidation and reduction potentials measured with cyclic voltammetry and HOMO and LUMO levels of PCBM from Reference 112 105

Figure 4.11. Current density versus voltage plots of PPBDTPBT:PCBM OPV devices (a) with no thermal annealing and (b) after annealing at 50 °C for 15 minutes 107

Figure 4.12. UV-Vis absorbance spectra of PPBDTPBT as a film and films made by blending PPBDTPBT and PCBM at 1:1 by mass. As indicated by the legend, spectra were obtained for as cast blends and blends annealed at 50 °C, 100 °C, and 150 °C 109

Figure 5.1. The different sites of the purine scaffold highlight the tailorability of four distinct positions around the fused-ring heterocycle system 115

Figure 5.2. (a) Variations on the PBDTP building block and (b) variations of the benzothiadiazole acceptor monomer that are known to affect optoelectronic properties and active layer morphology 116

Figure 5.3. A representative 2,6-dithienylpurine monomer that can offer halogenation or stannylation functionality for cross-coupling polymerizations as well as solubilizing chains on the thiophene heterocycles or at the N-9 position of the purine..... 117

Figure 5.4. Various electron-donating and electron-accepting building blocks commonly found in conjugated polymers used for optoelectronic devices. These may be useful for developing structure-property relationships of purine-based chromophores 118

Figure A.1. ^{1}H NMR spectrum (300 MHz, 25 ˚C, $CDCl_3$) of M1; δ (ppm): 5.40 (s, 2H, CH_2), 7.20 (d, 2H, *J* = 9 Hz, Ph), 7.50 (d, 2H, *J* = 6 Hz, Ph), 8.11 (s, 1H, purine H), 8.73 (s, 1H, purine H) 140

Figure A.2. ^{13}C NMR spectrum (300 MHz, 25 ˚C, $CDCl_3$) of M1; δ, ppm: 47.29, 123.05, 129.54 (×2), 132.44 (×2), 133.48, 134.12, 143.41, 144.53, 150.51, 152.20 141

Figure A.3. ^{1}H NMR spectrum (300 MHz, 25 ˚C, $CDCl_3$) of M2; δ, ppm: 5.42 (s, 2H), 7.23 (m, 2H, PhH), 7.47 (m, 2H, PhH), 8.13 (s, 1H, purine H), 8.75 (s, 1H, purine H) 141

Figure A.4. ^{13}C NMR spectrum (300 MHz, 25 ˚C, $CDCl_3$) of M2; δ, ppm: 47.15, 123.25, 126.42, 130.80, 130.88, 132.06, 134.09, 136.69, 143.44, 144.56, 150.52, 152.25 142

Figure A.5. ^{1}H NMR spectrum (300 MHz, 25 ˚C, $CDCl_3$) of P1 (depicted in inset) 142

Figure A.6. ^{1}H NMR spectrum (300 MHz, 25 ˚C, $CDCl_3$) of P2 (depicted in inset) 143

Figure A.7. ^{1}H NMR spectrum (300 MHz, 25 ˚C, $CDCl_3$) of P3 (depicted in inset) 143

Figure A.8. ^{1}H NMR spectrum (300 MHz, 25 ˚C, $CDCl_3$) of P4 (depicted in inset) 144

Figure A.9. SEC traces of poly(purine)s P1-P4 synthesized using conventional heating 146

Figure A.10. SEC traces of polymer P1 that was synthesized using different palladium catalysts (identified in the legend) 146

Figure A.11. SEC traces showing the comparison of P1 to BDT stannyl comonomers to demonstrate successful coupling between the purine and BDT comonomers 147

Figure A.12. DSC traces for polymers P1-P4 on the second heat-cycle 147

Figure B.1. ^{1}H NMR spectrum (500 MHz, 25 °C, $CDCl_3$) of 6-Br-9-ethylhexylpurine; δ (ppm): 0.85-0.95 (m) 1.20-1.36 (m), 1.62 (br singlet), 1.91-2.03 (m), 4.18 (d, 2H, CH_2), 8.08 (s, 1H, purine H), 8.70 (s, 1H, purine H) 148

Figure B.2. ^{13}C NMR spectrum (500 MHz, 25 °C, $CDCl_3$) of 6-Br-9-ethylhexylpurine; δ (ppm): 10.39, 13.93, 22.82, 23.67, 28.35, 30.31, 39.75, 47.89, 123.04, 134.00, 143.07, 145.33, 150.92, 151.84 149

Figure B.3. ^{1}H NMR spectrum (500 MHz, 25 °C, $CDCl_3$) of P-BDT-P; δ (ppm): 0.88 (t), 0.94-0.98 (m), 1.08 (t), 1.24-1.40 (m), 1.41-1.52 (m), 1.55-1.84 (m), 1.91-1.97 (m), 2.00-2.05 (m), 4.21 (d), 4.40 (d) ,8.09 (s, 1H,), 8.99 (s, 1H, purine H), 9.27 (s, 1H, purine H) ... 150

Figure B.4. ^{13}C NMR spectrum (500 MHz, 25 °C, $CDCl_3$) of P-BDT-P; δ (ppm): 10.44, 11.41, 13.96, 14.19, 22.90, 23.17, 23.72, 23.87, 28.42, 29.29, 30.39, 30.50, 39.79, 40.79, 47.39, 75.55, 127.29, 129.88, 130.61, 134.01, 140.22, 145.05, 145.94, 149.79, 152.30, 152.42 151

Figure B.5. ^{1}H NMR spectrum (500 MHz, 25 °C, $CDCl_3$) of P-TBTT-P; δ (ppm): 0.88 (t), 0.95 (t), 1.24-1.40 (m), 1.60 (s, br), 2.01 (m), 4.22 (d), 8.06 (s, 2H, purine H), 8.09 (s, 2H, purine H), 8.31 (d, 2 H, thiophene H) 8.73 (d, 2H, thiophene H), 8.94 (s, 2H, BT H) .. 152

Figure B.6. ^{13}C NMR spectrum (500 MHz, 25 °C, $CDCl_3$) of P-TBTT-P; δ (ppm): 10.42, 13.97, 22.89, 23.71, 28.39, 30.36, 39.72, 47.39, 120.63, 126.08, 128.93, 129.20, 133.27, 140.89, 143.94 144.78, 149.49, 152.37, 152.44 153

Figure B.7. ^{1}H NMR spectrum (500 MHz, 25 °C, $CDCl_3$) of P-Th-P; δ (ppm): 0.88 (t), 0.94 (t), 1.24-1.39 (m), 2.01 (m), 4.21 (d), 8.10 (s), 8.77 (s, 1H, purine H), 8.94 (s, 1H, purine H) 154

Figure B.8. ^{13}C NMR spectrum (500 MHz, 25 °C, $CDCl_3$) of P-Th-P; δ (ppm): 10.43, 13.97, 22.89, 23.71, 28.40, 30.36, 39.75, 47.40, 129.26, 133.37, 144.40, 144.93, 149.51, 152.42, 152.61 155

Figure B.9. UV-Vis spectra of varying concentrations (2.5-20 μM) of P-BDT-P in chloroform scanning from 325-600 nm and the corresponding Beer's Law plots at the absorbance maximums 156

Figure B.10. UV-Vis spectra of varying concentrations (2.5-20 μM) of P-TBTT-P in chloroform scanning from 325-600 nm and the corresponding Beer's Law plots at the absorbance maximums 157

Figure B.11. UV-Vis spectra of varying concentrations (2.5-20 μM) of P-Th-P in chloroform scanning from 325-600 nm and the corresponding Beer's Law plots at the absorbance maximums 158

Figure B.12. Absorbance versus integrated fluorescence intensity plots used for calculated the quantum yield for P-BDT-P 159

Figure B.13. Absorbance versus integrated fluorescence intensity plots used for calculated the quantum yield for P-TBTT-P 160

Figure B.14. Absorbance versus integrated fluorescence intensity plots used for calculated the quantum yield for P-Th-P 161

Figure C.1. ^{1}H NMR spectrum (500 MHz, 25 °C, $CDCl_3$) of Br_2PBDTP; δ (ppm): 0.85-0.95 (m) 1.20-1.36 (m), 1.62 (br singlet), 1.91-2.03 (m), 4.18 (d, 2H, CH_2), 8.08 (s, 1H, purine H), 8.70 (s, 1H, purine H) 162

Figure C.2. ^{13}C NMR spectrum (500 MHz, 25 °C, $CDCl_3$) of Br_2PBDTP; δ (ppm): 10.54, 11.45, 13.97, 14.20, 22.91, 23.73, 23.90, 28.37, 29.28, 30.33, 30.48, 39.17, 40.71, 48.54, 62.72, 127.45, 130.04, 130.57, 133.76, 134.19, 139.91, 145.96, 148.52, 152.36, 153.50, 165.25 163

Figure C.3. ^{1}H NMR spectrum (500 MHz, 25 °C, $CDCl_3$) of PPBDTPBDT; δ (ppm): 0.85-0.95 (m) 1.20-1.36 (m), 1.62 (br singlet), 1.91-2.03 (m), 4.18 (d, 2H, CH_2), 8.08 (s, 1H, purine H), 8.70 (s, 1H, purine H) 163

Figure C.4. ^{1}H NMR spectrum (500 MHz, 25 °C, $CDCl_3$) of PPBDTPTh; δ (ppm): 0.85-0.95 (m) 1.20-1.36 (m), 1.62 (br singlet), 1.91-2.03 (m), 4.18 (d, 2H, CH_2), 8.08 (s, 1H, purine H), 8.70 (s, 1H, purine H) 164

Figure C.5. ^{1}H NMR spectrum (500 MHz, 25 °C, $CDCl_3$) of PPBDTPBT; δ (ppm): 0.85-0.95 (m) 1.20-1.36 (m), 1.62 (br singlet), 1.91-2.03 (m), 4.18 (d, 2H, CH_2), 8.08 (s, 1H, purine H), 8.70 (s, 1H, purine H) 164

Figure C.6. SEC traces for PPBDTPBDT, PPBDTPTh, and PPBDTPBT synthesized by Stille cross-coupling polymerizations 165

Figure D.1. ^{1}H NMR spectrum (500 MHz, 25 °C, $CDCl_3$) of 6-chloro9-ethylhexylpurine; δ (ppm): 0.81-0.95 (m) 1.18-1.36 (m), 1.90-2.01 (m), 4.18 (d, 2H, CH_2), 8.07 (s, 1H, purine H), 8.73 (s, 1H, purine H) 167

Figure D.2. ^{13}C NMR spectrum (500 MHz, 25 °C, $CDCl_3$) of 6-chloro-9-ethylhexylpurine; δ (ppm): 10.38, 13.92, 22.81, 23.67, 28.35, 30.31, 39.75, 47.86, 131.38, 145.46, 150.95, 151.89, 152.15 168

Figure D.3. ^{1}H NMR spectrum (500 MHz, 25 °C, $CDCl_3$) of 2-amino-6-bromo-9-ethylhexylpurine; δ (ppm): 0.84-0.93 (m) 1.19-1.34 (m), 1.72 (br singlet), 1.84-2.93 (m), 3.95 (d, 2H, CH_2), 5.13 (s, br, $-NH_2$), 7.73 (s, 1H, purine H) 168

Figure D.4. ^{13}C NMR spectrum (500 MHz, 25 °C, $CDCl_3$) of 2-amino-6-bromo-9-ethylhexylpurine; δ (ppm): 10.42, 13.98, 22.87, 23.65, 28.38, 30.29, 39.49, 47.24, 127.71, 142.63, 143.29, 152.79, 158.79 169

Figure D.5. ^{1}H NMR spectrum (500 MHz, 25 °C, $CDCl_3$) of 2,6-diamino-9-ethylhexylpurine; δ (ppm): 0.84-0.92 (m) 1.21-1.35 (m), 1.85-1.92 (m), 2.62 (br singlet), 3.91 (d, 2H, CH_2), 4.77 (s, br, $-NH_2$), 5.57 (s, br, $-NH_2$), 7.48 (s, 1H, purine H) 169

Figure D.6. ^{13}C NMR spectrum (500 MHz, 25 °C, $CDCl_3$) of 2,6-diamino-9-ethylhexylpurine; δ (ppm): 10.44, 14.00, 22.91, 23.64, 28.41, 30.29, 39.52, 46.81, 114.31, 138.55, 152.51, 155.63, 159.58 170

Figure D.7. UV-Vis spectra of varying concentrations (2.5-20 μM) of $(NH_2)_2$P-BDT-P in chloroform scanning from 325-600 nm and the corresponding Beer's Law plots at the absorbance maximums 171

Figure D.8. UV-Vis spectra comparing the absorbance of P-BDT-P (red) and $(NH_2)_2$P-BDT-P (black) in chloroform 172

LIST OF SCHEMES

Scheme 1.1. General illustration of how purines will be incorporated into a polymer backbone through a Stille cross-coupling reaction using dihalides and stannylated reagents 7

Scheme 1.2. The catalytic cycle for Stille cross-coupling reactions. Inspiration for this scheme comes from Reference 38 8

Scheme 2.1. Synthesis of M1 via Mitsunobu conditions 31

Scheme 2.2. Synthesis of M1 via alkylation conditions 32

Scheme 2.3. Synthesis of M2 via Mitsunobu conditions 34

Scheme 2.4. Polymerization attempts using 2,6-dichloropurine as the dihalo monomer and either (*i*) 1,4-bis(tributylstannyl)benzene as the stannyl monomer or (*ii*) 2,5-bis(trimethylstannyl)thiophene as the stannyl monomer to yield purine-based copolymers 37

Scheme 2.5. Polymerization attempts using 6-bromo-9-(4-bromophenyl)purine and (*i*) 1,4-bis(tributylstannyl)benzene or (*ii*) 2,5-bis(trimethylstannyl)thiophene by Stille cross-coupling. The former did not appear to work while the latter resulted in mostly an insoluble product 38

Scheme 2.6. Polymerization of M1 and M2 to yield P1-P4 40

Scheme 2.7. Reaction scheme used for examining regioselectivity of M1 43

Scheme 3.1. Synthesis of 6-bromo-9-ethylhexylpurine by alkylation 59

Scheme 3.2. Synthesis of purine dyads via Stille cross-coupling 62

Scheme 4.1. Synthesis of Br_2PBDTP 85

Scheme 4.2. Synthesis of conjugated poly(purine)s by Stille cross-coupling polymerizations 88

Scheme D.1. Synthesis of N-9 functionalized purines by alkylation 166

Scheme D.2. Synthesis of $(NH_2)_2$P-BDT-P via Stille cross-coupling 171

CHAPTER 1
INTRODUCTION

1.1 Motivation

Purines (Figure 1.1) have proven to be interesting and useful molecules due to the way their molecular design, which provides functionality and tailorability, gives rise to a wide array of molecular properties. Due to their high tailorability and given that two purines, adenine and guanine, are building blocks of life, purines are widely used in medicine. By extension, it stands to reason that purine-based materials may be useful as advanced materials. In particular, using purines as building blocks of novel functional polymers may allow for the development of a new class of semiflexible, highly-tailorable polymers with unusual properties, and because of the tailorability of the purine scaffold, these materials may allow useful insights between molecular design and macromolecular properties.

Purine derivatives have been studied in medical science because of the diverse biological properties that purines possess.[1,2] For example, while 6-methylpurine has been found to be highly cytotoxic,[3] other modified purines have shown to have antiviral and anticancer effects,[4] as well as cytokinin activity.[5] Because of these potentially beneficial characteristics, a large number of commercially available drugs are based on the purine scaffold.[1] The pursuit of these purine-based drugs has allowed many synthetic avenues to be explored and developed, which has advanced the development of purine derivatives and related heterocyclic systems.[1,6] This variety of known synthetic transformations provides a broad foundation for this work.

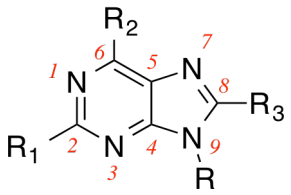

Figure 1.1. The purine scaffold with the corresponding numbering scheme of each position of the fused heterocyclic system. Motivation for this figure comes from References 1 and 2.

The diverse functionality of purines enables their use in a variety of applications. Modified purines have proven to be useful in an effort to image cell nuclei due to their biocompatability,[7] and the ability to tune their emission wavelength by introducing multiple functional groups around the purine scaffold suits them in organic light emitting diodes (OLEDs).[8,9] Their tunability and ability to interact with metals have driven efforts to use purines to nucleate and to template the growth of inorganic nanomaterials.[10,11] The unusual H-bonding character of purines also has provided motivation for designing advanced materials.[12-15] For instance, the H-bonding character of the purines has been exploited to study photogenerated charge-transfer pathways,[16] to provide a template for conjugated polymer synthesis,[17] and to create well-defined nanostructures by self-assembly.[18,19] To take advantage of the H-bonding character of purines, well-defined polymers containing purine pendants have been synthesized using a variety of controlled polymerization methods, including atom transfer radical polymerization (ATRP),[20-22] reversible addition-fragmentation chain transfer (RAFT) polymerization,[18,19] and ring-opening metathesis polymerization (ROMP).[23]

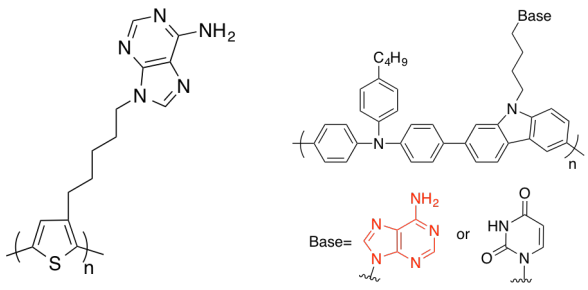

(a) (b)

Figure 1.2. Chemical structures of purine-functionalized conjugated polymers from (a) Reference 24 and (b) Reference 25.

Purines have also been incorporated as side-chain functionalities of conjugated polymers through non-controlled polymerization methods such as Suzuki cross-coupling and oxidative polymerizations.[24,25] The purine-functionalized conjugated polymers (Figure 1.2) found applicability as electron storage/transport layer and hole injection/transport layer materials for high-performance electrochemical devices and OLEDs, respectively.

For example, purine-functionalized poly(triphenylamine-carbazole)s (PTCs) exhibit high thermal stability and solvent resistance due to their H-bonding induced self-assembly, which led to the purine-functionalized PTCs outperforming OLED devices using the traditional injection/transport layer PEDOT:PSS.[25] Further, purine-containing poly(acrylate) copolymers have exhibited enhanced mechanical properties for polymer systems studied for thermoplastic elastomers and tunable adhesion/cohesion properties of copolymers used for supramolecular adhesives.[19,26] Because side-chain purine-functionalized polymers and copolymers show enhancement and tailorability of properties needed for applications they have been studied for, it raises the question:

"*What properties will poly(purine)s exhibit when a purine is directly incorporated into the polymer backbone*?" Addressing this simple question will allow me to generate a foundation of structure-property relationships for a novel class of polymeric material, "poly(purine)s", synthesized using a highly tailorable monomeric building-block.

1.2 Synthesis of Poly(purine)s

1.2.1 Purines and Palladium Catalyzed Reactions

Purines are able to participate in metal-mediated coupling reactions, especially palladium (Pd) catalyzed Stille cross-coupling reactions, to create modified purines that are functionalized at the 2-, 6-, or 8- position of the purine heterocycle.[27-34] Gunderson was the first to demonstrate that 6-chloropurines (without N-9 functionalization) readily participate in Stille cross-coupling reactions with a diverse group of stannyl coupling partners, leading to 6-subtituted purines that are desirable for medicinal studies.[32] Gunderson and coworkers expanded upon those initial findings by studying whether N-9 functionalized 6-chloropurines participated in Stille cross-coupling reactions. These studies successfully showed that a variety of stannyl reagents were effective cross-coupling partners with 6-chloropurines, allowing 6-functionalized purines to be made in high yields.[33] To further investigate the viability of functionalizing halopurines to create therapeutic agents, Gunderson and coworkers also examined the reactivity and selectivity of 2,6-dichloropurines in Stille cross-coupling reactions. Their efforts revealed that alkenyl-, alkynyl-, and thienyl-tin reagents coupled selectively at the 6-position, while other stannylated reagents (furyl and phenyl, for example) were not regioselective without using more reactive catalyst.[29] However, their findings highlight the viability of

halopurines to participate in Stille cross-coupling reactions at multiple positions around the purine heterocycle, which motivates the use of Stille cross-couplings as a way to synthesize poly(purine)s.

As suggested by the efforts of Gunderson and coworkers, the primary focus of purine chemistry has been directed toward therapeutic applications. However, it has been recently realized that Pd-catalyzed reactions are useful for synthesizing purine-based donor-acceptor small-molecule chromophores.[35] Castellano et al. successfully demonstrated that introducing purines (and pyrimidines) into π-conjugated systems can systematically tune the resulting optical and electrochemical properties. The ability to design π-conjugated building blocks that have distinct effects on optical and electrochemical properties is important for designing functional conjugated polymers.[36,37] Stille cross-coupling reactions are widely used for synthesizing conjugated polymer materials for organic photovoltaics (OPVs), OLEDs, and organic field effect transistors (OFETs).[38-42] (Stille cross-coupling polymerizations will be expanded upon in Section 1.2.2 of this chapter.) Based on these foundational pieces, it seems reasonable to conclude that purines could be incorporated into the repeat unit of a conjugated polymer (Scheme 1.1) through Pd-catalyzed Stille cross-coupling reactions and their properties altered through peripheral functionalization. As a result, so-called poly(purine)s may be attractive as novel polymeric materials and used for establishing links between macromolecular properties and design.

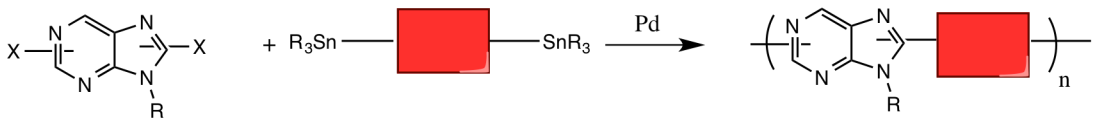

Scheme 1.1. General illustration of how purines will be incorporated into a polymer backbone through a Stille cross-coupling reaction using dihalides and stannylated reagents.

1.2.2 Stille Cross-Coupling Mechanism and Step-Growth Polymerization

The mechanistic cycle of a Stille coupling reaction, which is shown in Scheme 1.2, consists of three steps: oxidative addition, transmetallation, and reductive elimination.[28,38,39] Oxidative addition of the organohalide (step (I) in Scheme 1.2) begins the cycle, resulting in the oxidation of the palladium catalyst from Pd(0) to Pd(II). Transmetallation (step (II) in Scheme 1.2) creates a palladium intermediate having both the organohalide and organotin reagents to be coupled together. With the reductive elimination (step (III) Scheme 1.2), a new C-C bond is formed with the desired coupled product being released with simultaneous regeneration of the Pd(0) catalyst complex.

For the Stille cross-coupling reaction, thienyl monomers are preferred because thienyl monomers readily undergo the transmetallation step (compared to stannylbenzenes) because of the relatively electron-rich nature of the thienyl ring systems.[38,39,42] In general, electron-rich distannyl monomers are used for this reason.[38] On the other hand, electron-deficient halides are needed to facilitate the oxidative addition step and the formation of the desired C-C bond.[38,42]

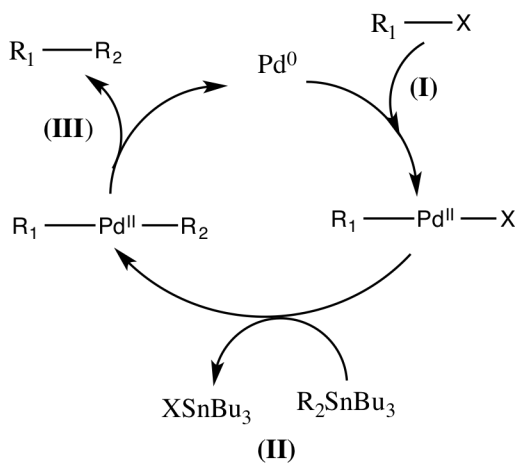

Scheme 1.2. The catalytic cycle for Stille cross-coupling reactions. Inspiration for this scheme comes from Reference 38.

Furthermore, dihalides are usually synthesized as dibromo monomers due to higher reactivity compared to dichloro monomers (reactivity follows the order of I > Br >> Cl), and increased stability compared to diiodo monomers.[38,42,43]

When the Stille cross-coupling mechanism is applied to make polymers, it falls under the classification of a step-growth polymerization. Step-growth polymerizations occur when bifunctional monomers (AB) or pairs of difunctional monomers (AA+BB reactions) are allowed to react: Generally speaking, long reaction times are needed in order to achieve high molecular weight polymers.[44] In step-growth polymerizations, the number-average degree-of-polymerization, X_n, (or number of repeat units) is determined by the Carothers Equation,[45] which is shown as Equation 1.1. This equation shows that the degree of polymerization (X_n) depends on the monomer conversion (ρ) during the polymerization:

$$X_n = \frac{1}{1-\rho} \tag{1.1}$$

Equation 1.1 shows that obtaining high molecular weight polymer requires high monomer conversions. Generally values of ρ>98% is required to generate polymers exhibiting acceptable mechanical strength, which allows them to be incorporated into useful materials.[44] In addition to using long reaction times, high temperatures, and active catalysts, another strategy for increasing ρ in step-growth polymerizations is through microwave-assisted synthesis.[46] In comparison to conventional synthetic strategies, microwave synthesis has shown to increase monomer conversion,[47,48] and has proven to be a reliable method for obtaining polymers with targeted molecular weights.[49,50] This technique is attempted to synthesize high molecular weight poly(purine)s. The ability to control molecular weight is essential to efforts to clarify links between macromolecular size and polymer properties.[45]

1.2.3 N-9 Protection of Purines: For Monomers and/or Solubilizing Groups

The 9-position of the purine is synthetically accessible through several reactions. Alkylation reactions are widely used to functionalize purines that lead to regio-isomeric products of N-7 and N-9 alkylpurines, with the N-9 product being the major product.[6] Mitsunobu reactions involving primary or secondary alcohols were found to produce, with high regioselectivity, N-9 functionalized purines.[6,51] Due to large amount of primary alcohols that are commercially available,[6,52] the Mitsubobu reaction is an attractive option for functionalizing purines. For this work, alkylation and Mitsunobu reactions are utilized to functionalize the 9-position to introduce Br-functionalized phenyl pendants, as

discussed in Chapter 2, and ethylhexyl solubilizing chains, which is described in Chapter 3.

1.2.4 Design of Donor-Acceptor Chromophores and Copolymers

As mentioned in Section 1.1 of this dissertation, purines have found applicability in organic electronics. One attribute of purines that enables their use in these applications is the ability to be synthetically designed as "push-pull" molecules, which is common strategy utilized for optoelectronic organic materials. Conjugated polymers have been studied in a variety of organic electronic applications, including organic photovoltaics OPVs,[36,53-55] OLEDs,[56] and OFETs.[57] Common goals for improving optoelectronic properties of conjugated polymers include, for example, increasing the absorbance of low energy photons near the infrared (IR) region of the visible spectrum,[36] or facilitating charge separation via intramolecular charge transfer (ICT). Both of these are beneficial when conjugated polymers are used in OPVs.[58,59] The most efficient way for modulating the energy levels of semiconducting copolymers and chromophores, and generating differences in dipoles between the ground and excited state of conjugated polymers,[58,59] has been through the design and synthesis of donor-acceptor (D-A) copolymers.[36,42,53] Due to the ability to rationally design monomers for D-A copolymers, D-A copolymers have had significant impact on the field of organic electronics, especially OPVs[36,42,53] and OFETs.[60-62]

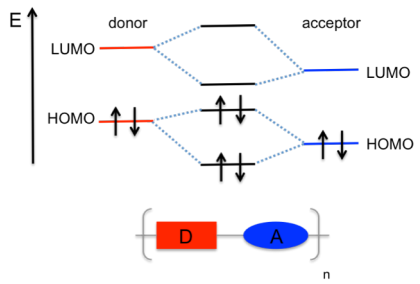

Figure 1.3 Illustration of orbital mixing in a donor-acceptor conjugated polymer. Inspiration for this illustration was gained from Reference 36.

The D-A concept consists of covalently linking electron-rich (donor) and electron-deficient (acceptor) moieties in alternating succession (i.e. D-A-D-A…). The D-A design approach results in a narrowing of the optical bandgap *and* systematic control of the HOMO and LUMO energy levels.[36,53,63] This is advantageous because the HOMO and LUMO levels of the D/A materials are set mainly by the HOMO of the donor and the LUMO of the acceptor, respectively, as illustrated in Figure 1.3.[36,53,58]

Due to the fact that the donor and acceptor moieties contribute to (dominate) the HOMO and LUMO levels, respectively, of a D-A copolymer, judicious design of monomer building blocks allow HOMO/LUMO to be tailored. For example, in OPV systems the difference between the LUMO level of the donor copolymer and the LUMO level of the acceptor PCBM must be ~0.3 eV to facilitate charge dissociation.[64] Therefore, in D/A conjugated copolymers, acceptor building blocks are chosen in order to keep the LUMO levels at or near that threshold. Similarly, the open-circuit voltage (V_{OC}) of an OPV device is directly related to the difference between the HOMO of the donor

copolymer and the LUMO of the acceptor. Therefore, donor moieties that have "deep" HOMO levels are highly desired in order to maximize this difference, which leads to increases in the V_{OC} and (generally) in device performance. The success D-A copolymers have exhibited in organic electronics, in conjunction with the ability to alter properties at the molecular level drives the development of new monomer building blocks for D/A copolymers. These efforts contribute to the advancement of organic electronics.

1.3 Characterization of Physical Properties

All monomers, oligomers, and polymers are characterized using common characterization techniques. ^{1}H and ^{13}C nuclear magnetic resonance (NMR) spectroscopy is used to confirm successful synthesis of the materials through comparison of the proton and carbon shifts between starting materials and final products. Masses of the synthesized monomers are determined with Direct Analysis in Real Time (DART) mass spectrometry. Given the potential application of purine-based chromophores and copolymers in optoelectronic devices, photophysical properties of the conjugated oligomers and copolymers are investigated using UV-Vis and fluorescence spectroscopies. Size-exclusion chromatography is used to determine the molecular weight and dispersity (M_w/M_n) of the synthesized purine copolymers. Cyclic voltammetry also is used to examine changes in oxidation and reduction potentials of the purine-based materials. Furthermore, the thermal stability of the conjugated oligomers are investigated via thermal gravimetric analysis (TGA) and differential scanning calorimetry (DSC) to determine thermal properties such as melting (T_m), crystallization (T_c), and glass-transition (T_g) temperatures, respectively.

1.4. Optoelectronic Characterization of Chromophores

1.4.1. Photophysical Characterization of Chromophores in Solution

As highlighted in Section 1.2.4, increasing the absorbance of visible light is a design goal for conjugated polymers. For this reason, understanding the photophysical processes of newly synthesized D/A and π-conjugated materials is imperative. Absorbance (process (1) in Figure 1.4) is the process of an electron being excited from the ground state to the excited state of a chromophore, generating an electron-hole pair, which is known as an exciton.

For organic molecules, energetically favored transitions correspond to excitation of an electron from the HOMO to LUMO. Relating the absorbance to the abundance of chromophore present is necessary for evaluating light-absorbing materials as candidates for optoelectronic applications. The relationship between absorbance and concentration is proportional, as highlighted through Beer's Law, which is shown in Equation 1.2.

$$A = \varepsilon bc \tag{1.2}$$

In Equation 1.2, A is the absorbance, ε is the molar absorptivity of the material, b is the cell pathlength, and c is the concentration of material in solution. The molar absorptivity is an important trait for conjugated molecules, and it is determined by measuring the absorbance of a chromophore at various concentrations.

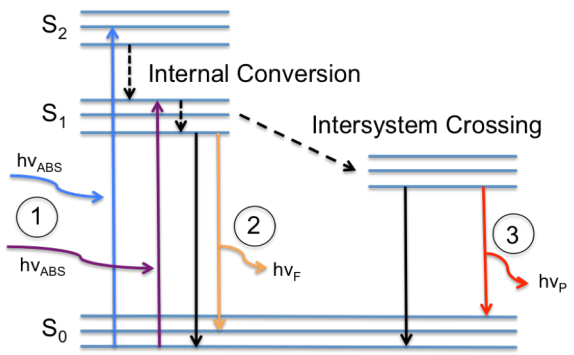

Figure 1.4. Jablonksi diagram illustrating photophysical processes. (1) represents the absorbance of photons from the singlet ground electronic state (S_0) to the first (S_1) and second (S_2) singlet electronic excited state by photons (hv) of arbitrary energy, process (2) is the emission of photons ($hv_F \neq hv_{abs}$) through fluorescence from the lowest vibrational energy state following internal conversion (vibrational relaxation), and (3) represents emission of photons through phosphorescence (hv_P) following intersystem crossing from the sinlget excited state to the triplet excited state. Solid black lines represent non-radiative relaxation pathways from the excited state to the ground state. Dashed black lines represent non-radiative relaxation pathways in the excited state.

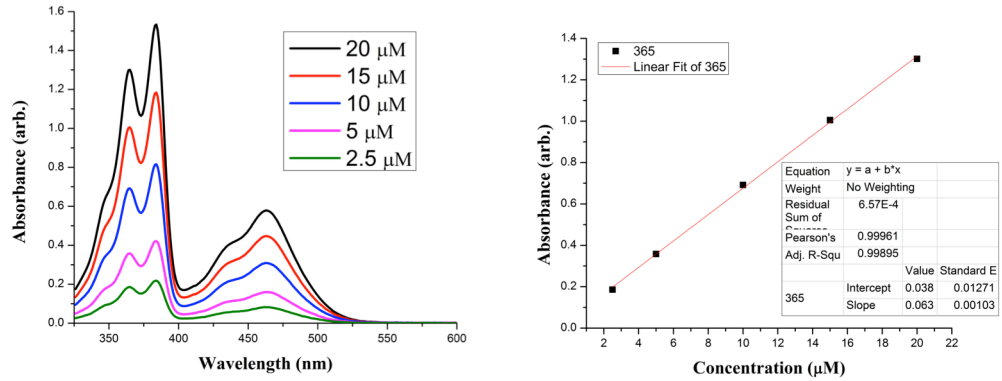

Figure 1.5. Absorbance spectra of **P-BDT-P** at various concentrations (left) and the corresponding Beer's Law plot (right), which is used to calculate the molar absorptivity.

A plot of absorbance versus concentration is generated and the slope of the line of best fit is the term εb in Equation 1.2. Molar absorptivity (ε) can be calculated by dividing the obtained value by the cell pathlength b. A series of absorbance spectra and a Beer's Law plot is presented in Figure 1.5 as an example.

Following absorbance to promote electrons to the excited state, the electron begins to relax to the ground state. One such relaxation process involving radiative decay results in the process of fluorescence. This is depicted as process (2) in Figure 1.4. Relaxation of the excited state follows an exponential decay, shown as Equation 1.2.

$$I(t) = I_0 \exp(-t/\tau) \tag{1.2}$$

Here I_0 is the intensity at time zero and τ is the characteristic decay constant, which is a measure of the excited state lifetime. The excited state lifetime is defined as the average time the molecule spends in the excited state before returning to the ground

state.[65] For a single exponential decay, 63% of chromophores decay before $t = \tau$ and 37% of chromophores decay at $t > \tau$.[65] Long-lived excited states lifetimes will, in principal, lead to higher performance in organic electronic devices.[66] As shown in Equation 1.3, the excited state lifetime is related to the radiative decay rate (k_r) and the nonradiative decay rate (k_{nr}):

$$\tau = \frac{1}{k_r + k_{nr}} \tag{1.3}$$

Due to the relationship between excited state lifetime and the relaxation rates, a link between the excited state lifetime and the fluorescence quantum yield can be derived. Quantum yield is an important property for OLEDs, as quantum yield is an indicator for OLED device efficiency. The fluorescence quantum yield is expressed as the ratio of the number photons emitted versus the number of photons absorbed, as shown by Equation 1.4.

$$\Phi = \frac{photons_{em}}{photons_{abs}} \tag{1.4}$$

In terms of the excited state relaxation rates, the quantum yield is expressed as

$$\Phi = \frac{k_r}{k_r + k_{nr}} \tag{1.5}$$

To experimentally calculate the fluorescence quantum yield the most accurate method is the comparative method. In the comparative method, the quantum yield of a new compound is determined by comparison to the fluorescence quantum yield of a known standard. This is accomplished by measuring the absorbance and fluorescence intensity of solutions at various concentrations. A plot of integrated fluorescence intensity

versus absorbance is generated and the slope of the best-fit line is inserted into Equation 1.6.

$$\Phi_S = \Phi_R \left(\frac{m_S}{m_R} \right) \left(\frac{\eta_S^2}{\eta_R^2} \right) \tag{1.6}$$

In Equation 1.6, Φ_i is the fluorescence quantum yield, m_i is the slope of the line obtained from the plot of absorbance versus the integrated fluorescence intensity, and η_i is the refractive index of the solvent where R and S refer to the reference fluorophore and sample fluorophore being studied, respectively. An example of a comparative method plot is shown in Figure 1.6.

The relationship between the excited state lifetime and quantum yield allows the radiative decay rate to be determined, which provides additional insight into the excited state dynamics of fluorophores. The radiative decay rate, k_r, can be calculated according to Equation 1.7.

$$k_r = \frac{\Phi}{\tau} \tag{1.7}$$

In Equation 1.7, Φ is the quantum yield of the chromophore and τ is the excited state lifetime of the chromophore. By measuring the absorbance, excited state lifetime, quantum yield, and radiative decay constant for designed chromophores, it is possible to develop clear insights between chromophore design and photophysical properties. This information is useful in efforts to design better materials for efficient organic electronic devices.

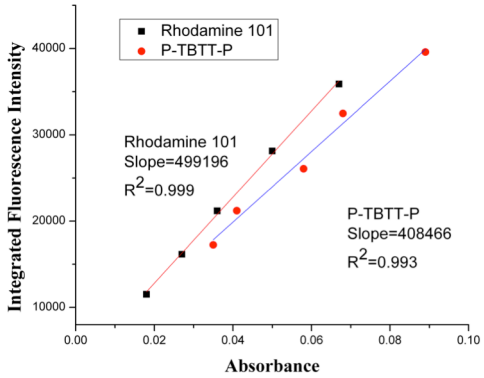

Figure 1.6. Integrated fluorescence intensity versus absorbance plot of Rhodamine 101 (black) and the purine chromophore **P-TBTT-P** (red) used for calculating the fluorescence quantum yield with the comparative method.

1.4.2 Photophysical Characterization of Chromophores as Thin Films

UV-Vis spectroscopy of thin films is used to study the optical properties of the fully conjugated poly(purine)s in the solid state. Packing orientation affects photophysical properties and performance of optoelectronic devices made from conjugated polymers.[67] For example, poly(3-hexylthiophene) (P3HT), a well-studied polymer for organic electronics,[68] exhibits a broad featureless absorbance pattern in solution. However, the absorbance profile of a P3HT film exhibits a distinct red shift (compared to its solution profile) and two "shoulders" are observed around $\lambda = 600$ nm.[69] These shoulders arise due to vibronic coupling and are attributed to an increase in π-π interactions.[70] Furthermore, variations of the polymer backbone can lead to differences in π-π interactions that impact the UV-Vis spectra of conjugated polymers in thin films. This is highlighted by Yang and Swager who, in an attempt to stabilize conjugated

polymer films for sensing applications, showed that the π-stacking of conjugated polymers is disrupted by introducing a bulky three-dimensional pentiptycene building block into the repeat unit of a poly(p-phenyleneethynylene) (Figure 1.7).[71] Disruption of π-stacking was evident by much smaller red shifts in the UV-Vis spectra between solution and a thin film. Because UV-Vis is sensitive to the design and π-interactions of π-conjugated materials, it will be a simple, yet powerful, technique for understanding how the design of the purine monomer and choice of comonomer affect photophysical properties of poly(purine)s.

Given the potential application of poly(purine)s as emitters in OLEDs, fluorescence spectroscopy also will be used to study the conjugated poly(purine)s in the solid state. Fluorescence intensity and quantum yield are affected by polymer architectures. Osaheni and Jenekhe reported that systematic manipulations block sizes of rod-coil copolymers based on benzothiadiazole (BZT) led to drastic differences in the photophysical properties of the copolymers in thin films.[67] The distinct changes in the shape and intensity of the fluorescence spectrum highlight the ability to tune thin film photophysical properties through specific design strategies. Yang and Swager also used fluorescence measurements to examine how bulky substituents in a poly(p-phenyleneethynylene) backbone affected π-π interactions. Consistent with the UV-Vis measurements, the introduction of the bulky pentiptycene comonomer to the repeat unit of poly(p-phenyleneethynylene) led to smaller red shifts in the fluorescence spectrum compared to poly(p-phenyleneethynylene),[71] again showing fluorescence spectroscopy to be an effective way to investigate π-π interactions in thin films of conjugated polymers.

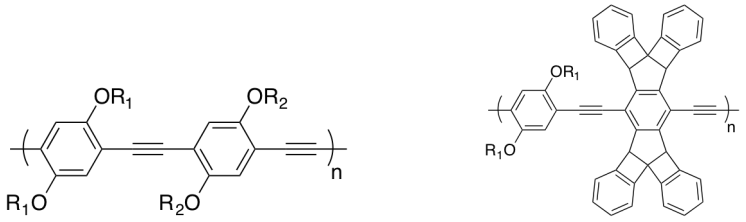

(a) (b)

Figure 1.7. Chemical structures of (a) poly(p-phenyleneethynylene) and (b) pentiptycene substituted poly(p-phenyleneethynylene) from Reference 71.

UV-Vis and fluorescence spectroscopies have proven to be sensitive to design-structure-property relationships for conjugated materials, which find applicability in OPVs and chemical sensing. Understanding the photophysical properties of conjugated poly(purine)s in the solid-state will allow for optimization of poly(purine)s for optoelectronic applications. Specifically, UV-Vis and fluorescence spectroscopies will provide valuable insight into solid-state characteristics, such as π-π interactions, and ultimately the role purine monomer design has on macromolecular properties of conjugated poly(purine)s in the solid state.

1.5 Research Objectives

Although much of my dissertation work may be regarded as exploratory, the overarching goal of my research is to establish a foundation for design principles of purine-based copolymers. Specifically, creating structure-property relationships of purine-based copolymers is an important first step for development of poly(purine)s as

material with potential application in organic electronics. In that pursuit, the specific goals of my research are to:

1. Provide the first example of "poly(purine)s" – polymers having purine monomers incorporated in the backbone of a polymer – and study the effect of monomer design on macromolecular properties;
2. Synthesize purine-based conjugated chromophores by coupling purines with donor or acceptor molecules and investigate their photophysical properties; and
3. Synthesize the first example of fully conjugated poly(purine)s and investigate the effect purine monomer design and comonomer choice on thermal, photophysical, and morphological properties in solution and thin films.

In Chapter 2, the first example of poly(purine)s is described. In this study, two dibromopurinyl monomers (with different substitution patterns) were synthesized via N-9 functionalization and polymerized with benzodithiophene (BDT) derivatives via Stille cross-coupling polymerizations. Through screening studies in which reaction time, solvent, and catalyst were examined, it was found that similar molecular weights were obtained. TGA and DSC were used to study the thermal properties of the resulting polymers. Thermal stability measured via TGA was found to be dependent on the choice of side-chain of the BDT comonomer while thermal transitions measured with DSC were dependent on BDT side-chain and purinyl monomer substitution pattern. In addition to studying thermal properties, optical properties were investigated via UV-Vis and fluorescence spectroscopies. The charge transfer character of the synthesized polymers

varied depending on purinyl monomer design, and these behaviors led me to speculate that the purine moiety acts an electron-accepting moiety with a BDT comonomer.

Chapter 3 describes a systematic study of purines in D/A chromophores to understand the charge transfer (CT) characteristics of poly(purine)s. Specifically, conjugated oligomers are synthesized by Stille cross-coupling reactions between a halopurine and the stannylated reagents of either BDT, thiophene (Th), or benzothiadiazole (BT). Thermal properties are investigated using TGA and DSC and the chromophores are susceptible to thermal annealing processes used in organic electronics. The photophysical properties are measured using UV-Vis and fluorescence spectroscopy. Through UV-Vis spectroscopy it was observed that the BDT and BT systems exhibit CT character while the Th system does not. The quantum yields were measured with fluorescence spectroscopies and all three chromophores exhibit high quantum yields. The excited state characteristics were further studied by measuring the excited state lifetime. The BDT possessed the longest excited state lifetime and by calculating the radiative rate constant it was determined this system exhibited the most charge-transfer character. Overall, this work also highlights that purine-based materials are highly tailorable and potentially functional materials.

In Chapter 4, the first synthesis of fully conjugated poly(purine)s is presented. This is accomplished by synthesizing a π-conjugated dibromopurinyl monomer that was polymerized with BDT, Th, or BT distannyl comonomers via Stille cross-coupling polymerizations. UV-Vis absorbance of the conjugated poly(purine)s revealed ~60 nm red shift of the π-π* transition compared to "Generation 1" poly(purine)s (synthesized in Chapter 2) and the purine chromophores (Chapter 3), which indicates an extension of the

π-conjugation. Furthermore, poly(purine)s constructed with the strong-acceptor benzothiadiazole shows the largest red shift with an absorbance onset of ~650 nm. This demonstrates low-band gap poly(purine)s can be constructed through the donor-acceptor design concept. Thin films of conjugated poly(purine)s also are studied using UV-Vis and fluorescence spectroscopies. The UV-Vis and fluorescence spectra indicate increased π-π interactions in solid state and provide insight about the arrangement of conjugated poly(purine)s in thin films. Conjugated poly(purine)s are also studied as the photoactive polymer in OPV devices. Preliminary OPV device performance is low and this is attributed to the low absorbance of photons in the region because of a disruption of interchain interactions between polymers and the short excited state lifetime of the conjugated polymer.

Chapter 5 summarizes the main findings of this dissertation and highlights the importance this work has in the field of polymer science and purine-based systems. Important obstacles in the development of functional purine-based materials are also discussed.

This dissertation closes with references and appendices containing information that supports the work described in Chapters 2-4. Examples include ^{1}H and ^{13}C NMR, molar absorbance plots, quantum yield plots, and SEC elugrams of synthesized polymers.

CHAPTER 2
SYNTHESIS OF MAIN CHAIN PURINE-BASED COPOLYMERS AND EFFECTS OF MONOMER DESIGN ON THERMAL AND OPTICAL PROPERTIES

This chapter describes the work published in ACS Macro Letters, 5, (2016), 682-687. I synthesized all monomers and polymers described in this work and performed all of the photophysical and thermal characterizations. Coauthors include Lauren A. Brown and Evan S. Boone, who assisted with purification and characterization of monomers and polymers, Prof. Brian K Long, who advises Lauren A. Brown, provided helpful suggestions regarding monomer and polymer synthesis, and Prof. S. Michael Kilbey II, who advised this work.

2.1 Abstract

The ability to incorporate diverse monomeric building blocks enables the development of advanced polymeric materials possessing a wide range of properties that suits them for myriad applications. Herein, I expand that synthetic toolbox by making the first report of purine-based copolymers in which purines are incorporated directly into the polymer main chain. Stille cross-coupling of dibromopurine monomers with benzodithiophene (BDT) comonomers are used to generate these "poly(purine)s". Variations in the substitution pattern of the purine monomer and BDT side-chains are studied to derive insight into the role of monomer design on the resultant thermal and photophysical properties. Specifically, thermal analyses show that poly(purine)s exhibit high thermal stability and high glass transition temperatures depending on the BDT side-chain substituents and substitution pattern of the purine-derived comonomer. Furthermore, optical properties measured via UV-Vis and fluorescence spectroscopies are dependent on monomer substitution pattern. These findings demonstrate the viability of

synthesizing poly(purine)s via metal-catalyzed cross-coupling reactions and highlight the potential to tailor poly(purine) properties via simple alterations of comonomers.

2.2 Introduction

Purines are a remarkably interesting class of molecules from both conceptual and practical points-of-view. The various positions on the fused heterocyclic ring, which was shown in Figure 1.1 of Chapter 1, can be synthetically accessed, providing functionality and tailorability that enables their use in a host of applications. Specifically, purines have been extensively studied in medicinal chemistry,[1,2] stemming from the role of adenine and guanine as building blocks of life in DNA and their importance as neurotransmitters. Due to their biocompatibility, modified purines ligated to gold nanoparticles have been used to image cell nuclei.[7] From a materials science perspective, the high fluorescence quantum yields[72] and ability to tune emission wavelengths by introduction of multiple functional groups around the periphery of the purine scaffold[8,9,73] has driven their use in organic light emitting diode (OLED) devices. Similarly, purines have been combined with small-molecule thiophene derivatives to develop electroactive, nucleobase functionalized π-oligomers[35] and push-pull purines have been synthesized and used for heavy metal-sensing.[74] The multi-dentate hydrogen-bonding character of purines has also motivated their application in advanced materials[12-15] in which the H-bonding nature of purines has been utilized to affect photogenerated charge-transfer pathways,[16] to template the synthesis of conjugated polymers,[17] and to nucleate and grow metal/inorganic nanoparticles.[10,11] Figure 2.1 shows some of the structures from works described in this paragraph.

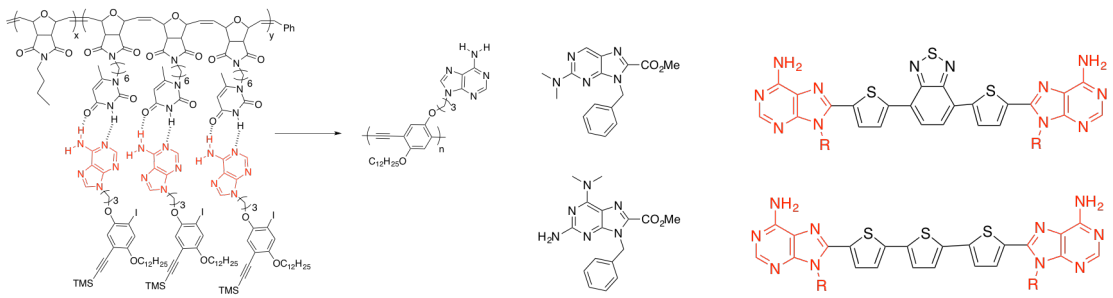

Figure 2.1. Chemical structures of purine inspired functional materials. (a) To template the synthesis of conjugated polymers from Reference 17, (b) push-pull purines for blue emitting OLEDs from References 8 and 9, and (c) donor-acceptor purine π–conjugated chromophores from Reference 35.

To further exploit the intriguing properties of purines for the development of advanced soft materials, purines have been incorporated into polymeric systems as side-chain substituents. Polymers bearing nucleobase (purine and pyrimidine) side-chains were studied extensively to investigate how complementary hydrogen-bonding impacts the self-assembly and morphological behaviors of soft materials. These side-chain functionalized polymers find potential applicability as thermoplastics,[26,75] drug delivery systems,[76,77] and electron storage/transport layers.[24,25] Inspired by the biological process of nucleic acid replication, Marsh et al. synthesized poly(methacryloyl nucleoside)s on solid supports and used them in template-directed polymerization of the complementary base pairing polymer that interacts through multi-dentate hydrogen-bonding interactions.[78] By and large, these purine (and pyrimidine) pendant-functionalized

polymers were synthesized using a variety of controlled polymerization methods such as atom transfer radical polymerization (ATRP),[20-22] reversible addition-fragmentation chain-transfer (RAFT) polymerization,[18,19] and ring-opening metathesis polymerization (ROMP).[23] Despite this, (co)polymers in which the purine unit is directly incorporated into the polymeric backbone, or main chain, have yet to be investigated and their resultant properties elucidated.

Inspired by the wide-spread use of palladium catalyzed cross-coupling chemistry for the synthesis of conjugated polymers[38-41] and by previous reports demonstrating that halopurine derivatives could be modified via transition metal-mediated cross-coupling reactions, especially Stille cross-coupling reactions,[27-33] I hypothesized that "poly(purine)s" could likewise be synthesized using Pd-catalyzed reactions. This route would involve the use of dihalopurine monomers, created using well-established synthetic methodologies that chemically transform the purine. The synthetic tailorability of the purine would, by extension, enable investigations of how the design of purinyl building block affects macromolecular properties when incorporated directly into the polymeric main chain. Herein I describe the first report of the preparation of purine containing copolymers, which were synthesized by step-growth, Stille cross-coupling polymerizations with aromatic comonomers. In addition to characterizing the molecular weight and dispersity of these novel copolymers, their thermal and photophysical properties are investigated in an initial attempt to elucidate relationships between purine monomer structure and their resultant copolymer properties.

2.3 Synthesis and Characterization

2.3.1 Materials and Methods

All chemicals used were commercially available from Sigma-Aldrich or Fisher Scientific and used without further purification unless otherwise stated. (4,8-Didodecylbenzo[1,2-b:4,5-b']dithiophene-2,6-diyl)bis(trimethylstannane) was purchased from Solarmer Energy Inc. and used without further purification. All solvents, except anhydrous *o*-xylenes, 1-methyl-2-pyrrolidinone (NMP) and anhydrous chlorobenzene (PhCl), were purified using an Innovative Technologies MD-5 Solvent Purification System and degassed prior to use. All other materials were synthesized using standard Schlenk line techniques under an argon atmosphere and purified via column chromatography using 60 Å silica gel (230-400 mesh size).

Reactions using microwave heating were performed using a Biotage Initiator 2.5 microwave reactor. ^{13}C and ^{1}H NMR spectra of synthesized monomers in $CDCl_3$ were obtained using a Varian Mercury Vx 300 MHz NMR at room temperature. 2-D HMBC NMR spectroscopy experiments were performed using a Varian VNMRS 500 MHz NMR and solutions were made using $CDCl_3$. Chemical shifts are reported in ppm and referenced to the residual solvent peak. Mass spectral analyses were performed using 1 mg/mL solutions in toluene with a JEOL AccuTOF DART Mass Spectrometer. Polymer molecular weights are reported relative to polystyrene standards and were measured using a Polymer Labs SEC 120 or Tosoh EcoSEC SEC system, both of which are operated at 40 °C and use tetrahydrofuran (THF) as the mobile phase. Concentrations of injected polymer solutions were nominally 1 mg/mL in THF. Thermogravimetric

analyses (TGA) were performed using a TA Instruments Q-50 TGA thermogravimetric analyzer with platinum pans under N_2. A scan used a ramp from room temperature to 800 °C at a heating rate of 10 °C/min. Differential scanning calorimetry (DSC) measurements were made using a TA instruments Q-2000 DSC with a heat-cool-heat cycle from -25 °C to 260 °C at a heating rate of 5 °C/min. The T_g values reported were obtained from the second heating cycle. UV-Vis spectroscopy was performed by diluting a polymer solution in chloroform with a nominal concentration of 1 mg/mL to 0.01 mg/mL. Absorbance transitions of the polymers were subsequently measured with a Thermo Scientific Evolution 600 spectrophotometer scanning from 325-600 nm. Fluorescence spectroscopy was performed by diluting UV-Vis solutions to 0.0025 mg/mL in chloroform and measuring the photoluminescence of the polymers using a Perkin Elmer LS-55 fluorescence spectrophotometer scanning from 370-700 nm after excitation at 360 nm.

2.3.2 Synthesis of 6-bromo-9-(4-bromobenzyl)-9H-purine (M1) using the Mitsunobu reaction:

M1 was synthesized following a literature procedure reported by Lu et al.[51] with slight modifications. A solution of PPh_3 (5.535 g, 21.1 mmol) and 4-bromobenzyl alcohol (3.947 g, 21.1 mmol) was prepared using dimethylformamide (DMF) (100 mL) in a 250 mL 3-neck round-bottom flask. 6-Bromopurine (2.000 g, 10.05 mmol) was added to the reaction flask under a stream of Ar, followed by the addition of diisopropyl azodicarboxylate (DIAD) (4.15 mL, 21.1 mmol) via syringe. The reaction was stirred for 24 h at 70 °C. See Scheme 2.1 below.

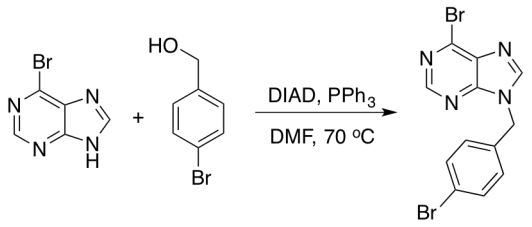

Scheme 2.1. Synthesis of **M1** via Mitsunobu conditions.

M1 was isolated and purified by a multi-step process. This work-up included addition of the reaction mixture to 50 mL of dichloromethane (DCM), washing with water (3×100 mL), drying the combined organic layers with $MgSO_4$, and filtering. The filtrate was purified by column chromatography using a gradient of hexanes and ethyl acetate. Initially the mobile phase was 100% hexanes, followed by 4:1 hexanes:ethyl acetate and finally 1:1 hexanes:ethyl acetate. The column fractions were collected and concentrated, yielding a light yellow solid that was subsequently recrystallized from a mixture of DCM and hexanes to yield white needles (42% yield). R_f (1:1 (v/v) hexanes:ethyl acetate) = 0.25, ^{1}H NMR (300 MHz, $CDCl_3$), δ (ppm): 5.40 (s, 2H, CH_2), 7.20 (d, 2H, J = 9 Hz, Ph), 7.50 (d, 2H, J = 6 Hz, Ph), 8.11 (s, 1H, purine H), 8.73 (s, 1H, purine H). ^{13}C NMR (300 MHz, $CDCl_3$), δ (ppm): 47.29, 123.04, 129.55 (×2), 132.44 (×2), 133.47, 134.09, 143.39, 144.58, 150.49, 152.19. AccuTOF DART (ESI): calc'd [M+H$^+$]: 368.9173, found [M+H$^+$]: 368.9165.

2.3.3 Synthesis of 6-bromo-9-(4-bromobenzyl)-9H-purine (M1) by alkylation:

A solution of 6-bromopurine (2.000 g, 10.05 mmol) in DMF (75 mL) was prepared in a 250 mL 3-neck round-bottom flask. Potassium carbonate (4.17 g, 30.2 mmol) was added and the resulting mixture was stirred for 20 min. 4-Bromobenzyl chloride (3.10 g, 10.05 mmol) was then added and the reaction mixture was stirred for 24 h. After 24 h, the reaction mixture was poured into DCM (50 mL), washed with H_2O (3×100 mL), and the combined organic layers were dried with $MgSO_4$ and filtered. The crude product was purified by flash chromatography on silica gel using ethyl acetate and hexanes (1:1 v/v). The collected fractions were dried, yielding a white powdery solid (55% yield). All characterizations were identical to those presented in Section 2.3.2 above. See Scheme 2.2 for the synthesis of **M1** via alkylation conditions.

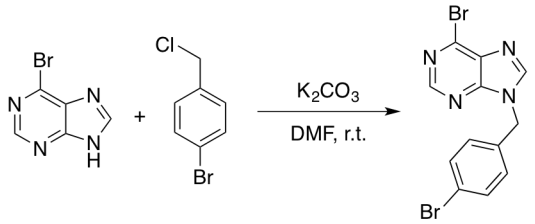

Scheme 2.2. Synthesis of **M1** via alkylation conditions.

2.3.4 Synthesis of 6-bromo-9-(3-bromobenzyl)-9H-purine (M2) by the Mitsunobu reaction:

A solution of PPh_3 (2.630 g, 10.04 mmol) and 3-bromobenzyl alcohol (1.877 g, 10.04 mmol) was prepared using DMF (50 mL) in a 250 mL 3-neck round-bottom flask. 6-Bromopurine (1.000 g, 5.02 mmol) was added, followed by addition of DIAD (1.97 mL, 10.04 mmol) via syringe. The reaction was stirred for 24 h at 70 °C. Subsequently, the reaction mixture was poured into DCM (50 mL), washed with H_2O (3×100 mL), and the combined organic layers were dried with $MgSO_4$ and filtered. The filtrate was purified by column chromatography using a gradient of hexanes and ethyl acetate. Initially, the mobile phase was 100% hexanes, followed by 4:1 hexanes:ethyl acetate and finally 1:1 hexanes:ethyl acetate. The column fractions were collected and then concentrated *in vacuo* to yield a light yellow oil. This oil was dissolved in hot DCM and hexanes and upon cooling yielded the product as a white powder that was filtered and dried *in vacuo* (37% yield). R_f (1:1 (v/v) hexanes:ethyl acetate)= 0.23, ^{1}H NMR (300 MHz, $CDCl_3$), δ (ppm): 5.42 (s, 2H, CH_2), 7.20-7.29 (m, 2H, Ph), 7.45-7.53 (m, 2H, Ph), 8.13 (s, 1H, purine H), 8.75 (s, 1H, purine H). ^{13}C NMR (300 MHz, $CDCl_3$), δ (ppm): 47.15, 123.25, 126.42, 130.80, 130.88, 132.06, 134.09, 136.69, 143.44, 144.56, 150.52, 152.25. AccuTOF DART (ESI): calc'd [$M+H^+$]: 368.9173, found [$M+H^+$]: 368.9174. See Scheme 2.3 for the synthesis of **M2** via Mitsunobu conditions.

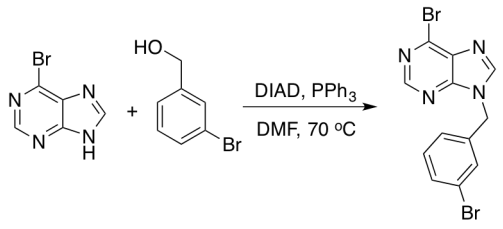

Scheme 2.3. Synthesis of **M2** via Mitsunobu conditions.

2.3.5 General Procedure for the Synthesis of Poly(purine)s P1-P4 using Conventional Heating:

The following procedure was used to prepare poly(purine)s from the dibromopurine monomers **M1** or **M2**. The polymers are referred to as **P1**, **P2**, **P3**, and **P4** with the numbers depending on the purine monomer substitution pattern (**M1** or **M2**) and the identity of the side chain on the comonomer. The desired dibromopurine monomer (1 equiv., 1 mmol), distannylbenzodithiophene (1 equiv., 1 mmol), and Pd catalyst (0.1 mmol, 10 mol%) were added to a 25 mL 3-neck round bottom flask and sealed with rubber septa. Solvent (10 mL) was then added via syringe to the reaction flask and the reaction mixture was heated at 100 °C for 24-72 hours. After the prescribed time, the reaction mixture was cooled to room temperature and the polymer was precipitated into copious amounts of methanol (MeOH). The precipitate was collected in a Soxhlet thimble and purified by successive extractions with methanol and acetone. The polymeric material was then extracted with chloroform and concentrated *in vacuo*, yielding a solid (color identified below). The solid was dissolved in a minimal amount of benzene and freeze-dried under reduced pressure. Molecular weight data (relative to polystyrene

standards) for these polymers are given in Table 2.1 and Table 2.2 of this chapter. The specific design of these poly(purine)s is presented in Scheme 2.6 in Section 2.4.

P1: Red solid. 82% yield. ^{1}H NMR (300 MHz, $CDCl_3$), δ (ppm): 0.31-2.73, 3.77-4.92, 5.18-5.79, 7.11-8.61, 8.87-9.55.

P2: Red solid. 61% yield. ^{1}H NMR (300 MHz, $CDCl_3$), δ (ppm): 0.85, 0.98-1.60, 1.71-1.96, 2.92-3.40, 5.23-5.63, 7.07-7.82, 8.00-8.20, 8.84-9.18.

P3: Orange solid. 75% yield. ^{1}H NMR (300 MHz, $CDCl_3$), δ (ppm): 0.43-1.95, 3.95-4.37, 5.27-5.60, 7.05-7.85, 8.01-8.20, 9.02, 9.12-9.28.

P4: Yellow solid. 81% yield. ^{1}H NMR (300 MHz, $CDCl_3$), δ (ppm): 0.82, 0.98-1.59, 1.75-1.98, 3.02-3.42, 5.39-5.67, 7.37-7.89, 8.17-8.23, 8.98-9.09, 9.11-9.20.

2.3.6 General Procedure for the Synthesis of Poly(purine)s P1-P4 using Microwave Heating:

The desired dibromopurine monomer (0.20 mmol), distannylbenzodithiophene (0.20 mmol), and the Pd catalyst (0.02 mmol, 10 mol%) were added to a microwave reaction vessel equipped with a Teflon stir bar. The flask was sealed and the atmosphere was rendered inert through a series of evacuation and backfilling with Ar (×3). After the final backfilling with Ar, the solvent (2 mL of either toluene, DMF, NMP, PhCl or *o*-xylenes) was added under positive Ar pressure to yield a 0.1 M solution. The reaction vessel was placed in a Biotage Initiator 2.5 microwave reactor and heated to 90-150 °C using microwave irradiation for 10 min. Upon completion, the reaction was cooled to room temperature and precipitated into a copious amount of MeOH. The precipitate was collected in a Soxhlet thimble was purified by successive washes with MeOH and

acetone. The polymeric material was then extracted with chloroform and concentrated *in vacuo*, yielding a solid (color identified above in 2.3.5). The resulting solid was dissolved in a minimal amount of benzene and freeze-dried under reduced pressure. SEC characterization results for these polymers are given in Appendix A, Table A.1.

2.4 Results and Discussion

Initial efforts to obtain purine-based polymers focused on using 2,6-dichloropurine as an organohalide coupling partner due to its common use in small-molecule Pd-catalyzed syntheses as well as its commercial availability. Previous reports of Pd-catalyzed coupling reactions involving purines demonstrated that N-9 functionalization/protection was not necessary for successful coupling of halopurines;[32] however, my initial efforts to synthesize poly(purine)s by cross-coupling 2,6-dichloropurine with 1,4-bis(tributylstannyl)benzene or 2,5-bis(trimethylstannyl)thiophene (Scheme 2.4) proved to be difficult for a number of reasons. These reasons include differences in reactivity of the C-2 and C-6 positions of the purine ring,[29,31,34] the low reactivity of the Cl substituents relative to Br and I,[43] and poor solubility. As a result, an alternative strategy involving N-9 functionalization/protection of 6-bromopurine to construct a more reactive and soluble dibromo-purinyl monomer was investigated.

Efficient N-9 functionalization or protection of purines is most commonly accomplished using either Mitsunobu reactions or simple alkylations,[1,6,51] both of which were investigated for the synthesis of dibromopurine monomer **M1**, as shown in Scheme 2.1 and Scheme 2.2.

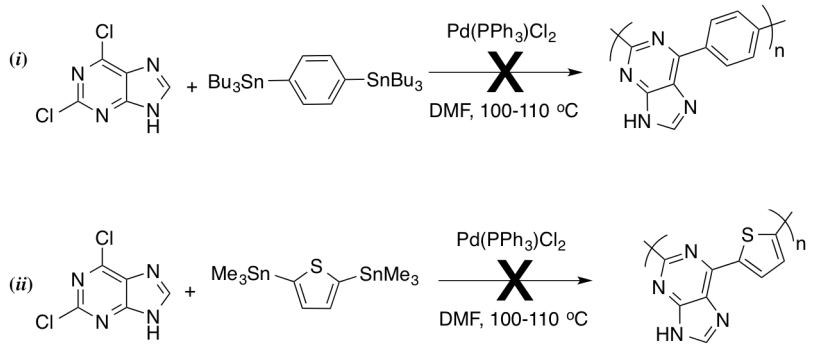

Scheme 2.4. Polymerization attempts using 2,6-dichloropurine as the dihalo monomer and either (*i*) 1,4-bis(tributylstannyl)benzene as the stannyl monomer and or (*ii*) 2,5-bis(trimethylstannyl)thiophene as the stannyl monomer to yield purine-based copolymers.

Through those efforts, alkylation conditions were found to provide slightly higher yields of **M1** compared to reactions using Mitsunobu conditions (55% versus 42%, respectively).

Additionally, driven by an interest to probe the effect that halide substitution pattern of the purinyl monomer would have on polymer synthesis and resulting polymer properties, 6-bromo-9-(3-bromophenyl)-purine (**M2**) was synthesized successfully with an overall yield of 37%. This monomer was synthesized via Mitsunobu reaction conditions (Scheme 2.3) rather than alkylation because 3-bromobenzyl chloride was not commercially available at the time of this work.

A series of test polymerizations involving **M1** and either 1,4-bis(tributylstannyl)benzene or 2,5-bis(trimethylstannyl)thiophene (see Scheme 2.5) were

performed to determine if purine-based copolymers could be synthesized by Stille cross-coupling polymerization. Reactions involving 1,4-bis(tributylstannyl)benzene yielded no evidence of polymer formation; however, cross-coupling reactions using 2,5-bis(trimethylstannyl)thiophene and monomer **M1** yielded a brown, insoluble suspension. A small amount of material was able to be dissolved in chloroform and size-exclusion chromatography (SEC) indicated this soluble recovered material had an M_n = 1,000 g/mol (relative to polystyrene standards); however, the majority of the product was insoluble and could not be characterized. This result suggested that the thienyl monomer was more efficient than the phenyl monomer in the Stille cross-coupling reaction, ostensibly due to the electron-rich nature of the sulfur-based heterocycle that may accelerate transmetallation during the cross-coupling catalytic cycle.[39]

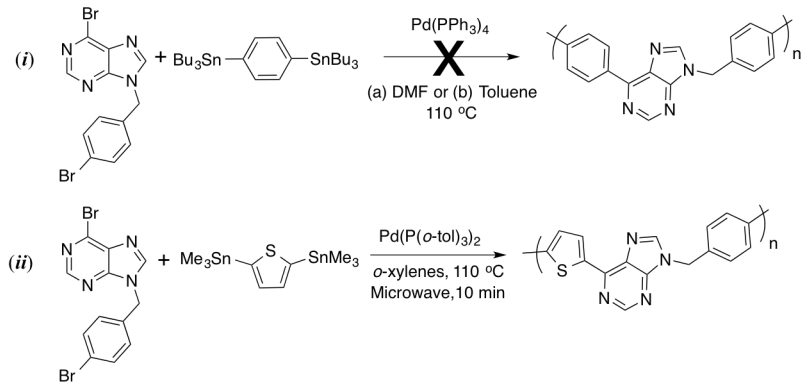

Scheme 2.5. Polymerization attempts using 6-bromo-9-(4-bromophenyl)purine and (*i*) 1,4-bis(tributylstannyl)benzene or (*ii*) 2,5-bis(trimethylstannyl)thiophene by Stille cross-coupling. The former did not appear to work while the latter resulted in an insoluble product.

Based on the results derived from the test polymerizations, including that solubility in organic solvents would be a challenge, various stannylated monomers were considered for use to produce poly(purine)s. A benzodithiophene (BDT)-based distannyl monomer (Scheme 2.6) was chosen because the long alkyl chains connected to the fused ring system by ether linkages are known to increase the electronic character of the monomer and to dramatically enhance solubility. The polymerizations were conducted using a 1:1 ratio of the dibromopurine **M1** and distannyl-benzodithiophene monomers in toluene with $Pd(PPh_3)_4$ (10 mol %) as the catalyst (Scheme 2.6). After stirring for 24-72 h at 100 °C, the reaction mixture was precipitated into MeOH to yield a red solid that was purified by a series of washes using MeOH and acetone in a Soxhlet extractor. The polymeric material was then extracted into chloroform, and recovered yields of 65-82% were determined. The recovered material was found to be readily soluble in many organic solvents such as THF, chloroform, and toluene, but demonstrated limited solubility in polar organic solvents such as DMF and DMSO. SEC analysis indicated the formation of polymeric material and number average molecular weight (M_n) values in the range of 5,600-7,200 g/mol (relative to polystyrene standards using THF as the mobile phase) were measured. The relevant data are reported as entries 1-3 in Table 2.1, and elugrams are shown in Appendix A, Figure A.1.9. These results demonstrate that purine-based copolymers could be synthesized using Stille cross-coupling and they also show that extended reaction times did not drastically affect molecular weights.

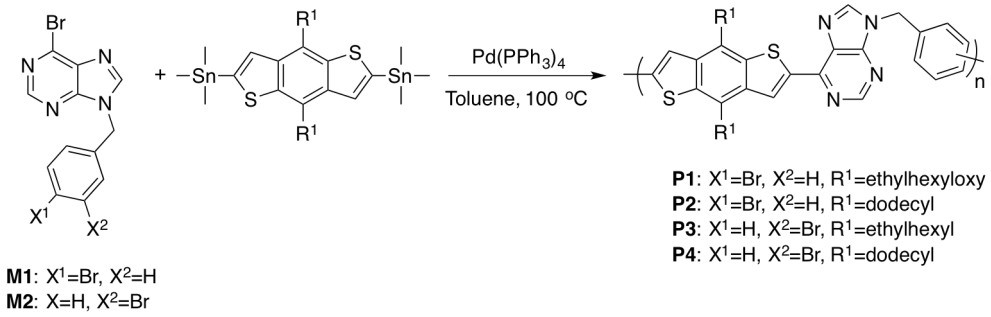

Scheme 2.6. Polymerization of **M1** and **M2** to yield **P1**-**P4**.

In an effort to increase molecular weights of the purine-containing copolymers, I chose to screen various Pd-based catalysts and solvent conditions. A variety of palladium catalysts commonly used in Stille cross-coupling reactions were investigated, and the results are shown in Table 2.1, entries 4-7. Catalyst screening studies in toluene at 100 °C indicate that both $Pd(PPh_3)_4$ and $Pd(PPh_3)_2Cl_2$ are suitable for synthesizing poly(purine)s, whereas $Pd(dba)_2/P(o\text{-tol})_3$, $PdCl_2(P(o\text{-tol})_3)_2$, and $Pd(t\text{-}Bu_3P)_2$ were ineffective. Although cross-coupling polymerizations using $Pd(PPh_3)_2Cl_2$ led to the highest molecular weights during these trials, the molecular weights obtained were inconsistent. In contrast, $Pd(PPh_3)_4$ was found to deliver the most reproducible polymer molecular weights. Based on these findings, the polymerization was then optimized relative to solvent type: *o*-xylene, chlorobenzene (PhCl), N-methylpyrrolidinone (NMP), and N,N-dimethylformamide (DMF) were each tested (Table 2.1, entries 8-11). For each solvent, the molecular weights of the resultant polymers remained similar.

Table 2.1. Molecular weight data from the synthesis of **P1** using conventional heating methods.[a]

entry	solvent	catalyst	time (h)	M_n (g/mol)[b]	M_w (g/mol)[b]	M_w/M_n[b]	yield (%)[c]
1	toluene	$Pd(PPh_3)_4$	24	5,600	7,600	1.36	82
2	toluene	$Pd(PPh_3)_4$	40	7,200	12,100	1.68	80
3	toluene	$Pd(PPh_3)_4$	72	6,900	11,100	1.61	78
4	toluene	$Pd(PPh_3)_2Cl_2$	24	7,300	10,000	1.37	74
5	toluene	$Pd(dba)_2/P(o\text{-tol})_3$	24	-	-	-	-
6	toluene	$PdCl_2(P(o\text{-tol})_3)_2$	24	-	-	-	-
7	toluene	$Pd(t\text{-}Bu_3P)_2$	24	-	-	-	-
8	*o*-xylene	$Pd(PPh_3)_4$	24	6,300	8,900	1.41	65
9	PhCl	$Pd(PPh_3)_4$	24	6,700	9,700	1.45	78
10	NMP	$Pd(PPh_3)_4$	24	5,200	6,700	1.29	69
11	DMF	$Pd(PPh_3)_4$	24	6,500	9,100	1.40	67

[a]All reactions were run at 100 °C in a 0.1 M solution with respect to purine. Ratio of **M1** to BDT was 1:1, [catalyst]=10 mol%. [b]Measured by SEC in THF at 40 °C relative to polystyrene standards. [c]Recovered yields after freeze-drying.

Polymerizations also were conducted using a microwave reactor to determine if higher monomer conversions could be obtained. Heating via microwave irradiation has shown to be an efficient method for increasing monomer conversions in many palladium-catalyzed polymerizations.[47-50] In the case of coupling the dibromopurine monomers with BDT, polymerizations using microwave irradiation led to molecular weights and yields consistent with those obtained using conventional heating methods. The molecular weight and yields are given in Appendix A, Table A.1. It is also worth noting that in multiple trials for conventional and microwave heating, there were small amounts of

material remaining in the Soxhlet thimble that was insoluble in common organic solvents. This is believed to be higher molecular weight poly(purine)s, which would indicate solubility remains a limiting factor, or that the Stille polymerizations suffer from side-reactions that result in crosslinked material.

In an attempt to circumvent the solubility issues encountered while synthesizing **P1**, a different comonomer, (4,8-didodecylbenzo[1,2-b:4,5-b']dithiophene-2,6-diyl)bis(trimethylstannane), which has dodecyl rather than ethylhexyloxy sidechains, was used as the distannyl monomer for the synthesis of **P2**. However, heating the purine-based monomers and BDT monomers in the presence of $Pd(PPh_3)_4$ in toluene at 100 °C led to molecular weights similar to **P1** (Table 2.2, entry 2). To investigate how halide substitution of the purine monomer impacts polymeric properties, 6-bromo-9-(3-bromophenyl)-9H-purine (**M2**) was incorporated yielding **P3** and **P4** (see Scheme 2.6).The molecular weights obtained for the polymerizations using conventional heating methods, reported as entries 3 and 4 in Table 2.2, are consistent with molecular weights and recovered yields obtained for **P1** and **P2**. This indicates that substitution pattern of the N-9 phenyl pendant did not affect polymerizability.

Given that the synthesized poly(purine)s were of modest molecular weights, I postulated that a difference in reactivity of the two Br-substituted positions of the dihalopurine monomer might be limiting monomer conversion. Halopurines are known to participate in regioselective cross-coupling reactions,[27,29-31,34,79] with reactivity generally following the trend of C-6 > C-8 > C-2.

Table 2.2. Polymerization data for **P1-P4** synthesized via conventional heating methods.[a]

entry	polymer	M_n (g/mol)[b]	M_w (g/mol)[b]	M_w/M_n[b]	Yield (%)[c]
1	**P1**	5,600	7,600	1.36	82
2	**P2**	6,900	10,700	1.55	61
3	**P3**	6,200	12,100	1.95	75
4	**P4**	8,000	14,100	1.75	81

[a]All reactions used $Pd(PPh_3)_4$ (10 mol%) in toluene at 100 °C for 24 h. [b]Measured by SEC in THF at 40 °C relative to polystyrene standards. [c]Recovered yields after freeze-drying.

To test the regioselectivity of the dibromopurine monomers, I performed Stille cross-coupling reactions using **M1** and the monostannylated cross-coupling partner 2-tributylstannylthiophene in a 1:1 stoichiometric ratio at the same concentrations used for polymerizations ([**M1**] = 0.1 M) (see Scheme 2.7). After heating a reaction mixture of **M1**, the monostannylthiophene, and $Pd(PPh_3)_4$ in toluene at 100 °C for 24 h, thin layer chromatography (TLC) indicated only one product is formed.

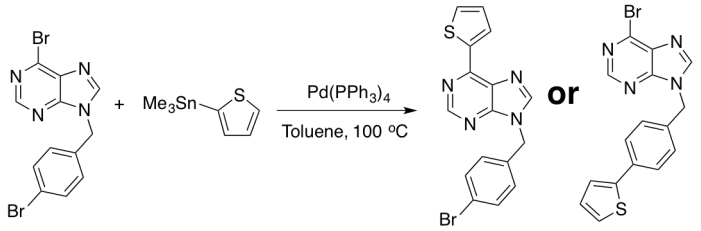

Scheme 2.7. Reaction scheme used for examining the regioselectivity of M1.

The solvent was evaporated and the product was purified via column chromatography using a 1:1 hexanes:ethyl acetate mobile phase to provide the mono-coupled product in 82% yield.

^{1}H NMR spectroscopy showed that the purine protons at 8.73 ppm and 8.11 ppm shifted to 8.92 ppm and 8.07 ppm, respectively, but the phenyl doublets at 7.50 ppm and 7.20 ppm did not shift. These results (see Figure 2.2) provide preliminary evidence of regioselective coupling at the C-6 position of the purine. This finding was confirmed by examining multi-bond proton-carbon correlations of both **M1** and the purified mono-coupled product via heteronuclear multiple-bond correlation (HMBC) NMR analysis.

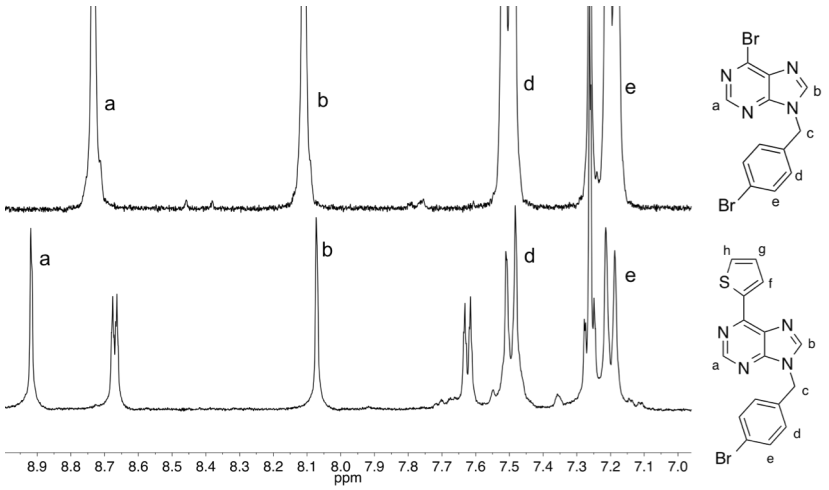

Figure 2.2. Comparison of ^{1}H spectra of **M1** (top) and a mono-substituted thienyl-purine (bottom) that shows a shift in the purine protons from 8.73 ppm and 8.11 ppm to 8.92 ppm and 8.07 ppm upon thiophene substitution at C-6 position of the purine ring.

From the results shown in Figure 2.3, it is seen that the thiophene protons (8.60 ppm) correlate with the purine C-6 (150.5 ppm), which is indicative of substitution at the C-6 position on the purine ring. Furthermore, when comparing the phenyl region of the HMBC spectra for **M1** and the mono-substituted thienylpurine, the proton signal at 7.20 ppm, which results from protons *ortho* to the -Br substituted carbon in **M1**, correlate to the same ^{13}C shift (123.3 ppm). This shows that substitution did not occur at the 4-bromo position of the N-9 appended phenylbromide substituent. These HMBC experiments provide strong evidence that cross-coupling reactions are regioselective at the C-6 position, and this regioselectivity is likely limiting the polymerization by Stille cross-coupling.

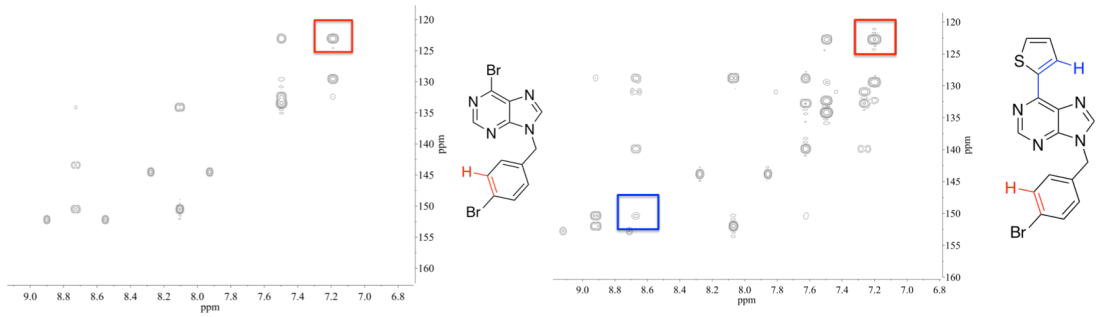

(a) (b)

Figure 2.3. HMBC of **M1** (a) and a mono-substituted thienyl-purine (b). The red box highlights the unchanged shifts of the *ortho* protons on the phenyl pendant while the blue box shows the correlation between the proton located at the 3-position of the thienyl ring and the C-6 position of the purine ring.

The differences in reactivity of the Br-substituted positions, specifically the lower reactivity of the phenyl Br, accounts for the observation that catalyst and solvent choice did not dramatically affect monomer conversion in the synthesis of **P1**-**P4**, whether by conventional heating or microwave-assisted cross-coupling. Furthermore, it is reasonable to anticipate that the polymer repeat units are not strictly regioregular, but regiorandom due to the observed differences in reactivity of the dihalide purinyl monomer.

Thermal properties such as degradation temperature (T_d) and glass transition temperature (T_g) of polymers **P1**-**P4** listed in Table 2.2 were measured using TGA and DSC, respectively, to investigate effects of monomer substitution pattern on polymeric properties. As observed in Figure 2.4, polymer **P1** exhibited a T_d at 311 °C, which is within the T_d range reported for BDT-based polymers used in organic photovoltaic devices.[80-83] The corresponding weight loss is attributed to the loss of side-chains on the BDT comonomer connected by ether linkages. When the phenyl-Br substitution pattern was changed from the 4-position to the 3-position, (**P3**) a T_d of 280 °C was measured. Comparison of the thermal stability of polymers **P1** and **P3** to **P2** and **P4** shows poly(purine)s synthesized with BDT comonomers with alkyl substituents (**P2** and **P4**) have greater thermal stability than BDT comonomers containing ethylhexyloxy substituents (**P1** and **P3**), which is consistent with behaviors reported in the literature.[84] Polymers **P2** and **P4** both show T_d values near 340 °C.

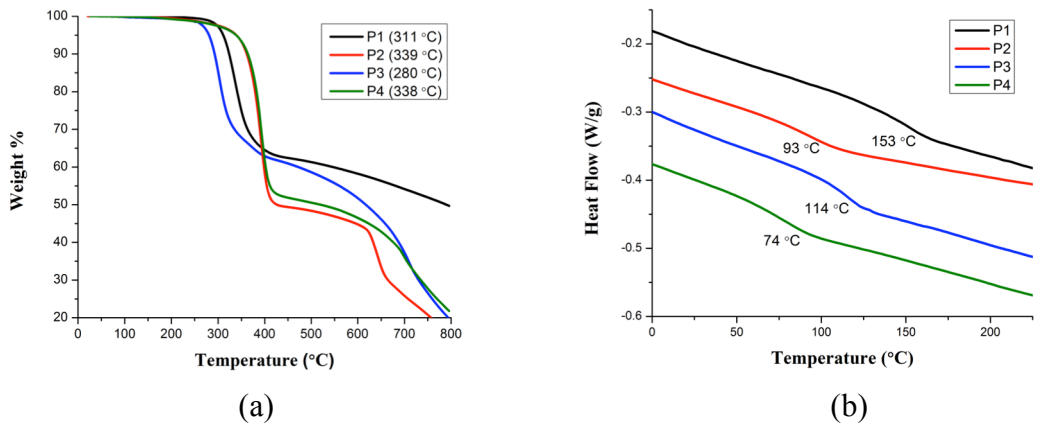

(a) (b)

Figure 2.4. Thermal characterization of poly(purine)s **P1-P4**. Data shown are (a) thermogravimetric analysis of **P1-P4** (20°C to 800°C), with T_d values given in the legend, and (b) differential scanning calorimetry traces for **P1-P4** (second heating cycle), with T_g values listed adjacent to each trace.

DSC measurements presented in Figure 2.4(b) reveal that these poly(purine)s are amorphous, exhibiting T_g values ranging from 74–153 °C, but no melting transition (T_m), as evident from the lack of an endothermic peak in the full DSC scans (see Appendix A, Figure A.12). The T_g measured for **P1** is similar to T_g values reported for previously synthesized BDT polymers.[80] Comparison of **P1** and **P3**, which were synthesized with the ethylhexyloxy-BDT comonomer but differed in Br substitution on the N-9 phenyl pendant, shows that **P1** has a T_g higher than **P3**, indicating that purine substitution impacts brittleness. This same trend is seen when comparing T_g values of polymers **P2** and **P4**, which again shows that coupling through the 4-position of the phenyl pendant leads to more brittle polymers. DSC measurements also show that polymers **P1** and **P3**, which have ethylhexyloxy side-chains, have higher T_g values than polymers **P2** and **P4**,

which have dodecyl side-chains. Given that the T_d temperatures are much higher than the measured T_g values, it is reasonable to anticipate that purine-BDT polymers are amendable to thermal processing without degradation, which may facilitate their eventual use in organic electronic devices.

Purines have been studied for a variety of optical and optoelectronic applications,[8,9,35,72-74] which motivated our investigations of photophysical properties of our main chain poly(purine)s **P1**-**P4** using UV-Vis and fluorescence spectroscopies. As illustrated in Figure 2.5, **P1**-**P4** show peak absorbance maximums ranging from 357–371 nm (see Table 2.3) that are attributed to π–π^* transitions.[85] Additionally, small shoulders appear, and these are likely due to the fine structure of the polymer, which may result from a regiorandom arrangement of comonomers. The spectra of **P1**, **P2**, and **P4** also show distinct secondary absorbance peaks at 440, 437, and 430 nm, respectively, but **P3** does not. This secondary absorbance exhibited by **P1**, **P2**, and **P4** is attributed to donor–acceptor internal charge transfer (ICT)[35,86-88] originating from the strong electron-donating characteristics of the BDT comonomer, which also has been seen in related systems.[89,90] The varying intensities of ICT bands for **P1**, **P2**, and **P4**, along with the lack of an ICT band in the spectrum of **P3,** is further indication of the regiorandom nature of the repeat units in which the conjugation is interrupted by the methylene group of the purinyl monomer. (Possible regiorandom configurations arising due to differences in reactivity of dibromo monomers are presented in Figure 2.6.)

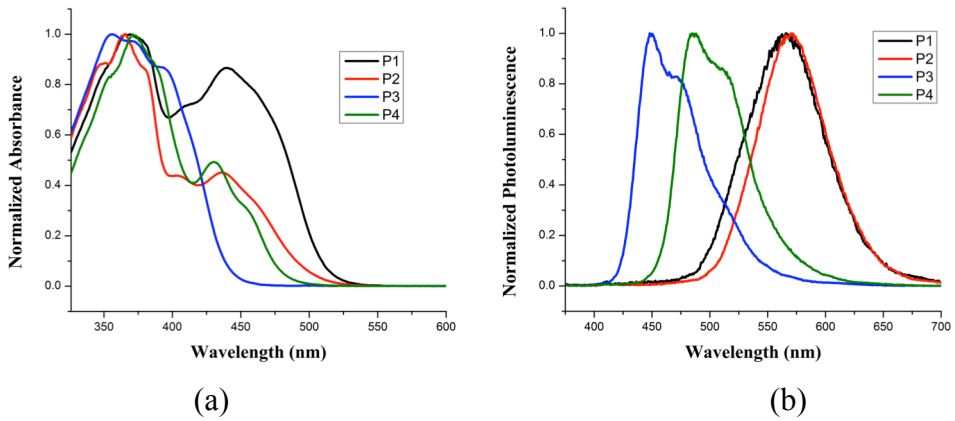

(a) (b)

Figure 2.5. (a) Normalized UV-Vis spectra for **P1-P4** at 0.01 mg/mL in chloroform and (b) normalized fluorescence spectra for **P1-P4** at 0.0025 mg/mL in chloroform.

Table 2.3. Absorbance and emission maximums of **P1**–**P4** measured in chloroform.

entry	polymer	λ_{abs} (nm)	λ_{em} (nm)	Stokes shift (nm)[a]
a	**P1**	370, 440	565	195
b	**P2**	365,437	569	204
c	**P3**	357	448, 471	91
d	**P4**	371, 430	486, 511	115

[a]Stokes shifts are calculated as the difference between the absorbance and fluorescence maximums.

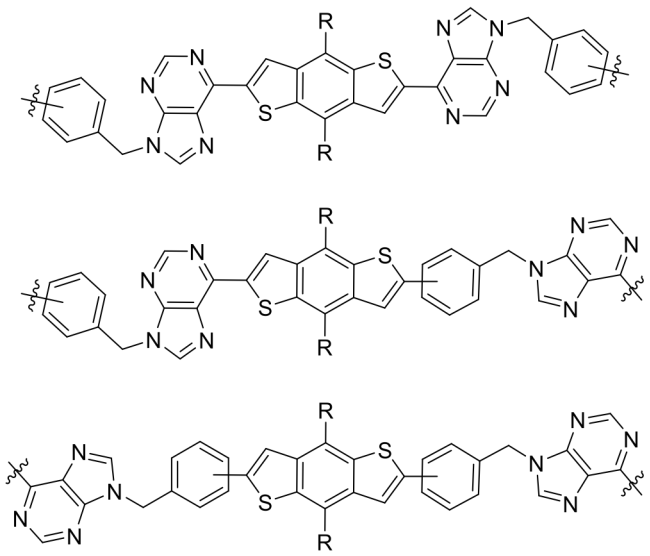

Figure 2.6. Possible repeat unit configurations of regiorandom poly(purine)s.

Comparison of the UV-Vis spectra indicates that polymers coupled via *para*-substituted benzyl moieties (**P1** and **P2**) display more red-shifted ICT bands than polymer **P4**, which is constructed by coupling through the *meta*-position. UV-Vis spectroscopy was also used to investigate whether the main chain poly(purine)s aggregate in solution via hydrogen-bonding. To test this, sequential additions of LiBr were made to a solution of **P1** in DMF. No changes in the UV-Vis spectra were noted as a function of LiBr concentration, indicating that strong H-bonding interactions are not operative at the concentrations used for these experiments. The spectra are presented in Figure 2.7.

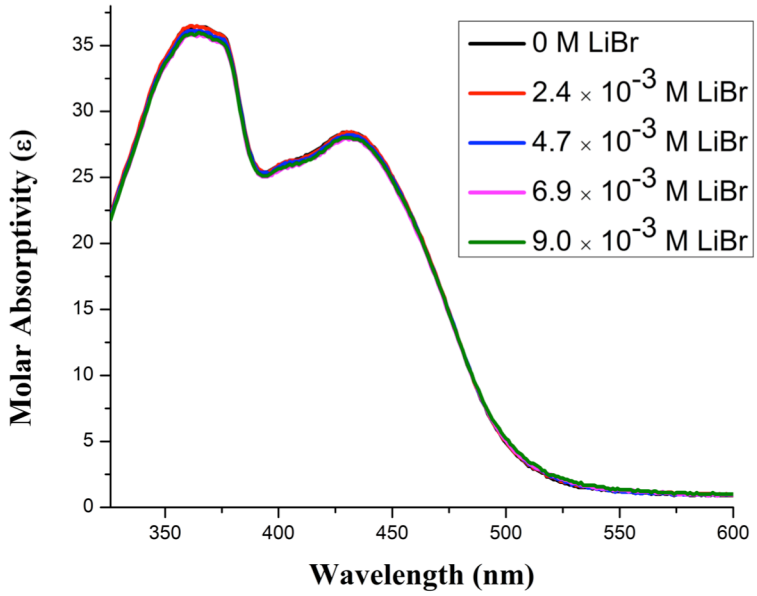

Figure 2.7. UV-Vis spectra of the soluble fraction of **P1** in DMF measured after sequential additions of a 0.1 M LiBr solution (in DMF) to investigate the possibility of hydrogen-bonding.

Fluorescence spectroscopy measurements of poly(purine) solutions presented in Figure 2.5(b) show that **P1** and **P2** exhibit significantly red-shifted emission maximums as compared to **P3** and **P4**, and this pattern of behavior is in good agreement with the red-shifted UV-Vis absorbance spectra. The featureless emission profiles of **P1** and **P2** are indicative of ICT,[35] while the two features observed at 471 and 511 nm in the emission profiles of **P3** and **P4**, respectively, are attributed to fine-structure vibrational progressions.[35,91]Additionally, when comparing the Stokes shifts of polymers **P1-P4** (Table 2.3), **P1** and **P2** display larger Stokes shifts than **P3** and **P4,** which is generally

indicative of greater structural reorganization upon photoexcitation.[35,73,92] These characteristics lend further support the contention that substitution pattern of the purinyl monomer distinctly affects polymer photophysical properties, providing a pathway for tuning the emission characteristics across much of the visible spectrum.

2.5 Conclusions

This study provides synthetic pathways to two new dibromopurine monomers that are shown to participate in palladium-catalyzed, Stille cross-coupling polymerizations to demonstrate the first examples of modified purines being directly incorporated into the main chain of a copolymer. Thermal analysis of the synthesized polymers show these "poly(purine)s" have high thermal stability, and variations in purine monomer design and type of side-chains on the BDT-comonomer led to distinct changes in glass transition temperatures. In addition, the substitution pattern of the purine monomer dramatically affects photophysical properties of poly(purine)s, as notably evidenced by the observed changes in charge transfer characteristics and dependence of emission maximums on purinyl monomer design. This study provides the foundation for a new class of polymeric material possessing tunable thermal and optoelectronic properties based on monomer substitution and motivates future investigations into the effect of purine monomer substitution on polymeric properties.

CHAPTER 3
SYNTHESIS OF DONOR-ACCEPTOR PURINE-BASED CHROMOPHORES AND AN INVESTIGATION OF THERMAL, PHOTOPHYSICAL, AND ELECTROCHEMICAL PROPERTIES

3.1 Abstract

Creating new building blocks for donor-acceptor conjugated systems is an important task for continued development of materials for organic electronics. Purines were introduced into small-molecule π-conjugated systems via Stille cross-coupling using benzodithiophene, thiophene, or dithienylbenzothiadiazole derivatives as stannyl coupling agents to generate a series of "purine-π-purine" chromophores. Photophysical and electrochemical property characterization indicate that depending on the choice of a conjugated bridging unit, purines behave as either an electron-donating or an electron-accepting unit in these small-molecule donor-acceptor chromophores. Specifically, while purine chromophores do not exhibit charge transfer character when linked to a thiophene unit, purinyl units act as a weak acceptor when coupled with benzodithiophene and a weak donor when coupled with dithienylbenzothiadiazole. The tunable charge-transfer character and their synthetic tailorability through numerous synthetic transformations suggest that purine based chromophores may be useful for synthesizing conjugated systems with high thermal stability, long excited-state lifetimes, and high quantum yields.

3.2 Introduction

Conjugated polymers and small-molecules are important materials because of their utility in fields of photovoltaics,[36,93] light-emitting diodes,[56] electrochromic devices,[94] and field-effect transistors,[57] as well as their applicability in chemical sensors.[95] Due to the desired processing properties organic materials possess, a large library of conjugated polymers and small-molecules have been developed and extensively studied leading to well-defined structure-property relationships for many conjugated

systems.[36,53] One class of π-conjugated building blocks that has drawn recent attention in the field of organic electronics is nucleobases (purine and pyrimidine). Generally, when nucleobases are incorporated into organic electronics their primary function is to manipulate molecular orientation and morphology through hydrogen-bonding.[24,25] However, the feasibility of using nucleobase building blocks as photoactive components for conjugated polymers,[96] small-molecule chromophores,[35] sensors,[74] and emitters[8,9,72,73] has been realized, highlighting their functionality beyond morphological manipulations.

As highlighted in Chapter 2 of this dissertation, I reported the first example of the synthesis of "poly(purine)s" synthesized by cross-coupling dibromo-purinyl monomers with benzodithiophene (BDT) comonomers.[97] Studies of photophysical properties revealed that poly(purine)s exhibit intramolecular charge transfer (ICT) characteristics, where the BDT unit acts as the intramolecular donor and the purine moiety of the polymer repeat unit acts as the intramolecular acceptor. In another report, Castellano et al. synthesized nucleobase π-conjugated oligomers and investigated the resulting photophysical and electrochemical properties.[35] Their purine-based conjugated systems made with a benzothiadiazole (BT) linker exhibited ICT characteristics, with the purine acting as the intramolecular *donor* and the BT acts as the intramolecular acceptor.[35] Both studies highlight the tunability of photophysical properties by varying the role (donor or acceptor) of purine building blocks in donor/acceptor π-conjugated systems. The recognition that purines are synthetically addressable at different positions of the fused ring heterocycle plus the ability of purines to behave as either a donor or an acceptor and the applicability of the donor/acceptor concept to guide the development of conjugated

polymers for applications such as high-performance organic photovoltaics,[36,53] motivate further studies of donor/acceptor purine chromophores.

While results from our group[97] and by Castellano et al.[35] point to purines behaving either as a donor or as an acceptor, there is no systematic study elucidating the optimal role for purines in donor/acceptor chromophores. Specifically, Castellano et al. reported π-conjugated oligomers (purine-π-purine) constructed through the *8-position* of the purine heterocycle,[35] while our poly(purine)s were constructed via coupling through the *6-position* of the purine and either a 3-bromo or 4-bromo benzylic pendant group installed at the *N-9 position*.[97] It is well known that changing the substitution pattern and functionality around a purine scaffold has a dramatic effect on properties such as absorbance, fluorescence, and dipole moment.[8,9,35,72-74,98] This motivates designing and synthesizing purine-containing π-conjugated oligomers constructed through the same position of the purine heterocycle (i.e. 6- or 8-position) and systematically studying the resulting thermal, photophysical, and electrochemical properties of the resultant materal. The structure-property relationships that emerge as donor- or acceptor-type building blocks and guide future development of donor-acceptor purine-based conjugated polymers.

In this Chapter, I report the synthesis of three π-conjugated purine-containing chromophores coupled through the 6-position of the purine heterocycle and describe their resulting thermal, photophysical, and electrochemical properties. The electron-donating and electron-accepting ability of the conjugated bridging unit was varied to construct an acceptor-donor-acceptor (A-D-A), a purine-π-purine (P-π-P), and a donor-acceptor-donor

(D-A-D) system, where the role of purine acting as a donor or acceptor varies based on the choice of the π-bridging unit.

3.3 Experimental

3.3.1 Materials and Methods

All chemicals and solvents were purchased from Sigma-Aldrich or Fisher Scientific and used without purification unless otherwise noted. 2,6-bis(trimethylstannyl)-4,8-bis(2-ethylhexyloxy)benzo[1,2-*b*:4,5-*b*′]dithiophene was purchased from Solarmer Energy Inc. and used without further purification. Tetrakistriphenylphosphine palladium (0) ($Pd(PPh_3)_4$) was purchased from Strem Chemicals and used without purification. Toluene and N,N-dimethylformamide (DMF) were purified using an Innovative Technologies MD-5 Solvent Purification System and degassed prior to use. All materials were synthesized using standard Schlenk line techniques under an argon atmosphere and purified via column chromatography using 60 Å silica gel (230-400 mesh size). 4,7-dithienyl-2,1,3-benzothiadiazole and 4,7-bis(5-(trimethylstannyl)thiophene-2-yl)-2,1,3-benzothiadiazole were synthesized according to previously reported procedures.[35,99]

^{13}C and ^{1}H NMR spectra of synthesized molecules were obtained using a Varian VNMRS 500 MHz NMR at room temperature in $CDCl_3$. Chemical shifts are reported in ppm and referenced to the residual solvent peak. Mass spectral analyses were performed using 1 mg/mL solutions in toluene with a JEOL AccuTOF DART mass spectrometer. Thermal stability of the chomorphores was determined via thermogravimetric analysis (TGA) in an inert atmosphere of N_2 or Ar using a TA Instruments Discovery thermogravimetric analyzer ramping from room temperature to 800 °C at a heating rate

of 10 °C/min. Thermal transitions were measured by differential scanning calorimetry (DSC) using a TA instruments Q-2000 DSC and a protocol consisting of a heat-cool-heat cycle from 0 °C to 270 °C with a heating rate of 10 °C/min and a cooling rate of 10 °C/min. Optical absorbance spectra were obtained via UV-Vis spectroscopy with a Thermo Scientific Evolution 600 spectrophotometer by scanning from 325-600 nm using 2.5-20 μM solutions of the chromophores in chloroform ($CHCl_3$). Steady-state photoluminescence was measured with a Perkin Elmer LS-55 fluorescence spectrophotometer using 0.1-2.0 μM solutions of the purine chromophores in $CHCl_3$. Time-resolved photoluminescence profiles were measured with Jobin Yvon-Spex Fluorolog equipped with 389 nm diode laser using 0.3 μM purine chromophore in $CHCl_3$. Redox potentials were measured via cyclic voltammetry (CV) using a CH Instruments potentiostat. For these measurements, 0.002 M solutions were created by dissolving 0.01 mmol of each purine oligomer in 5 mL of dichloromethane (DCM). This solution also contained tetrabutylammonium hexafluorophosphate ($(n\text{Bu})_4\text{NPF}_6$) at 0.2 M as the supporting electrolyte. The cell consisted of an using Ag/AgCl as the reference electrode, a gold working electrode, and a tungsten counter electrode and a scan rate of 100 $mV \cdot s^{-1}$ was used. All potentials are referenced to a ferrocene-ferrocenium redox couple.

3.3.2 Synthesis of 6-bromo-9-ethylhexyl-purine

A solution of 6-bromopurine (3.000 g, 15.07 mmol) and potassium carbonate (6.25 g, 45.22 mmol) in DMF (100 mL) was prepared in a 250 mL 3-neck round-bottom flask equipped with a Teflon stir bar and the resulting mixture was stirred for 20 min.

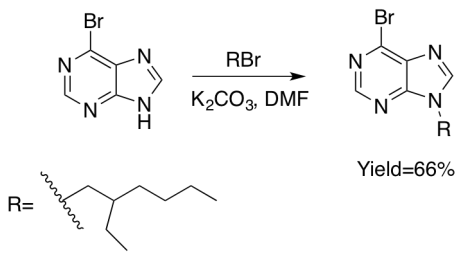

Scheme 3.1. Synthesis of 6-bromo-9-ethylhexylpurine by alkylation.

Ethylhexyl-bromide (5.36 mL, 30.15 mmol) was then added and the reaction mixture was stirred for 24 h. After 24 h, the reaction mixture was poured into DCM (50 mL), washed with H_2O (3×100 mL), and the combined organic layers were dried with $MgSO_4$ and filtered. The crude product was purified by flash chromatography on silica gel using hexanes and ethyl acetate (4:1 v/v). The collected fractions were dried, yielding a white solid (68% yield). ^{1}H NMR (500 MHz, $CDCl_3$), δ (ppm): 0.85-0.95 (m) 1.20-1.36 (m), 1.62 (br singlet), 1.91-2.03 (m), 4.18 (d, 2H, CH_2), 8.08 (s, 1H, purine H), 8.70 (s, 1H, purine H). ^{13}C NMR (500 MHz, $CDCl_3$), δ (ppm): 10.39, 13.93, 22.82, 23.67, 28.35, 30.31, 39.75, 47.89, 123.04, 134.00, 143.07, 145.33, 150.92, 151.84. AccuTOF DART (ESI): calc'd [$M+H^+$]: 310.079, found [$M+H^+$]: 310.080.

3.3.3 General Stille Cross-Coupling Procedure

6-bromo-9-ethylhexyl-purine (2 mol. equiv.), the distannyl monomer (1 mol. equiv.), and $Pd(PPh_3)_4$ (5 mol. %) were added to a single-neck 15 mL round bottom flask equipped with a Teflon stir bar and the flask was sealed with a rubber stopper. The atmosphere was rendered inert via three evacuation and refill cycles with argon. Degassed toluene was then added via syringe under an argon atmosphere and the reaction flask was placed in an

oil bath set to 100 °C and the mixture was stirred for 18-24 h. After the allotted stirring time, the toluene was removed and the crude mixture was dissolved in DCM. The crude mixture was then passed through a pad of celite to remove palladium. The filtrate was then concentrated in *vacuo* and the desired product was purified via column chromatography.

***P-BDT-P**:* Mobile phase: 6:1 v/v hexanes:ethyl acetate. Orange solid. ^{1}H NMR (500 MHz, $CDCl_3$), δ (ppm): 0.88 (t), 0.94-0.98 (m), 1.08 (t), 1.24-1.40 (m), 1.41-1.52 (m), 1.55-1.84 (m), 1.91-1.97 (m), 2.00-2.05 (m), 4.21 (d), 4.40 (d) ,8.09 (s, 1H,), 8.99 (s, 1H, purine H), 9.27 (s, 1H, purine H). ^{13}C NMR (500 MHz, $CDCl_3$), δ (ppm): 10.44, 11.41, 13.96, 14.19, 22.90, 23.17, 23.72, 23.87, 28.42, 29.29, 30.39, 30.50, 39.79, 40.79, 47.39, 75.55, 127.29, 129.88, 130.61, 134.01, 140.22, 145.05, 145.94, 149.79, 152.30, 152.42. AccuTOF DART (ESI): calc'd [$M+H^+$]: 906.53, found [$M+H^+$]: 906.35

***P-Th-P**:* Mobile phase: 2:1 v/v hexanes:ethyl acetate. Yellow powder. ^{1}H NMR (500 MHz, $CDCl_3$), δ (ppm): 0.88 (t), 0.94 (t), 1.24-1.39 (m), 2.01 (m), 4.21 (d), 8.10 (s), 8.77 (s, 1H, purine H), 8.94 (s, 1H, purine H). ^{13}C NMR (500 MHz, $CDCl_3$), δ (ppm): 10.43, 13.97, 22.89, 23.71, 28.40, 30.36, 39.75, 47.40, 129.26, 133.37, 144.40, 144.93, 149.51, 152.42, 152.61. AccuTOF DART (ESI): calc'd [$M+H^+$]: 544.3096, found [$M+H^+$]: 544.3086.

***P-TBTT-P**:* Mobile phase: 100% DCM. Red solid. ^{1}H NMR (500 MHz, $CDCl_3$), δ (ppm): 0.88 (t), 0.95 (t), 1.24-1.40 (m), 1.60 (s, br), 2.01 (m), 4.22 (d), 8.06 (s, 2H, purine H), 8.09 (s, 2H, purine H), 8.31 (d, 2 H, thiophene H) 8.73 (d, 2H, thiophene H), 8.94 (s, 2H, BT H). ^{13}C NMR (500 MHz, $CDCl_3$), δ (ppm): 10.42, 13.97, 22.89, 23.71, 28.39, 30.36,

39.72, 47.39, 120.63, 126.08, 128.93, 129.20, 133.27, 140.89, 143.94 144.78, 149.49, 152.37, 152.44. AccuTOF DART (ESI): calc'd [$M+H^+$]: 761.2990, found [$M+H^+$]: 761.2956.

3.4 Results and Discussion

Purines are known to have limited solubility in common organic solvents such as tetrahydrofuran (THF), toluene, and chloroform. To ensure solubility of donor-acceptor purine chromophores, 6-bromopurine was functionalized at the N-9 position via alkylation with 2-ethylhexyl bromide as shown in Scheme 3.1. Yields of 66% were obtained and the isolated N-9 alkylated purine, 6-bromo-9-ethylhexyl-purine, was readily soluble in hexanes, THF, chloroform, and toluene.

6-bromo-9-ethylhexylpurine was then used as the halogen coupling partner for Stille cross-coupling reactions with distannyl conjugated linkers. Cross-coupling reactions using either a distannylated benzodithiophene (BDT) or a distannylated thiophene (Th) coupling partner were performed in toluene at 100 °C using $Pd(PPh_3)_4$ (5 mol %) as the catalyst. After workup, the purine (P) dyads **P-BDT-P** and **P-Th-P** were isolated in yields of 56% and 58%, respectively. (See Scheme 3.2.)

Incorporating a benzothiadiazole (BT) linker proved more challenging. Initial attempts to incorporate a BT moiety as a linker using Suzuki cross-coupling reactions under either anhydrous or aqueous conditions did not yield product, which stands in contrast to the work of Hocek and coworkers.[34,100] These approaches failed ostensibly due to the electron deficient nature of 2,1,3-benzothiadiazole-4,7-bis(boronic acid pinacol ester).[38,42]

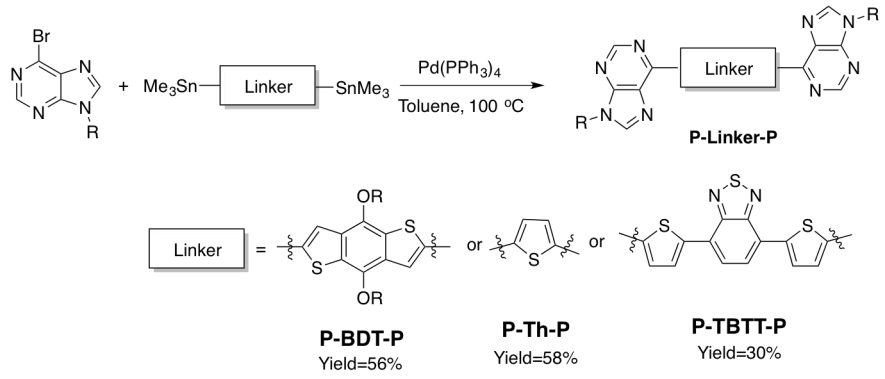

Scheme 3.2. Synthesis of purine dyads via Stille cross-coupling.

To circumvent this problem, 4,7-bis(5-(trimethylstannyl)thiophene-2-yl)-2,1,3-benzothiadiazole was prepared, as this building block is commonly used for the synthesis of conjugated polymers for OPV applications.[101] After synthesis and isolation of 4,7-bis(5-(trimethylstannyl)thiophene-2-yl)-2,1,3-benzothiadiazole, a Stille cross-coupling reaction was performed in toluene at 100 °C using $Pd(PPh_3)_4$ (5 mol %) as the catalyst to generate in **P-TBTT-P** with a yield of 30% as shown in Scheme 3.2.

Given the potential applicability of purine compounds in organic electronics, the thermal stability of **P-BDT-P**, **P-TBTT-P**, and **P-Th-P** was examined using TGA. As shown in Figure 3.1, **P-TBTT-P** showed the highest thermal stability with a degradation temperature (T_d) of 443 °C followed by **P-BDT-P** (T_d = 332 °C) and finally **P-Th-P** (T_d = 295 °C). The mass loss at the T_d values for **P-BDT-P** and **P-TBTT-P** are attributed to the loss of the N-9 ethylhexyl solubilizing group, while **P-Th-P** exhibits a single degradation event.

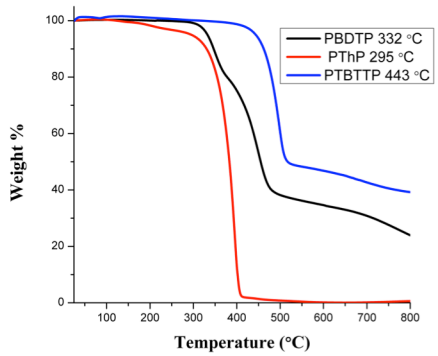

Figure 3.1. Thermogravimetric analysis of **P-BDT-P**, **P-Th-P**, and **P-TBTT-P** (20-800 °C).

To further probe the thermal properties of the purine chromophores, the melting temperatures of **P-BDT-P**, **P-Th-P**, and **P-TBTT-P** were measured using DSC. As shown in Figure 3.2, **P-Th-P** exhibits a sharp melting (T_m) transition at 158 °C and a crystallization (T_c) transition at 137 °C. **P-BDT-P** exhibits a T_m = 102 °C without an observable T_c while **P-TBTT-P** did not exhibit a T_m or T_c over the experimental temperature range accessed. The low melting temperatures observed for **P-Th-P** and **P-BDT-P** are attributed to the branched ethylhexyl solubilizing groups. The higher T_m measured for **P-Th-P** is an indication of more rigid packing, which is likely disrupted in **P-BDT-P** due to the ethylhexyl chains on the BDT linker. Because the measured T_m and T_c are much lower than the measured T_d's, these purine chromophores are amendable to processing by thermal annealing.

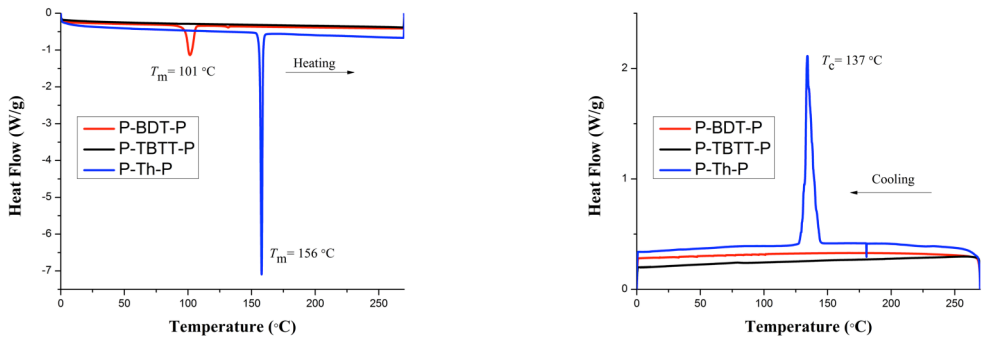

(a) (b)

Figure 3.2. Differential scanning calorimetry traces of **P-BDT-P**, **P-Th-P**, and **P-TBTT-P** showing the heating (a) and cooling (b) cycles.

While characterizing the purine chromophores using ^{1}H NMR spectroscopy, differences in aromatic ^{1}H chemical shifts were observed, as represented in the spectra shown in Figure 3.3. Specifically, when the purines are coupled with the very strong electron-donating BDT linker there is a downfield shift of the proton at the 2-position of the purine (labeled as *proton a* in Figure 3.3) as compared to the corresponding proton in either **P-TBTT-P** or **P-Th-P**. Furthermore, there is negligible difference between *proton a* in the ^{1}H spectra measured for **P-Th-P** (π-conjugated) and **P-TBTT-P** (electron accepting linker), which indicates similar electron density (proton shielding) in the purine ring for these two chromophores. The different π-electron distributions are a good indication that electronic properties of the purine chromophores can be tuned based on the nature of the linker as well as the substituents (*vide infra*).

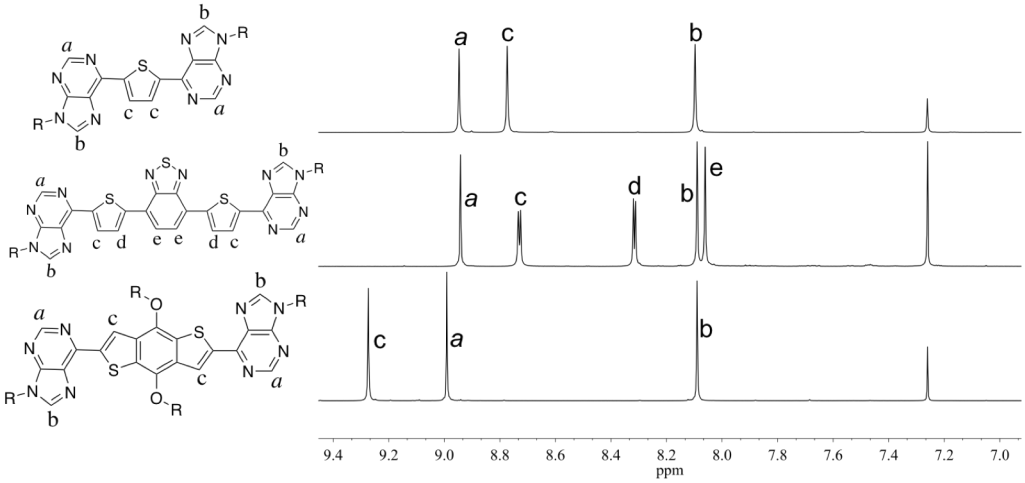

Figure 3.3. ^{1}H NMR spectra of the aromatic regions of the three purine chromophores. The R-groups are representative of the ethylhexyl solubilizing chains.

The UV-Vis spectra of **P-BDT-P**, **P-TBTT-P**, and **P-Th-P** are shown in Figure 3.4(a) with the absorbance maximums, $\lambda_{\max}^{abs}$, for each chromophore presented in Table 3.1. All three chromophores exhibit absorbance maximums between 350-400 nm, and this corresponds to their respective π-π* transitions.[35,97] **P-BDT-P** and **P-TBTT-P** exhibit a second transition at 463 nm and 488 nm, respectively, which is characteristic of intramolecular charge-transfer (ICT).[35,97] The ICT band in **P-BDT-P** originates from charge transfer (CT) processes from the strong-electron donor BDT to the purine, which also was observed for the poly(purine)s described in Chapter 2,[97] while the ICT is from the purine to the strong electron-acceptor in **P-TBTT-P**, a characteristic that is consistent with the behavior of purine-based chromophores constructed through the 8-position.[35]

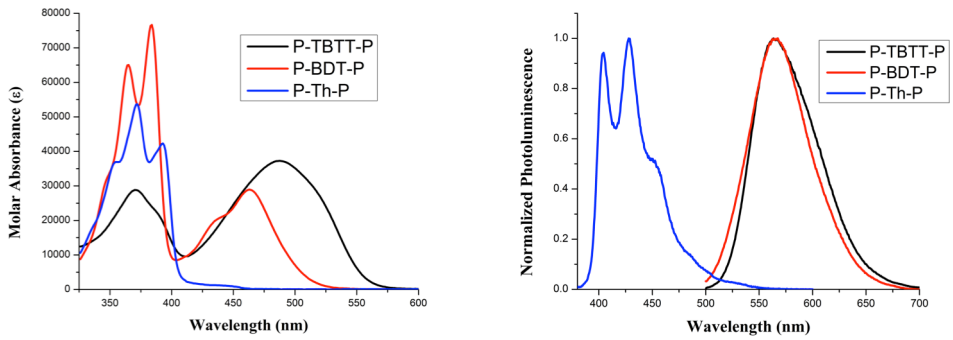

(a) (b)

Figure 3.4. (a) UV-Vis and (b) photoluminescence spectra of **P-BDT-P**, **P-TBTT-P**, and **P-Th-P** in chloroform.

On the other hand, **P-Th-P** does not exhibit ICT characteristics due to the weak electron-donating nature of the thiophene linking unit.The absence of CT character for my thienyl-based purine chromophore constructed through the 6-position of the purine heterocycle is consistent with the absence of CT processes observed in thienyl-linked purines coupled through the 8-position, as reported by Castellano et al.[35]

Stemming from purines finding applicability in OLEDs due to high fluorescence quantum yields,[8,9,72,73] I measured the photoluminescent (PL) properties of **P-BDT-P**, **P-TBTT-P**, and **P-Th-P** via fluorescence spectroscopy. The normalized fluorescence spectra of the chromophores are shown in Figure 3.4(b) and the fluorescence maxima, $\lambda_{\max}^{em}$, are presented in Table 3.1. Both **P-BDT-P** and **P-TBTT-P** exhibit broad, featureless emission profiles, and large Stokes shifts (of 97 nm and 72 nm, respectively).

Table 3.1. Photophysical properties of purine chromophores.

compound	λ_{max}^{abs}	λ_{max}^{em}	Stokes shift (nm)[a]	φ[b]	τ (ns)	$k_r=\varphi/\tau \times 10^9$ (s^{-1})
P-BDT-P	365, 383, 463	560	97	0.50	8.01	0.062
P-Th-P	372, 393	405, 428	12	0.52	1.32	0.39
P-TBTT-P	370, 488	560	72	0.93	4.57	0.20

[a]Stokes shift calculated as the difference between absorbance and fluorescence maximums. [b]Quantum yields were calculated using the comparative method.

These traits provide further evidence of **P-BDT-P** and **P-TBTT-P** possessing ICT character. On the other hand, a small Stokes shift (~12 nm) and fine-structure vibrational progressions are observed in the **P-Th-P** fluorescence spectrum, which are consistent with the absence of ICT processes.[35]

Quantum yields were determined using the comparative method, which is embodied in Equation 1.6.[65,102]

$$\varphi_x = \varphi_s \left(\frac{m_x}{m_s}\right)\left(\frac{\eta_x^2}{\eta_s^2}\right) \tag{1.6}$$

Rhodamine 101 in ethanol (φ_s = 1.00) was used as the fluorescence standard for **P-BDT-P** and **P-TBTT-P** and quinine sulfate at 0.05 M in H_2SO_4 (φ_s = 0.52) was used as the standard for **P-Th-P**. **P-BDT-P** and **P-Th-P** exhibited lower quantum yields (φ_x = 0.50 and 0.52, respectively) in comparision to **P-TBTT-P**, whose quantum yield was measured as 0.93. The measured quantum yields of **P-BDT-P**, **P-TBTT-P**, and **P-Th-P** are higher than purines coupled through the 8-position,[35] further highlighting that purine properties are tailorable through the specific functionalization (type of functionality and

location) of the fused ring heterocycle structure.[97] The high quantum yields exhibited by **P-TBTT-P** makes this molecule a promising candidate for OLED applications.

Photoluminescent properties of the purine chromophores were measured in solvents of different polarity to investigate solvatochromic behavior. **P-Th-P** did not exhibit any changes in the emission profile when measured in solvents of varying polarity, which is consistent with a lack of intramolecular charge-transfer characteristics. **P-BDT-P** exhibited the most dramatic changes in the emission profile when changing the solvent: As shown in Figure 3.5(a), **P-BDT-P** shows a clear redshift in the fluorescence spectrum with increasing solvent polarity. When **P-BDT-P** is measured in hexanes, a vibronic progression is apparent, but when the solvent is changed to toluene or chloroform there are clear redshifts and the vibronic progression is no longer visible. The shifts in the PL spectra with increasing solvent polarity are an indication that the excited state dipole moment is larger than the ground state dipole moment.[103] Larger dipole moments in the excited state were also observed in the purine-based donor-acceptor systems studied by Castellano et al.[35]

A thorough investigation of the solvatochromic properties of **P-TBTT-P** was difficult because of the limited solubility of this chromophore in several solvents. When the PL spectra of **P-TBTT-P** were measured in toluene, THF, and chloroform, there were no substantial differences between the PL profiles, as shown in Figure 3.5(b).

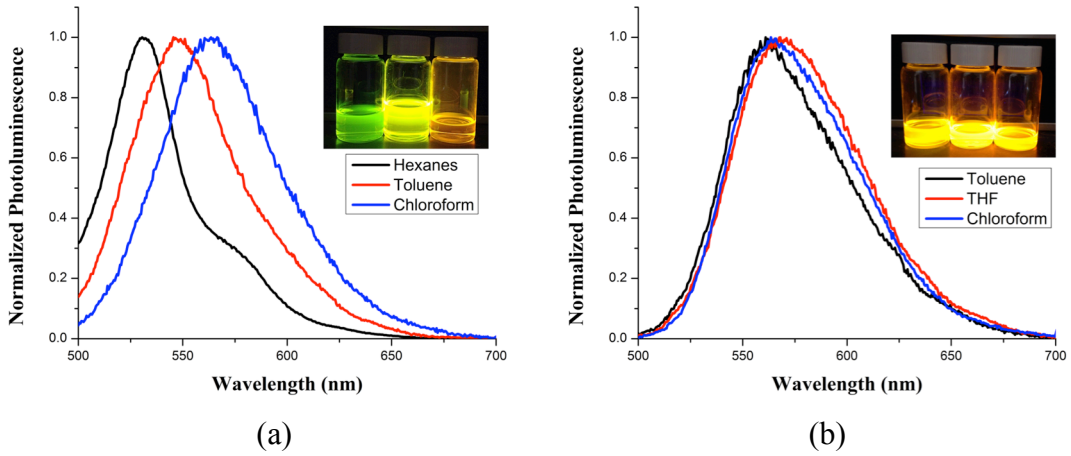

Figure 3.5. Normalized photoluminescence spectra of (a) **P-BDT-P** and (b) **P-TBTT-P** in solvents of varying polarity.

The emission profile of **P-TBTT-P** in toluene was narrower than the emission profiles in the more polar solvents, THF and chloroform. The small changes in the PL profile when changing solvent polarity indicates that there is not a significant difference between ground state and excited state dipole moments. The distinct changes seen in the PL spectra of **P-BDT-P**, such as vibronic progressions in nonpolar solvents and increasing red shifts with increasing solvent polarity, is evidence that **P-BDT-P** possesses more CT character than **P-TBTT-P**.

The excited state fluorescence lifetimes (τ) of the purinyl chromophores were determined using time-resolved photoluminescence. The fluorescence decay profiles of **P-BDT-P** and **P-TBTT-P** were measured in $CHCl_3$ by exciting at 389 nm and monitoring the fluorescence decay at 550 nm. Measurements of **P-Th-P** in $CHCl_3$ used

the same excitation wavelength, but the decay was measured at 425 nm. As shown in Figure 3.6, donor-acceptor purine chromophores (**P-BDT-P** and **P-TBTT-P**) exhibit significantly longer excited-state lifetimes than the π-conjugated system that does not exhibit donor-acceptor character (**P-Th-P**). **P-BDT-P** exhibits the longest excited state lifetime (8.01 ns) followed by **P-TBTT-P** (4.57 ns), and **P-Th-P** (1.32 ns). Each of the decay profiles for the chromophores are well-described by a single exponential function. The large difference in fluorescence lifetimes is indicative that the singlet states of **P-BDT-P** and **P-TBTT-P** exhibit a higher degree of CT character, with **P-BDT-P** possessing more CT character than **P-TBTT-P**, while the singlet state of P-Th-P does not show CT character.[104] Furthermore, the fluorescence lifetimes measured for **P-TBTT-P** and **P-Th-P** are similar to those reported by Castellano et al.,[35] but **P-BDT-P** exhibits the longest lifetime reported for a purine based donor-acceptor system.

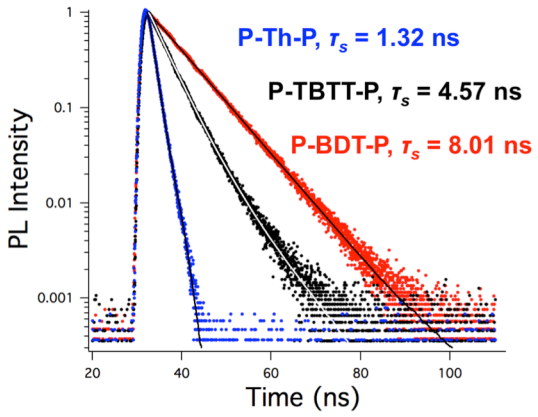

Figure 3.6. Time-resolved photoluminescence profiles of **P-BDT-P**, **P-TBTT-P**, and **P-Th-P** in $CHCl_3$.

Additional insight into the excited state photophysics of the purine chromophores was gained by calculating the excited state radiative decay constant, k_r: $k_r = \varphi/\tau$. **P-BDT-P** has a k_r one order of magnitude smaller than **P-TBTT-P** and **P-Th-P**, as seen in Table 3.1. This is indicative of a greater degree of CT character for **P-BDT-P** compared to **P-TBTT-P** and **P-Th-P**.[35,104] The smaller k_r for **P-TBTT-P** compared to **P-Th-P** is due to **P-TBTT-P** possessing more charge-transfer character than **P-Th-P**.[35,104] The k_r values indicating **P-BDT-P** and **P-TBTT-P** exhibit CT character while **P-Th-P** does not, are consistent with UV-Vis and fluorescence measurements. Furthermore, the k_r values show that **P-BDT-P** possesses more CT character than **P-TBTT-P**, which agrees with results of fluorescence lifetime and solvatochromic fluorescence measurements. It is also worth noting that the nonradiative decay rate constants ($k_{nr} = (1-\varphi)/\tau$) for each purinyl chromophore – **P-BDT-P** = 0.062×10^{-9} s^{-1}, **P-Th-P** = 0.15×10^{-9} s^{-1}, and **P-TBTT-P** = 0.36×10^{-9} s^{-1} – are similar to their k_r values. The similarity between the two constants is indicative there is minimal internal conversion or intersystem crossing.[105]

The redox properties of **P-BDT-P**, **P-TBTT-P**, and **P-Th-P** were measured with cyclic voltammetry (CV) in dichloromethane (DCM) with $(n\text{Bu})_4\text{NPF}_6$ as the supporting electrolyte. The oxidation and reduction onsets were used to estimate the HOMO and LUMO energy levels using Equations 3.1 and 3.2 based on the assumption that the Fc/Fc^+ redox couple is 5.1 eV relative to vacuum.[106]

$$E_{HOMO}(eV) = -(E^{ox}_{onsext} + 5.1)eV \tag{3.1}$$

$$E_{LUMO}(eV) = -(E^{red}_{onset} + 5.1)eV \tag{3.2}$$

E_{onsext}^{ox} and E_{onset}^{red} represent the onset oxidation and reduction potentials, respectively, via CV versus the Fc/Fc^+ couple, and from these values, the bandgap, ΔE_{gap}, was determined. As shown in Table 3.2, **P-TBTT-P** has the narrowest bandgap (2.19 eV), followed by **P-BDT-P** (2.27 eV), and subsequently **P-Th-P** (2.99 eV). An illustration of the relative HOMO/LUMO levels calculated from the redox onset potentials measured using CV is shown in Figure 3.7(b).

The lower lying HOMO exhibited by **P-TBTT-P** in comparison to **P-BDT-P** is an indication that **P-TBTT-P** follows the "weak donor-strong acceptor" concept used for constructing low bandgap conjugated polymers more closely than **P-BDT-P**.[53] Specifically, the purine moiety acts as the weak donor when coupled with the strong acceptor TBTT. The large band gap exhibited by **P-Th-P** is an indication the chromophore does not possess CT character that leads to a narrowing of the optical band gap.

Table 3.2. Molecular orbital data obtained via CV measurements.

compound	E_{onsext}^{ox} (V)	E_{onset}^{red} (V)	HOMO (eV)	LUMO (eV)	ΔE_{gap} (eV)
P-BDT-P	0.40	-1.87	-5.50	-3.23	2.27
P-Th-P	1.17	-1.82	-6.27	-3.28	2.99
P-TBTT-P	0.79	-1.40	-5.89	-3.70	2.19

[a]Electrochemical potentials are reported against the Fc/Fc^+ reference.

Cyclic voltammetry of **P-BDT-P**, **P-TBTT-P**, and **P-Th-P** indicates that each of the chromophores exhibit two reversible reductions within the DCM solvent window. (See Figure 3.7(a)) Both **P-TBTT-P** and **P-Th-P** show irreversible oxidations, with **P-TBTT-P** displaying multiple irreversible oxidations while **P-Th-P** exhibits only one. **P-BDT-P** on the other hand shows two reversible oxidations potentials. The large positive shift in the reduction onset potential when comparing **P-TBTT-P** to **P-Th-P** demonstrates the strong electron accepting nature of the BT moiety.[35]

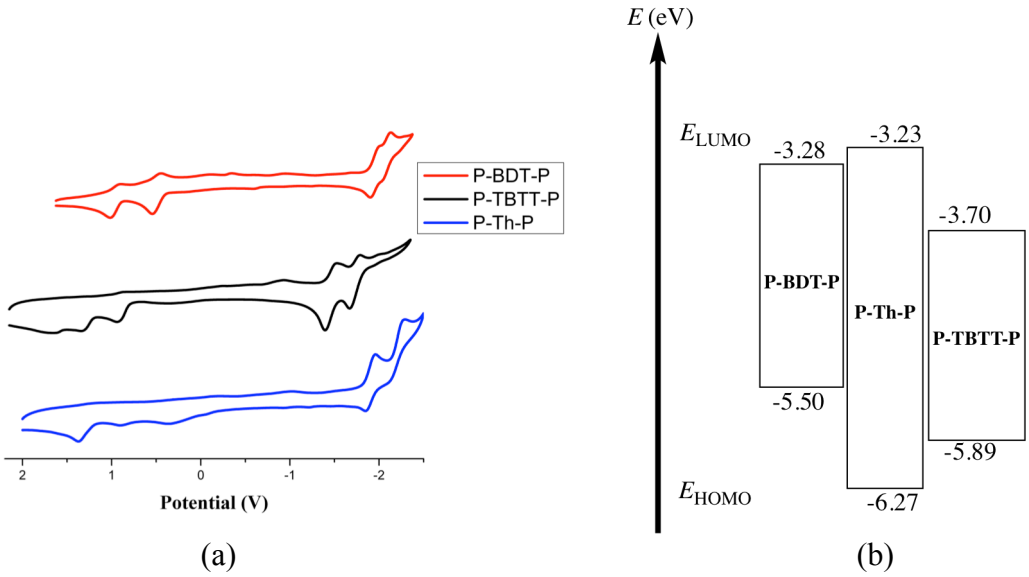

Figure 3.7. (a) Overlay of cyclic voltammetry traces illustrating redox potentials of **P-BDT-P**, **P-TBTT-P**, and **P-Th-P** and (b) HOMO/LUMO level diagrams of **P-BDT-P**, **P-TBTT-P**, and **P-Th-P** obtained via cyclic voltammetry measurements.

However, when the purine is functioning as the intramolecular acceptor in **P-BDT-P**, the reduction onset does not drastically change in relation to **P-Th-P**. This leads to the similar LUMO levels of **P-BDT-P** and **P-Th-P**, indicating that the purine is a weak acceptor unit, as illustrated in Figure 3.7(b).

3.5 Conclusions

Purines are useful molecules that provide a highly tailorable scaffold that can be exploited for designing bioinspired π-conjugated materials for next generation optoelectronics. For purines to find applicability in organic electronics, structure-property relationships of purine-functionalized chromophores must be established and understood. Three purine-based donor-acceptor chromophores – A-D-A (**P-BDT-P**), D-A-D (**P-TBTT-P**), and P-π-P (**P-Th-P**) – were synthesized via Stille cross-coupling reactions between a 6-bromopurine derivative and the corresponding distannyl π-linker. Thermal analyses revealed purine-based chromophores are thermally stable and amendable to processing techniques commonly used for organic electronics. The resulting photophysical and electrochemical properties reveal the purine acts as a weak-acceptor when coupled with BDT, as a weak-donor when coupled with BT, and forms a conjugated system with no ICT character when coupled with Th. The choice of the π-linker also has drastic effects on photophysical properties, such as ICT, quantum yield, and fluorescence lifetime of the chromophores. Results from these studies provide further motivation to study purine chromophores for organic electronic applications due to their high thermal stability, long excited state lifetimes, and high quantum yields. The large number of verified synthetic transformations of purines and their ability to participate in

cross-coupling reactions with donors or acceptors suggests these conjugated materials may find applicability in high-performance organic electronic devices or sensors. The reported purine chromophores can be incorporated into polymers and studies of the resulting photophysical properties will be presented in Chapter 4.

CHAPTER 4
SYNTHESIS OF PURINE-BASED DONOR-ACCEPTOR CONJUGATED POLYMERS AND THE EFFECT OF INCORPORATING PURINES ON PHOTOPHYSICAL PROPERTIES

4.1 Abstract

Creating new donor-acceptor conjugated polymer systems and understanding structure-property relationships is essential for their practical application in organic electronic devices. In this work, a dibromo purine-based donor-acceptor π-conjugated comonomer was synthesized and incorporated into the backbone of a conjugated polymer via Stille cross-coupling polymerizations. These polymerizations used distannylated versions of either benzodithiophene, thiophene, or dithienylbenzothiadiazole as the comonomer. The photophysical properties of the resulting conjugated polymers were studied in solution and as thin films to elucidate the effect comonomer type on charge transfer characteristics and morphological behaviors. It was determined that charge transfer character was enhanced by decreasing the electron donating ability of the comonomer, which ultimately led to a novel low bandgap conjugated polymer when dithienylbenzothiadiazole was used as the comonomer. The low bandgap "poly(purine)" has photophysical and electrochemical properties that suit its application as the donor-type polymer in organic photovoltaic devices. Preliminary device performance measurements using the low bandgap poly(purine) were marked by extremely low power conversion efficiencies, which point to a clear need to improve the underlying morphology in order to optimize the device performance. These findings highlight the ability to incorporate purines into low bandgap polymers and provide a foundation for future studies of purine-based conjugated polymers as materials for organic electronic device applications.

4.2 Introduction

Conjugated polymers have been extensively studied because of their applicability in optoelectronic devices, such as organic photovoltaics (OPVs),[36,37,54] organic light-emitting diodes (OLEDs),[56] chemical sensors,[95] and electrochromic devices.[94] The ability to systematically alter the optical properties through polymer design and to utilize solution-based processes in order to manufacture devices makes these systems conceptually attractive and practically important. Tuning the optical properties of conjugated polymers can be accomplished by varying the π-conjugated building blocks[42] comprising the polymer or by manipulating side-chain functionality.[87,107] The donor-acceptor design concept is one approach for manipulating optical properties, and it is widely pursued in efforts to construct new conjugated polymers,[36,42,53] especially conjugated polymers used in OPV devices. The donor-acceptor concept consists of linking electron-rich (donor) and electron-deficient (acceptor) building blocks in an alternating sequence. This alternating donor-acceptor repeat unit sequence creates a copolymer, and this approach has allowed a wide variety of donor and acceptor building blocks to be incorporated in conjugated polymers.[36,53] Even though there have been significant improvements in power conversion efficiency (PCE) of OPV devices, for example, these organic electronic systems still fall short of the efficiency achieved by inorganic counterparts and below the efficiency deemed commercially viable. For this reason, discovering new donor-acceptor building blocks for conjugated polymers and successfully incorporating them into polymer chains through synthesis could improve

optoelectronic properties. Thus, this endeavor is viewed as essential for advancing the field of organic electronics.

Stemming from the ability to synthesize highly fluorescent "push-pull" purine chromophores by functionalizing multiple positions of the fused heterocycle system,[72,73] electroactive purine materials have been studied as blue-ultraviolet emissive layers in OLEDs.[8,9] As the emissive layer in OLEDs, purine-based push-pull systems achieved performance comparable to organic chromophores used in state-of-the-art OLEDs at wavelengths below 450 nm.[8,9] The high performance of purine emitters for OLEDs, along with the ability to synthetically access and specifically functionalize the purine scaffold in order to tune optical properties, sets a clear precedent for studying purine-based chromophores as electro- or photoactive materials in organic electronic applications.

Nucleobases (purine and pyrimidine) also have drawn attention as building blocks in donor-acceptor π-conjugated chromophores.[35] The small molecule chromophores reported by Castellano et al. and the work described in Chapter 3 of this dissertation highlight the ability to use purines as either a donor or as an acceptor π-conjugated building block. Moreover, it is possible to tune absorbance and fluorescence properties, yielding materials exhibiting long excited state lifetimes, high fluorescence quantum yields, and high thermal stability.[35] Furthermore and as highlighted in Chapter 2 of this dissertation, purine-based monomers can be directly incorporated into the backbone of a polymer by Stille cross-coupling reactions.[97] Tunable optoelectronic properties, high thermal stability, and the ability of purinyl monomers to participate in metal-catalyzed

polymerizations, motivated my effort to incorporate purine-based building blocks into π-conjugated donor-acceptor copolymers.

Two drawbacks of the monomers I designed and used in Chapter 2 were the unequal reactivity of the Br-substituted positions of the purinyl monomer and the break in conjugation due to the methylene of the benzyl bromide attached at the N-9 position of the purine.[97] These motivated me to design a dihalo purinyl monomer with equal reactivity at the coupling positions. In addition, I also was motivated to extend work related to the donor-acceptor chromophores reported in Chapter 3 to determine whether the long excited-state lifetimes, high quantum yields, and high thermal stability would be preserved when the small molecule chromophores were used to create conjugated polymers.

Herein, I report the first example purine-based donor-acceptor conjugated polymers. The **P-BDT-P** chromophore described previously in Chapter 3 was chosen as the purine-based building block because it offered the potential to synthesize a dibromo monomer with equal reactivities, and also because it displayed intramolecular charge-transfer characteristics, long excited state lifetime, and high thermal stability. **P-BDT-P** was polymerized using distannylated versions of either BDT, Th, or BT, yielding a new class of purine-based conjugated polymers. The photophysical properties of the conjugated poly(purine)s in solution and as thin films were investigated to provide insight into how molecular design and comonomer selection affects the optoelectronic properties. The conjugated poly(purine)s were incorporated as the donor-type polymer in OPV devices and preliminary device performance data is presented.

4.3 Experimental

4.3.1 Materials and Methods

All chemicals and solvents were purchased from Sigma-Aldrich or Fisher Scientific and used without purification unless noted otherwise. 2,6-bis(trimethylstannyl)-4,8-bis(2-ethylhexyloxy)benzo[1,2-*b*:4,5-*b*′]dithiophene was purchased from Solarmer Energy Inc. and used without further purification. Tetrakistriphenylphosphine palladium (0) ($Pd(PPh_3)_4$) was purchased from Strem Chemicals and used without purification. [6,6]-Phenyl-C_{61}-butyric acid methyl ester (PCBM) was purchased from Sigma-Aldrich and was used without purification. Toluene was purified using an Innovative Technologies MD-5 Solvent Purification System and the solvent was degassed prior to use. All materials were synthesized using standard Schlenk line techniques under an argon atmosphere and purified via column chromatography using 60 Å silica gel (230-400 mesh size). 4,7-dithienyl-2,1,3-benzothiadiazole and 4,7-bis(5-(trimethylstannyl)thiophene-2-yl)-2,1,3-benzothiadiazole were synthesized according to previously reported procedures.[35,99] (Dithienylbenzothiadiazole will be abbreviated BT in this chapter for simplicity.)

^{13}C and ^{1}H NMR spectra (of synthesized monomers and polymers) were obtained using a Varian VNMRS 500 MHz NMR at room temperature using $CDCl_3$ as the solvent. Chemical shifts are reported in ppm and referenced to the residual solvent peak. Mass spectral analyses were performed with a Bruker microflex Matrix-assisted-laser-desorption-ionization time-of-flight (MALDI-TOF) mass spectrometer. The matrix compound was trans-2-[3-(4-tert-butylphenyl)-2-methyl-2-propenylidene]malononitrile.

Polymer molecular weights reported in this chapter are relative to polystyrene standards and were measured using a Tosoh EcoSEC SEC system operating at 40 °C using tetrahydrofuran (THF) as the mobile phase. Concentrations of injected polymer solutions were nominally 1 mg/mL in THF. The thermal stability of the poly(purine)s was determined via thermogravimetric analysis (TGA) using platinum pans in an inert atmosphere of N_2 or Ar. These experiments utilized a TA Instruments Discovery thermogravimetric analyzer. A temperature scan consisting of a ramp from room temperature to 800 °C at a heating rate of 10 °C/min was used. Thermal transitions were measured with differential scanning calorimetry (DSC) using a TA instruments Q-2000 DSC. A protocol of a heat-cool-heat cycle from 0 °C to 270 °C at a heating rate of 10 °C/min. Optical absorbance spectra of poly(purine)s in solution were obtained via UV-Vis spectroscopy with an Agilent Cary 5000 UV-Vis-NIR spectrophotometer. Spectra were acquired by scanning from 325-750 nm using 0.01 mg/mL solutions of poly(purine)s in chloroform ($CHCl_3$). Optical absorbance spectra of poly(purine)s as thin films were obtained via UV-Vis spectroscopy with a Agilent Cary 5000 UV-Vis-NIR spectrophotometer. These spectra also were acquired by scanning from 325-750 nm. Glass slides were prepared prior to use by immersing them for 30 min. in a boiling "piranha acid" solution (3:1 v/v H_2SO_4/30% H_2O_2). After cleaning, the slides were rinsed thoroughly with deionized water and dried under a stream of nitrogen (N_2). *Caution! Piranha acid is a strong oxidizer and strong acid; therefore it should be handled with extreme care as it reacts violently with organics.* Films were made by spin-coating 5 mg/mL solutions of poly(purine)s in chloroform onto a glass slide. Steady-state

photoluminescence of poly(purine)s in solutions was measured with a Perkin Elmer LS-55 fluorescence spectrophotometer using 0.0025 mg/mL of the poly(purine)s in $CHCl_3$. Fluorescence spectra of poly(purine) thin films deposited on glass slides from 5 mg/mL $CHCl_3$ solutions were acquired using a Jobin Yvon-Spex Fluorolog instrument. Time resolved photoluminescence profiles were measured with Jobin Yvon-Spex Fluorolog equipped with 389 nm diode laser using 0.0025 mg/mL poly(purine) in $CHCl_3$. Redox potentials were measured via cyclic voltammetry (CV) using a CH Instruments potentiostat. For these measurements, 3 mg/mL solutions were created by dissolving 10 mg of each purine polymer in 3 mL of dichloromethane (DCM). This solution also contained tetrabutylammonium hexafluorophosphate ($(n\text{Bu})_4\text{NPF}_6$) at 0.2 M as the supporting electrolyte. The cell used an Ag/AgCl reference electrode, a gold working electrode, and a tungsten counter electrode and a scan rate of 100 $\text{mV}\cdot\text{s}^{-1}$ was used. All potentials are referenced to a ferrocene-ferrocenium redox couple.

4.3.2 Organic Photovoltaic Device Fabrication

Patterned tin-doped indium oxide (ITO) electrodes with a resistance of ~18-20 Ω sq^{-1} were purchased from Ossila Limited and cleaned prior to use. Cleaning procedures involved consecutive sonication of ITO electrodes for 30 min. in 0.2 M sodium hydroxide (NaOH) solution, acetone, and isopropyl alcohol. After each sonication cycle, electrodes were rinsed thoroughly with Milli-Q water. Following the final Milli-Q water rinse, the electrodes were dried under a stream of N_2 gas and placed in an ozone cleaner for 30 min. poly(3,4-ethylenedioxythiophene)-poly(styrenesulfonate) (PEDOT:PSS) was filtered through a 0.2 μM filter and subsequently deposited onto a clean ITO electrode via

spin-coating. Active layer solutions were prepared at 1:1 by mass of poly(purine):PCBM in anhydrous chlorobenzene. The solutions were heated and stirred overnight at 50 °C in a N_2 filled glovebox. The polymer:PCBM active layer was deposited using spin-coat deposition in a N_2 filled glovebox followed by aluminum (Al) contact (100 nm) deposition under vacuum (10^{-6} mbar). The final device architecture was [ITO/PEDOT:PSS/Poly(purine):PCBM)/Al]. Illumination was provided by a Newport 300 W xenon lamp with an AM 1.5 solar spectrum filter calibrated with a Si photodiode to produce an illumination of 100 mW cm^{-2} of AM 1.5 G illumination (1 sun illumination).

4.3.3 Synthesis of Dibromo-P-BDT-P (Br_2PBDTP)

Degassed THF (1 mL) was added to an oven-dried round bottom flask filled to have an inert atmosphere (Ar). The flask had previously been equipped with a Teflon stir bar and the flask was cooled to -78 °C using a dry ice/acetone bath. Lithium diisoproplyamide (LDA) was then added dropwise at -78 °C with an oven-dried and Ar flushed syringe. In a separate round bottom flask, **P-BDT-P** (108.5 mg, 0.119 mmole) was dissolved in THF (2 mL) under Ar. The **P-BDT-P** solution was subsequently added dropwise at -78 °C to the LDA solution via cannula, and then the resulting reaction mixture was stirred at -78 °C for 3 h. In a third round bottom flask, a solution of 1,2-dibromotetrachloroethane ($BrCCl_2CCl_2Br$, 85.25 mg, 0.261 mmole) was dissolved in degassed THF (1 mL). After 3 h, the $BrCCl_2CCl_2Br$ solution was added dropwise at -78 °C to the solution containing **P-BDT-P**.

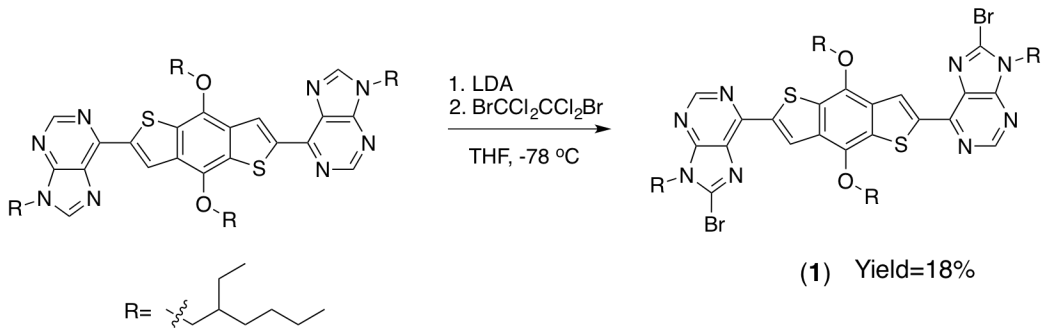

Scheme 4.1. Synthesis of Br_2PBDTP.

The resulting solution was stirred for 3 h at -78 °C. After that time had elapsed, saturated aqueous solution of ammonium chloride (NH_4Cl) was added. The mixture was warmed to room temperature and extracted three times with DCM. The combined organic layers were dried with $MgSO_4$, filtered, and then concentrated via rotary evaporation. The recovered product was purified via column chromatography using a mobile phase of 10:1 (v/v) hexanes:ethyl acetate to obtain Br_2PBDTP in yields of 18%. (See Scheme 4.1.) ^{1}H NMR (500 MHz, $CDCl_3$), δ (ppm): 0.88 (t), 0.95 (m), 1.13 (t), 1.24-1.64 (m), 1.72 (m), 1.84 (m), 1.94 (m), 2.14 (m) 4.19-4.22 (m), 4.33-4.42 (m), 8.93 (s, 2H, purine H), 9.22 (s, 2H, BDT H). ^{13}C NMR (500 MHz, $CDCl_3$), δ (ppm): 10.54, 11.45, 13.97, 14.20, 22.91, 23.73, 23.90, 28.37, 29.28, 30.33, 30.48, 39.17, 40.71, 48.54, 62.72, 127.45, 130.04, 130.57, 133.76, 134.19, 139.91, 145.96, 148.52, 152.36, 153.50, 165.25. MALDI-TOF: calc'd [M+H$^+$]: 1062.35, found [M+H$^+$]: 1062.98.

4.3.4 General Polymerization Procedure

Dibromopurine monomer **1** (1 equiv., 0.0359 mmole), the distannyl monomer (1 equiv, 0.0359 mmole), and 5 mol % $Pd(PPh_3)_4$ were combined in a round bottom flask

equipped with a Teflon stir bar. The atmosphere was rendered inert via 3 evacuation/backfill cycles using Ar. Degassed toluene (2 mL) was added via syringe and the resulting mixture was placed in an oil bath set to 110 °C. After stirring for 48 h, the reaction flask was removed from the oil bath and allowed to cool to room temperature. Then, the reaction mixture was precipitated into copious amounts of methanol (MeOH). The precipitate was filtered into a Soxhlet thimble and washed with subsequent MeOH and acetone washes. The final polymer was extracted from the Soxhlet thimble using $CHCl_3$ and concentrated via rotary evaporation. The polymer was finally isolated by freeze-drying.

PPBDTPBDT: Orange solid. M_n=7,700 g/mol, M_w=9,300 g/mol, M_w/M_n=1.2, and Yield=8%. ^{1}H NMR (500 MHz, $CDCl_3$), δ (ppm): 0.68-1.01, 1.02-1.14, 1.16-1.50, 1.51-1.81, 1.85-2.01, 2.17, 4.20-4.54, 4.58-4.68, 8.09-8.17, 8.99-9.05, 9.36-9.41.

PPBDTPTh: Orange solid. M_n=3,700 g/mol, M_w=4,100 g/mol, M_w/M_n=1.1, and Yield=12%. ^{1}H NMR (500 MHz, $CDCl_3$), δ (ppm): 0.68-1.01, 1.02-1.14, 1.16-1.50, 1.51-1.81, 1.85-2.01, 2.17, 4.20-4.54, 4.58-4.68, 7.87-7.99, 8.84-9.05, 9.16-9.41.

PPBDTPBT: Purple solid. M_n=4,4000 g/mol, M_w=9,700 g/mol, M_w/M_n=2.2, and Yield=21%. ^{1}H NMR (500 MHz, $CDCl_3$), δ (ppm): 0.68-1.01, 1.02-2.25, 3.95-4.64, 7.36-8.36, 8.67-9.17

4.4 Results and Discussion

As shown in Scheme 4.1, **P-BDT-P** described in Chapter 3 was chosen to become the dibromo commoner because of the charge transfer character, long excited-state lifetime, and ease of synthesis and purification. Bromination at the 8,8'-positions was attempted using n-bromosucciminde (NBS), but there was no evidence of the dibromo purine monomer being formed. Therefore, bromine functionality was introduced at 8,8'-positions following a procedure described by Gundersen and coworkers.[108] This procedure includes treating **P-BDT-P** with lithium diisopropylamide (LDA) and quenching the lithiated purines with a bromine electrophile ($BrCCl_2CCl_2Br$) to form **Br_2PBDTP**, as shown in Scheme 4.1. **Br_2PBDTP** was purified by column chromatography and isolated yields were low due difficulty separating **Br_2PBDTP** from products resulting from multiple side reactions, such as dimerization and bromination at positions other than the 8,8'-positions of the purine units.

Stille cross-coupling polymerizations were performed by combining **Br_2PBDTP** and one of the distannyl comonomers in a 1:1 ratio, and $Pd(PPh_3)_4$ (5 mol %) in toluene. The reaction mixture was heated at 110 °C for 48 h. After stirring for 48 h, the reaction mixture was precipitated into MeOH and was purified with a series of Soxhlet washes using MeOH and then acetone. The final polymer was extracted with $CHCl_3$ and isolated in low yields. **PPBDTPBDT** corresponds to using BDT as the distannylated comonomer, **PPBDTPTh** corresponds to using Th, and **PPBDTPBT** uses BT. (See Linker in Figure 4.2.)

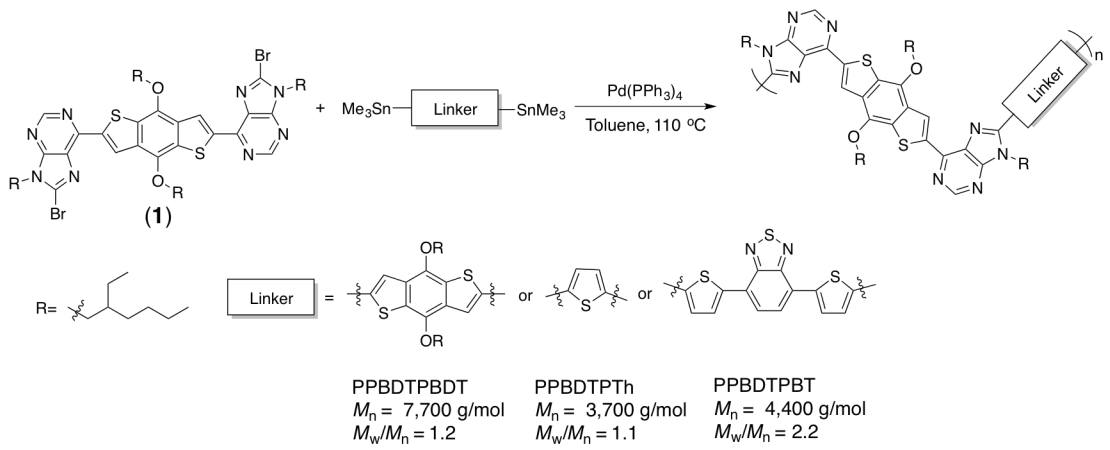

Scheme 4.2 Synthesis of conjugated poly(purine)s via Stille cross-coupling polymerizations.

The molecular weights of the resulting polymers were low, ostensibly due to electron richness of the **Br_2PBDTP** monomer, which decreases the efficiency of the oxidative addition step of the catalyst cycle, which was discussed in Chapter 1, and to a monomer that cannot be sufficiently purified for polymerizations. It is worth noting that polymerizations using the benzothiadiazole comonomer seemed to be very efficient. This was supported by a lack of **Br_2PBDTP** in the methanol and acetone washes, which indicates that **Br_2PBDTP** was fully consumed during the cross-coupling polymerization. Furthermore, after extracting with chloroform there was a significant amount of insoluble purple material remaining in the Soxhlet thimble. Based on the SEC results presented as Figure C.6 this insoluble materials is believed to be high molecular weight **PPBDTPBT**. In the chromatogram for **PPBDTPBT**, there is a shoulder at a retention time of ~7.75 min. and this shoulder corresponds to an M_n = 9,000 g/mol. The SEC results and a

presence of insoluble material in the thimble indicate that high molecular weight poly(purine)s might be obtained if the solubility of the **PPBDTPBT** copolymer were improved.

Given the extensive use of conjugated polymers in organic electronics and the importance of thermal annealing during processing, the thermal properties of conjugated poly(purine)s were investigated. The thermal stability was measured via TGA by determining the degradation behavior. As shown in Figure 4.1, the three polymers exhibited degradation temperatures ranging from 265 °C to 290 °C. The thermal stability of the conjugated poly(purine)s decreased compared to "Generation 1" poly(purine)s described in Chapter 2,[97] and the small molecule model compounds presented in Chapter 3 of this dissertation. The degradation temperatures are similar to other BDT-based copolymers, which suggests that they are acceptable for organic electronic applications.[109,110]

Thermal transitions of the fully conjugated poly(purine)s were also investigated with DSC. As illustrated in Figure 4.2, the three polymers do not exhibit thermal transitions below 270 °C. This is mainly due to the semicrystalline nature of the conjugated poly(purine)s, which is facilitated by increased π-π interactions. This finding is consistent with previously reported behaviors resulting from thermal investigations of BDT-based copolymers.[111,112]

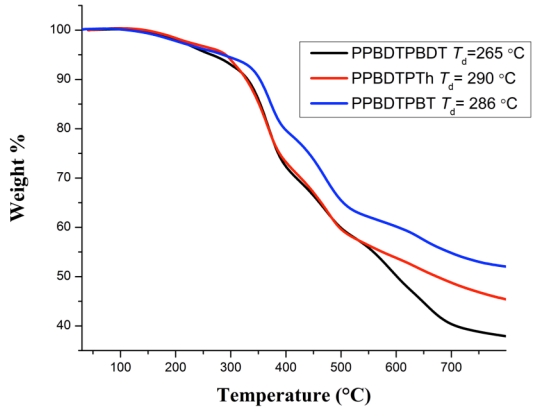

Figure 4.1. Thermal stability of **PPBDTPBDT**, **PPBDTPTh**, and **PPBDTPBT** polymers measured using TGA (25 °C to 800 °C).

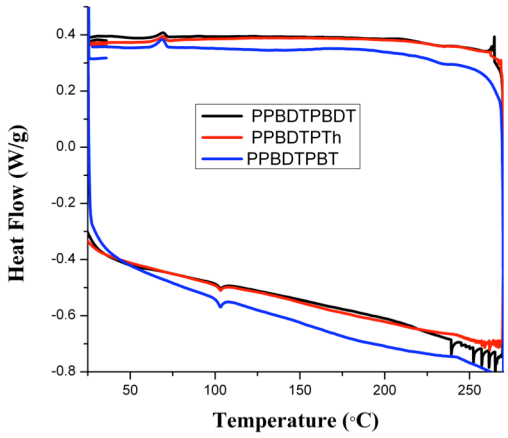

Figure 4.2 DSC traces for **PPBDTPBDT**, **PPBDTPTh**, and **PPBDTPBT** on the second heating cycle.

Due to the widespread use of conjugated polymers in optoelectronic devices such as OPVs, the absorbance transitions of the poly(purine)s were investigated by UV-Vis spectroscopy. As shown in Figure 4.3(a) and tabulated in Table 4.1, the three polymers exhibit absorbance transitions at ~400 nm, which correspond to the π-π* transitions. The π-π* transitions of the three polymers are red-shifted by ~60 nm compared to the Generation 1 poly(purine)s and the model chromophores described in Chapter 3 of this dissertation. This red-shift is indicative of an extended conjugated length in comparison to Generation 1 poly(purine)s and the small-molecule chromophores. The transitions at longer wavelengths in Figure 4.3(a) correspond to ICT due to the donor-acceptor nature of the polymers. **PPBDTPBT** absorbs further in the red region of the visible spectrum due to the donor-acceptor design concept narrowing the optical bandgap. The onset of absorbance of **PPBDTPBT** in chloroform is 614 nm, and this corresponds to an optical bandgap of 2.0 eV. **PPBDTPBDT** and **PPBDTPTh** possess similar absorbance profiles, but onsets of absorbance are at ~545 nm. The onset of absorbance at 545 nm for **PPBDTPBDT** and **PPBDTPTh** corresponds to an optical bandgap of 2.3 eV (in chloroform).

Because BDT is extensively used as a building block in conjugated polymers for optoelectronic devices such as OPVs,[113] the effect of introducing purines into the conjugated backbone on the optical properties can be compared to analogous conjugated BDT-based homo and copolymers.

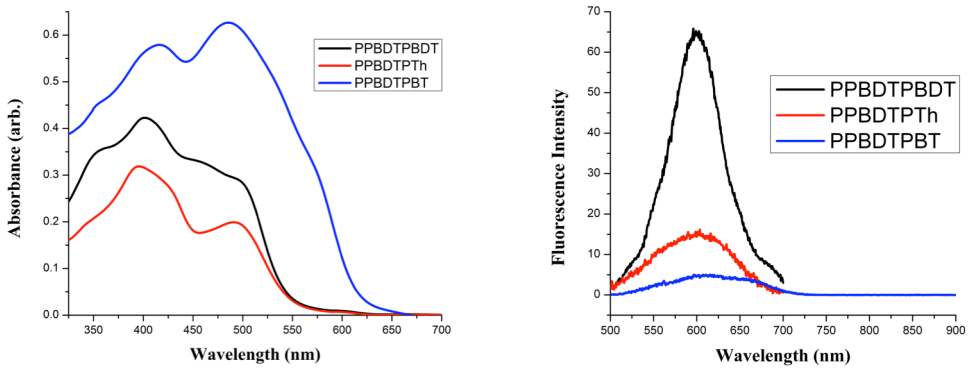

(a) (b)

Figure 4.3. (a) UV-Vis and (b) photoluminescence spectra of conjugated poly(purine)s in chloroform.

When comparing **PPBDTPBDT** to homo-BDT polymers (see Figure 4.4 for comparison of chemical structures), the π-π* transition of **PPBDTPBDT** is blue-shifted: BDT homopolymers (without purines in the backbone) exhibit π-π* transitions around ~500 nm.[109,114] The onset absorbance (λ_{onset}^{abs}) in chloroform of ~545 nm for **PPBDTPBDT** is slightly blue-shifted compared to BDT homopolymers chloroform (λ_{onset}^{abs} = 560 nm), which gives **PPBDTPBDT** a slightly larger optical bandgap (**PPBDTPBDT** E_{gap} = 2.3 eV, homo-BDT E_{gap} = 2.2 eV).[109] This indicates the purine disrupts the "electronic communication" between BDT repeat units along the conjugated backbone.

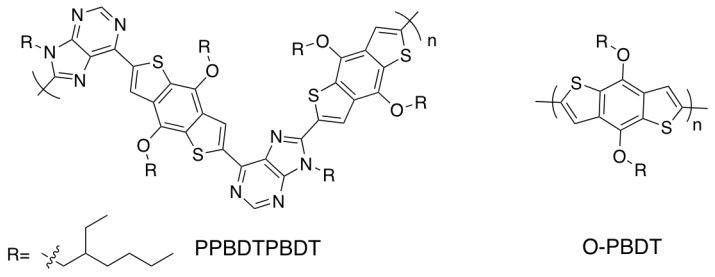

Figure 4.4. Chemical structures of **PPBDTPBDT** and O-PBDT. Absorbance onsets of the two polymers are 545 nm (poly(purine)) and O-PBDT 560 nm, Reference 112.

Incorporating a purine unit in the conjugated backbone of BDT-based copolymers when thiophene is used as the comonomer has similar effects as when purines are incorporated in BDT homopolymers in that the electronic communication is disrupted between BDT and Th units. **PPBDTPTh** exhibits an λ_{onset}^{abs} = 545 nm in chloroform, which is ~30 nm blue-shifted compared to BDTT (structure presented in Figure 4.5).[115] However, incorporating a purine in the polymer increases the CT character of the purine-based copolymers due the decrease of electron-donating ability of the thiophene comonomer compared to BDT. The increase CT character is evident by the more well-defined CT band in the absorbance spectra of **PPBDTPTh** compared to **PPBDTPBDT** in Figure 4.3(a). **PPBDTPTh** also exhibits more CT character than BDTT as BDTT exhibits a broad featureless absorbance profile.[115]

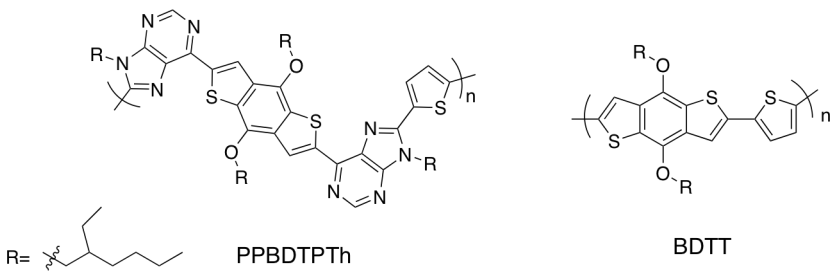

Figure 4.5. Chemical structures of **PPBDTPTh** and BDTT. Absorbance onsets of the two polymers are 545 nm (poly(purine)) and BDTT ~575 nm, Reference 115.

Introducing purines into BDT-based copolymers that use benzothiadiazole as the comonomer (BDT-BT based copolymers) has conflicting effects compared to the relationship between **PPBDTPBDT**, **PPBDTPTh**, and BDT homopolymers. When comparing **PPBDTPBT** to BDT-BT copolymers, the extent of electronic disruption, or enhancement of electronic communication, is dependent on substitution patterns of the BT comonomer. For example, when BDT is coupled with "DTBT", which has hexyl chains at the 3-position of the thiophene units straddling the benzothiadiazole (polymer Z3 in Figure 4.6), the polymer displays an λ_{onset}^{abs} < 600 nm absorbance.[110] Thus in comparison, **PPBDTPBT**, which has an λ_{onset}^{abs} = 614 nm, has a greater extent of electronic communication across the conjugated backbone.

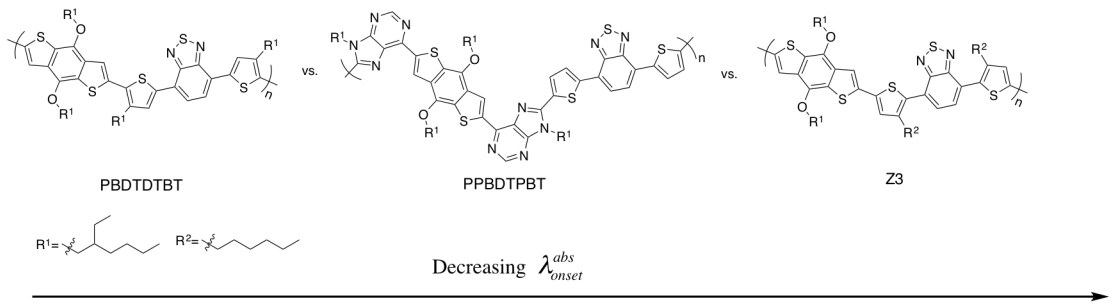

Figure 4.6. Chemical structures of **PPBDTPBT**, PBDTDTBT from Reference 114, and polymer Z3 from Reference 113 highlight the dependence of thiophene substitution on the onset of absorbance.

However, with ethylhexyl chains at the 4-position of the thiophene units of the PBDTDTBT copolymer (see Figure 4.6), the absorbance onset of my **PPBDTPBT** copolymer is blue shifted (λ_{onset}^{abs} = 614 nm) compared to the absorbance onset of the PBDTDTBT copolymer (λ_{onset}^{abs} = ~675 nm) without a purine unit.[116] Because substitution pattern of alkyl chains on the thiophene rings does impact photophysical tunability, it is important to investigate how optical properties of low bandgap conjugated poly(purine)s are affected by substitution patterns. These lines of inquiry are anticipated to be helpful efforts to develop poly(purine)s for optoelectronic applications and understand how molecular-level design impacts photophysical properties.

Fluorescence spectroscopy was performed to measure the photoluminescent properties of the conjugated poly(purine)s in solution. **PPBDTPBDT** and **PPBDTPTh** exhibit fluorescence maximums ($\lambda_{\max}^{em}$) at ~600 nm while **PPBDTPBT** shows a $\lambda_{\max}^{em}$ =

623 nm. (See Figure 4.3(b) and Table 4.1.) Each polymer exhibits a broad featureless emission profile and a large Stokes shift, which is consistent with ICT. As highlighted in Table 4.1 the Stokes shift of the purine-containing polymers increases as the electron donating ability of the comonomer decreases. Specifically, the Stokes shift is 106 nm for **PPBDTPBDT** and 110 nm for **PPBDTPTh** and 138 nm **PPBDTPBT**. The larger Stokes shift for PPBDTPBT is due to an increase in ICT character, brought on by using the strong electron-acceptor benzothiadiazole in the donor-acceptor design concept.

The fluorescence intensity also decreases upon changing the stannyl comonomer: **PPBDTPBDT** had the greatest fluorescent intensity, but the fluorescence intensity was greatly diminished for **PPBDTPTh** and almost nonexistent for **PPBDTPBT**. This indicates shorter excited state lifetimes of the singlet excited state with the less electron-donating comonomers.[117]

Table 4.1. UV-Vis and photoluminescence properties of conjugated poly(purine)s in chloroform solutions.

Polymer	λ_{max}^{abs}	λ_{max}^{em}	Stokes Shift (nm)[a]	λ_{onset}^{abs}	E_{gap} (eV) Optical
PPBDTPBDT	400, 497	600	106	545	2.3
PPBDTPTh	396,492	602	110	545	2.3
PPBDTPBT	415, 485	623	138	614	2.0

[a]Stokes shifts were calculated between the absorbance and fluorescence maximums.

To confirm this inference, the excited state dynamics of the conjugated poly(purine)s also were studied to investigate how the choice of comonomer affected the excited state lifetime. As seen in Figure 4.7, **PPBDTPBT** exhibits the longest excited state lifetime (3.24 ns), followed by **PPBDTPTh** (1.80 ns), and finally **PPBDTPBT** (1.49 ns). The excited state decay profiles for **PPBDTPBDT** and **PPBDTPTh** are well-described by a double exponential fit, while **PPBDTPBT** is well described with a triple exponential fit. Following the same trend of poly(purine) fluorescence intensity, going from electron-donating to electron-accepting comonomers, led to drastic decreases in the excited state lifetime (BDT > Th > BT). The need to use multiple exponential functions to fit the decay profiles indicates that there are multiple relaxation pathways. An increase in the number of radiative relaxation pathways gives rise to an increase in the number of nonradiative relaxation pathways in the conjugated polymers.

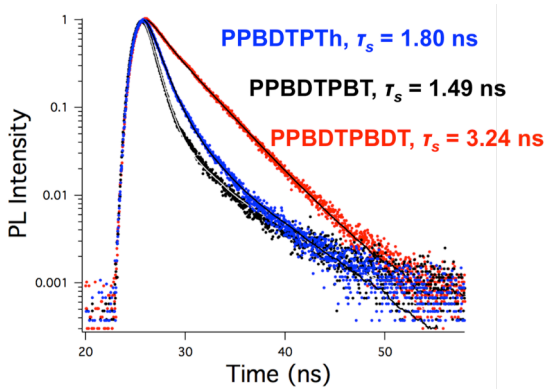

Figure 4.7. Time-resolved photoluminescence profiles of **PPBDTPBDT** (3.24 ns), **PPBDTPTh** (1.80 ns), and **PPBDTPBT** (1.49 ns) in $CHCl_3$.

This increase in nonradiative relaxation pathways is one reason for the significant decrease in excited state lifetimes and fluorescence intensity compared to the small molecules chromophores (described in Chapter 3) that are used as the polymer building block.

To probe the photophysical properties of the conjugated polymers in the solid state, the conjugated poly(purine)s were cast into films and the absorbance and fluorescence spectra were measured via UV-Vis and fluorescence spectroscopies, respectively, and these spectra are shown in Figure 4.8. As shown in Figure 4.9, which compares solution and thin film behaviors, the λ_{onset}^{abs} of the poly(purine)s is red-shifted as thin films compared to solution.

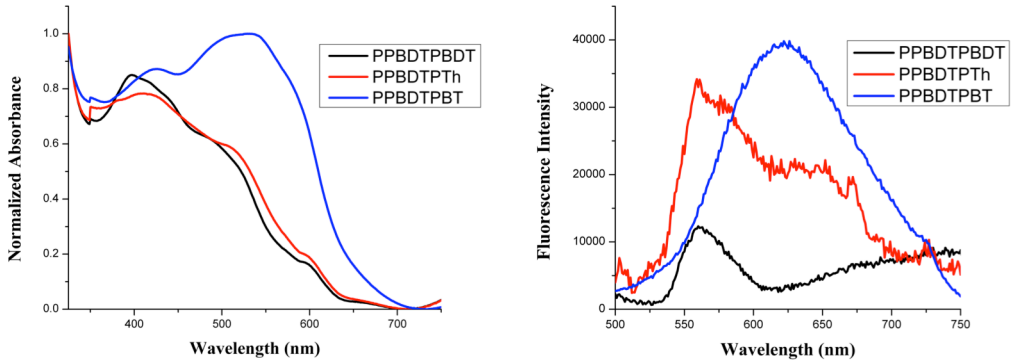

(a) (b)

Figure 4.8. (a) UV-Vis and (b) photoluminescence spectra of **PPBDTPBDT**, **PPBDTPTh**, and **PPBDTPBT** thin films made by spin-coating from chloroform solutions of 5 mg/mL.

This is attributed to an increase in π-π interactions in the solid state.[110,116] The absorbance spectra of **PPBDTPBDT** and **PPBDTPTh** each show the formation of shoulders aside the main absorbance peak at λ ≈ 430 nm. The shoulders at longer wavelengths are indicative of enhanced organization and interactions between aggregates in the solid state that leads to new transitions, similar to P3HT.[118,119]

To investigate the effect purine repeat units have on ordering of BDT-based copolymers in the solid state, the absorbance spectrum of **PPBDTPBDT** is compared to that of O-PBDT (structure shown in Figure 4.4). Lee et al. showed that when O-PBDT was cast as a thin film, the absorbance profile did not change drastically compared to the spectra recorded for O-PBDT in chloroform. Most notably the absorbance onset of O-PBDT as thin film was consistent with the absorbance onset measured for a solution.[109] The fact there was no change in the absorbance onset suggests that there are negligible interchain interactions driving the organization of O-PBDT. Given that films of **PPBDTPBDT** exhibit an 85 nm red-shift in the onset absorbance and form a shoulder at ~600 nm indicates that there is an increase of interchain interactions in the solid state for **PPBDTPBDT** compared to O-PBDT. The increase in interchain interactions could lead to higher hole mobility for **PPBDTPBDT** compared to O-PBDT, which would be beneficial for charge extraction in organic electronic devices and increase the fill-factor (*FF*) in OPV devices.[110]

Table 4.2. Absorbance onset data for conjugated poly(purine)s in solution and as thin films.

polymer	Soln. λ_{onset}^{abs} (nm)	Film λ_{onset}^{abs} (nm)	$\Delta\lambda_{onset}^{abs}$ (nm)
PPBDTPBDT	545	630	85
PPBDTPTh	545	636	91
PPBDTPBT	614	685	71

PPBDTPTh and BDTT (the structure of which is shown in Figure 4.5) both exhibit a red shift in their absorbance spectra as thin films compared to solution spectra. Based on the absorbance onsets, **PPBDTPTh** has a slightly smaller optical bandgap (1.9 eV) compared to BDTT (2.08 eV).[115] The larger red shift of the absorbance onset of **PPBDTPTh** ($\Delta\lambda_{onset}^{abs}$ = 91 nm) compared to BDTT ($\Delta\lambda_{onset}^{abs} \approx$ 50 nm) is due to increased π-π interactions in the solid state compared to BDTT. This is analogous to the absorbance behaviors of **PPBDTPBT** compared to O-PBDT, which highlights the conclusion that incorporating purines into the backbone of a conjugated polymer increases π-π interactions and subsequently enhances the ordering and organization of the polymers in thin films.

The absorbance spectrum of **PPBDTPBT** as a thin film is compared to analogous studies of PBDTDTBT and Z3. Both PBDTDTBT and Z3 exhibit distinct changes in the UV-Vis spectra of thin films compared to in solution.[110,116] PBDTDTBT exhibits a red shift of the absorbance onset of ~40 nm[116] while Z3 exhibits a ~51 nm red shift.[110] Similarly, **PPBDTPBT** exhibits a ~71 nm red shift of the absorbance onset when going from solution to the solid state. This pattern of behavior is attributed to the conjugated

polymers adopting a more planar geometry in the solid state, which is brought on by an increase of π-π interactions. The larger red shift of the absorbance onset observed for **PPBDTPBT** suggests **PPBDTPBT** has greater interchain interactions and is more planar in the solid state than PBDTDTBT and Z3. The enhancement in interchain interactions in **PPBDTPBT** compared to PBDTDTBT and Z3 may be attributed to the unsubstituted thiophenes in the BT comonomer. Also, as evident from UV-Vis studies of **PPBDTPBDT** and **PPBDTPTh** in thin films, introduction of a purine into the polymer backbone increases π-π interactions and manipulates the ordering of poly(purine)s in the solid state. Also, it would be anticipated that **PPBDTPBT** has a higher degree of crystallinity in the solid state compared to PBDTDTBT and Z3.[116]

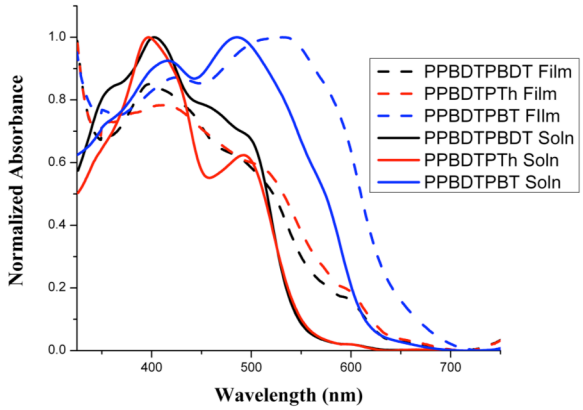

Figure 4.9. Comparison of normalized UV-Vis spectra of conjugated poly(purine)s in chloroform and as thin films.

The photoluminescence behavior of the poly(purine) films were also investigated to gain additional insight into the intermolecular interactions of poly(purine) chains in the solid state and these spectra are presented in Figure 4.8(b). **PPBDTPBDT** and **PPBDTPTh** exhibit substantial differences in their fluorescence profiles of thin films compared to solution. Most notably, **PPBDTPBDT** and **PPBDTPTh** both exhibit blue shifts in their fluorescence profiles as thin films compared to solution, which is accompanied with a 45 nm blue-shift of the emission maximum. The blue shift of the emission profile indicates that the radiative emission profile is of higher energy (shorter wavelength) than isolated polymer chains dissolved in chloroform. The disappearance of the emission peak from solution ($\lambda_{\max}^{em}$ = 600 nm) suggests the formation of H-aggregates in the solid state for **PPBDTPBDT** and **PPBDTPTh** because the fluorescence process of H-aggregates is inefficient.[120] On the other hand, **PPBDTPBT** exhibits a broad featureless emission profile in the solid state (Figure 4.8(b)), while the fluorescence was nearly non-existent in solution (Figure 4.3(b)).

Table 4.3. Photophysical properties of conjugated poly(purine)s as thin films.

Polymer	$\lambda_{\max}^{abs}$	$\lambda_{\max}^{em}$	Stokes Shift (nm)	λ_{onset}^{abs}	E_{gap} (eV) Optical
PPBDTPBDT	394, 490, 598	559	69	630	1.9
PPBDTPTh	412, 512, 600	559 (broad)	47	636	1.9
PPBDTPBT	424, 531	623	92	685	1.8

The fluorescence results for **PPBDTPBDT**, **PPBDTPTh**, and **PPBDTBT** as thin films are due to increased interchain interactions in thin films, and most likely the formation of aggregates since aggregation leads to drastic changes in photophysical properties.[121] Further studies of the conjugated poly(purine)s, such as grazing-incident wide-angle X-ray scattering (GIWAXS), are needed to quantify the amount of aggregates and orientation in thin films.

The favorable optical properties of **PPBDTPBT** suggests that it would be compelling to test their performance in organic electronic devices in order to assess whether incorporating a purine into a polymer backbone enhances device performance. To determine the viability of using **PPBDTPBT** as the donor polymer in an OPV device, the oxidation and reduction potentials of **PPBDTPBT** were measured by cyclic voltammetry. As introduced in Chapter 3, oxidation and reduction potentials are used to calculate the HOMO and LUMO levels according to Equation 3.1 and Equation 3.2, respectively.

$$E_{HOMO}(eV) = -(E_{onsext}^{ox} + 5.1)eV \tag{3.1}$$

$$E_{LUMO}(eV) = -(E_{onset}^{red} + 5.1)eV \tag{3.2}$$

PPBDTPBT exhibits an E_{onsext}^{ox} = 0.10 V and an E_{onset}^{red} = -1.52 V, which corresponds to an E_{HOMO} of -5.20 eV and a E_{LUMO}= -3.58 eV. The HOMO of **PPBDTPBT** (-5.20 eV) is similar to the HOMO of PBDTDTBT (-5.24 eV) but the LUMO is slightly higher (-3.58 eV) for **PPBDTPBT** than for PBDTDTBT (-3.71 eV).[116] This indicates that **PPBDTPBT** has a slightly larger energy bandgap compared to PBDTDTBT. (See Figure 4.6 for structure of PBDTDTBT.) The larger bandgap of

PPBDTPBT (compared to PBDTDTBT) is in consistent with the UV-Vis results described above. The difference between the LUMO of **PPBDTPBT** and the LUMO of the commonly-used electron acceptor PCBM (0.62 eV) is large enough to overcome the ~0.3 eV coulombic binding energy of an exciton, which means that **PPBDTPBT** can facilitate charge separation at the donor/acceptor interfaces within OPV devices.[64] Another noteworthy feature of the energy levels of **PPBDTPBT** is the 1.0 eV difference between the HOMO of **PPBDTPBT** and the LUMO of PCBM. The difference between the HOMO of the donor polymer and the LUMO of an electron acceptor is correlated to the open-circuit voltage of an OPV device,[122] and the electrochemical results point toward **PPBDTPBT** generating high a V_{OC} in OPV devices.

Table 4.4. Oxidation and reduction potentials measure with cyclic voltammetry and the resulting HOMO and LUMO levels for **PPBDTPBT**.

polymer	E_{onsext}^{ox} [a]	E_{onset}^{red} [a]	HOMO (eV)[b]	LUMO (eV)[b]
PPBDTPBT	0.10	-1.52	-5.20	-3.58

[a]Electrochemical potentials are referenced to the Fc/Fc^+ redox couple.
[b]HOMO and LUMO levels are calculated assuming the Fc/Fc^+ redox couple is 5.1 eV relative to vacuum.

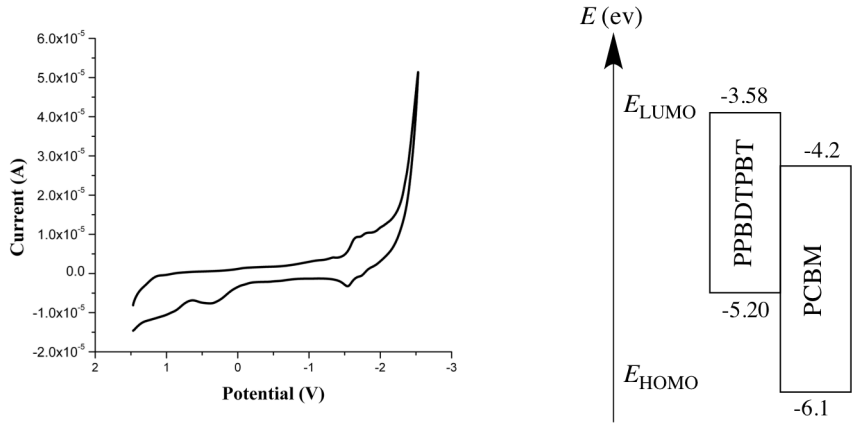

(a) (b)

Figure 4.10. (a) Cyclic voltammetry trace of **PPBDTPBT** in DCM illustrating redox behavior with potentials reported relative to the Fc/Fc^+ redox couple and (b) HOMO and LUMO levels of **PPBDTPBT** calculated from oxidation and reduction potentials measured with cyclic voltammetry and HOMO and LUMO levels of PCBM from Reference 112.

Given that **PPBDTPBT** exhibits absorbance and energy level alignment relative to PCBM that make it suitable for use as the donor-type polymer in OPV devices, some preliminary devices were made and tested in the lab of Professor Michael Walter at the University of North Carolina at Charlotte. Device architectures of ITO/PEDOT:PSS/**PPBDTPBT**:PCBM/Al were constructed and the results are presented in Figure 4.11 and Table 4.5. The most noteworthy feature of the preliminary device performance measurements is the open-circuit voltage (V_{OC}). Both sets of devices (one tested as-cast and the other annealed at 50 °C for 15 minutes) that are highlighted in this

dissertation had (average) V_{OC}'s commonly achieved for BDT-based copolymers.[113] More specifically, the BDT-BT copolymers discussed earlier (and whose structures are represented in Figure 4.5), have similar V_{OC}'s.[110,116] This is a sign that the E_{HOMO} level for **PPBDTPBT** determined from CV measurements is accurate and **PPBDTPBT**'s HOMO is significantly deeper than the LUMO of PCBM.

Overall, the OPV devices demonstrated low device performance – the short-circuit current density (J_{SC}), fill-factor (*FF*), and efficiency (η) were low, as highlighted in Table 4.5. It is likely that the J_{SC} of OPV devices incorporating **PPBDTPBT** as the donor-type polymer was low due to low absorbance of photons in the visible region.[53] The *FF* was low because charges that are generated are not being efficiently extracted, which therefore creates a large series resistance in the device.[53] The large series resistance is most likely due to an unfavorable morphology that leads to inefficient charge separation at donor-acceptor interfaces and charge transport through the bulk of the device.

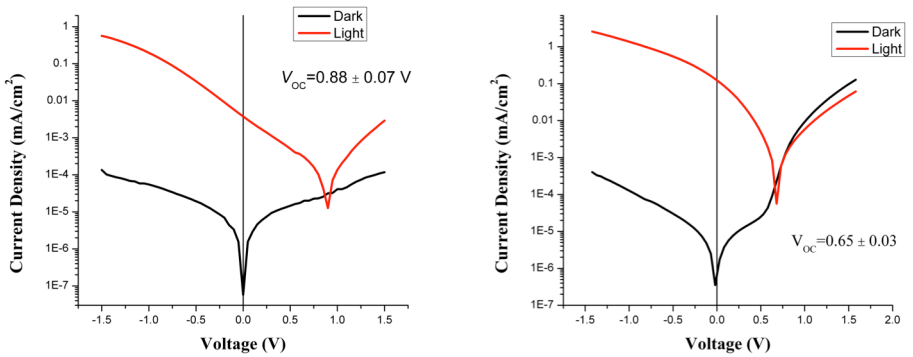

(a) (b)

Figure 4.11. Current density versus voltage plots of **PPBDTPBT**:PCBM OPV devices (a) with no thermal annealing and (b) after annealing at 50 °C for 15 minutes.

Table 4.5. Data for OPV devices made using **PPBDTPBT** as the donor-type polymer.

Annealing Temp. (°C)	V_{OC} (V)	J_{SC} (mA/cm^2)	*FF*	η (%)
N/A	0.88±0.08	0.005±0.003	0.13±0.05	0.0005±0.0003
50 °C	0.65±0.03	0.11±0.03	0.13±0.02	0.009±0.005

Furthermore, both J_{SC} and *FF* have been shown to be dependent on molecular weight of conjugated polymers.[50] Considering the molecular weight of **PPBDTPBT** is low, the device performance of **PPBDTPBT** could remain inefficient unless higher molecular weight poly(purine)s can be synthesized. Another factor that could be contributing to low J_{SC} and *FF* values is low hole-mobility of **PPBDTPBT**, brought on either by polymer design or an unfavorable morphology. A large number of additional studies are needed to confirm these hypotheses, such as constructing hole- and electron-only devices to measure the mobilities of **PPBDTPBT**. Another factor that may be contributing to the low OPV device performance is the short excited-state lifetime. As highlighted earlier and presented in Figure 4.7, **PPBDTPBT** had the shortest excited state lifetime in solution. The short lifetime most likely leads to intrachain quenching of excited states instead of electron transfer from **PPBDTPBT** to the acceptor PCBM.[117]

UV-Vis spectroscopy was used to measure the absorbance of **PPBDTPBT**:PCBM blends, and the spectra of as-cast and annealed blends are shown in Figure 4.12. First, the absorbance of **PPBDTPBT**/PCBM composite films decreases significantly in comparison to pure **PPBDTPBT** films. Specifically, the onset absorbance is blue-shifted by ~50 nm, which indicates that blending **PPBDTPBT** with PCBM disrupts the π-π interactions between poly(purine) chains in the solid state. To circumvent this problem, **PPBDTPBT** based copolymers with different functionalities (at the N-9 position of the purines, thiophene side-chains, etc.) can be synthesized to increase interchain interactions in the solid state, or the PCBM loading level can be varied.

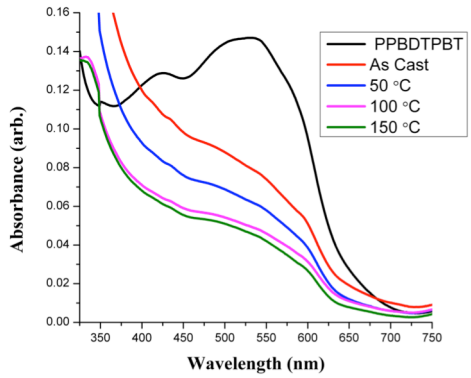

Figure 4.12. UV-Vis spectra of **PPBDTPBT** as a film and films made by blending **PPBDTPBT** and PCBM at 1:1 by mass. As indicated by the legend, spectra were obtained for as cast blends and blends annealed at 50 °C, 100 °C, and 150 °C.

The low absorbance of films made of **PPBDTPBT**:PCBM blends is consistent with the low J_{SC} because there are not enough photons being absorbed. Secondly, the absorbance profile is not affected by thermal annealing at 50 °C, 100 °C, or 150 °C. This is expected considering that no thermal transitions were observed below 270 °C, and it suggests that the resulting device morphology would be thermally stable.[112] Because of this, differences in the V_{OC} values (see Table 4.5) are attributed to films having different but unoptimized morphologies.

4.5 Conclusions

The plethora of synthetic transformations purines can participate in has led to the synthesis of a new dibromopurinyl monomer (**Br_2PBDTP**) that can be polymerized via Stille cross-coupling polymerizations to form conjugated poly(purine)s. While all

polymers isolated were of modest molecular weight, this study highlights the ability to manipulate photophysical properties of purine-based conjugated polymers through choice of the comonomer. Specifically, donor-acceptor purine-based conjugated polymers constructed with BDT and Th comonomers exhibit medium bandgaps, but the **PPBDTPBT**, which was synthesized using the strong acceptor benzothiadiazole has an optical bandgap of 2.0 eV in solution and 1.8 eV in a thin film. **PPBDTPBT** possesses photophysical and electrochemical properties that make it an attractive donor-type polymer suitable for OPV devices. Furthermore, preliminary OPV device performance indicate the possibility that **PPBDTPBT**-containing devices can possess high V_{OC}'s, but dedicated efforts are needed to optimize processing conditions optimize the active layer morphology. In combination with exploring donor/acceptor ratio, these efforts are anticipated to increase the J_{SC} and FF of devices. In addition, the low device performance also is affected by the short excited state lifetime of **PPBDTPBT**. All of these contribute to poor charge separation at donor-acceptor interfaces and poor transport to respective electrodes. Nevertheless, this work provides proof-of-concept and serves to motivate future studies of conjugated poly(purine)s for optoelectronic applications. By taking advantage of myriad synthetic transformations of the purine scaffold to alter the design of purine building blocks and the opportunity to choose different comonomers suggests that poly(purine)s are worth pursuing as materials for organic electronic devices.

CHAPTER 5
SUMMARY, FUTURE WORK, AND CONCLUSIONS

5.1 Summary

Linking monomer design to polymeric properties is crucial for developing polymer systems with desired attributes that suit them for targeted applications. The work I described in this dissertation provides baseline synthesis-structure-property relationships for purine-based copolymers and donor-acceptor molecular materials. The synthesis and structure-property relationships described herein will be useful for future endeavors to incorporate purines into polymeric materials and guide their application in organic electronic devices. The first accomplishment I described is the first example of purine-based comonomers being incorporated into a polymer backbone through Stille cross-coupling polymerizations. While polymerizations were hindered by low reactivity of one of the purine comonomer coupling sites, my work demonstrated that thermal and photophysical properties of the resulting purine-based copolymers can be impactfully manipulated based on 1) the side-chain functionalization of the comonomer and 2) the substitution pattern of the purinyl comonomer. This first accomplishment is also noteworthy because of the plethora of synthetic transformations by which purine can be manipulated.

Secondly, I investigated the role a purine plays in donor-acceptor small-molecule chromophores. I discovered purines act as a weak-acceptor when coupled with an electron rich π-conjugated linker, but as a weak donor when coupled with an electron-deficient π-conjugated linker. Furthermore, in these systems, when a purine is coupled through the 6-position and acts as an acceptor in the donor-acceptor chromophores, the excited state lifetime is nearly twice as long as compared to when the purine plays the

role of the donor in chromophores that are coupled through either the 6-position or the 8-position. The work I presented highlights that purines can be incorporated into donor-acceptor π-conjugated systems, and their resulting thermal and optoelectronic properties can be systematically tuned. This work is impactful because developing conjugated building blocks with tailored photophysical properties is crucial for developing π-conjugated materials for applications in organic electronics.

Finally, I presented the first example of fully conjugated donor-acceptor copolymers containing a purine repeat unit. This was accomplished through Stille cross-coupling polymerizations of purine chromophores with electron-rich or electron-deficient comonomers. While the molecular weight of the copolymers remained low, this new class of conjugated polymer exhibits photophysical tunability that depends on comonomer selection, and (*vide infra*) I expect additional functionalization of the purine can further expand copolymer properties. In the work I presented, a low bandgap polymer with photophysical and electrochemical properties suitable for organic electronic devices was synthesized by coupling an electron-deficient benzothiadiazole comonomer with the purine-based comonomer. This low bandgap poly(purine) was incorporated into an OPV device, and although the device performance was low due to the short excited state lifetime of the polymer and an undesirable active layer morphology, the open-circuit voltages obtained are highly encouraging. These results support the broader ideas that incorporating purine building blocks into conjugated polymers is attractive and functionally useful.

The largest hurdle remaining for advancement of poly(purine)s is addressing the reactivity of coupling sites on purine monomers. In the "Generation 1" poly(purine)s described in Chapter 2, the unequal reactivity of the halogens hindered polymerizations. In the "Generation 2" poly(purine)s described in Chapter 4, the design of the monomer rendered the comonomer more electron-rich which hindered its use in Stille cross-coupling polymerizations. In addition, purification of Generation 2 monomers could be simplified by adjusting the N-9 solubilizing group. Specifically, it may be useful to use linear alkyl chains or benzyl halides to protect the N-9, or to use preparatory thin-layer chromatography. Another fruitful pursuit would be to synthesize a diiodo purine monomer to see if higher molecular weight poly(purine)s result from the increased reactivity in Stille cross-coupling. It may also be the case that purines are not suitable as halogen coupling partners for polymerizations. For this reason, it may be beneficial to synthesize distannyl functionalized purine-based comonomers and run polymerization screenings with these analogues.

5.2 Future Work

The work I have described in this dissertation provides precedence for continuing to study purine-based materials as polymer and small-molecule systems for optoelectronic properties. As highlighted in Figure 5.1, there are four readily synthetically accessible positions of the purine heterocycle. (In my work I have used three of the four positions for various reasons.)

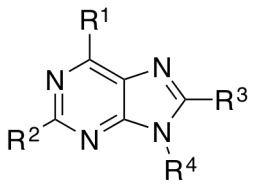

R^1 = Efficient cross-coupling center or H-Bonding site
R^2 = Cross-coupling center or Optoelectronic tunability or H-Bonding site
R^3 = Cross-coupling center or Optoelectronic tunability
R^4 = Solubilizing handle or Photo cross-linking functionalities

Figure 5.1. The different sites of the purine scaffold highlight the tailorability at four distinct positions around the fused-ring heterocycle system.

The ability to react at these positions allows purines to participate in metal-mediated cross-coupling reactions, provides the opportunity to introduce electron-donating or electron-accepting moieties for tuning optoelectronic properties, and enables introduction of solubilizing groups or other dynamic functionality that manipulate physical properties of the resulting materials. Given the wealth of synthetic transformations that can be applied to purines and the potential vast number of properties, there is a clear need to explore structure-property relationships of purine-based polymers and chromophores for advanced optoelectronic materials. I will now briefly describe what I believe are key areas that deserve focus for exploring purine-based materials.

5.2.1 Purines as Monomer Building Blocks for π-Conjugated Polymers

By showing that low bandgap conjugated polymers can be synthesized with purines in the polymer backbone, it becomes compelling to design a copolymer with an increased excited state lifetime and that adopts a more favorable morphology in an active layer blend. To accomplish this, different N-9 solubilizing groups on the purine monomer or solubilizing side-chains on the BDT linker can be investigated. (See Figure 5.2(a).) As

highlighted in Chapter 2, varying the functionality at these positions changes both thermal and photophysical properties. Therefore, different side-chains are expected to alter thermal and photophysical properties compared to the copolymers I described in Chapter 4, and these changes could improve the optoelectronic properties of the conjugated polymers. In addition, it is possible to change the design of the acceptor comonomer to increase solubility and tune optoelectronic properties by introducing solubilizing chains on the thiophene units of the electron-acceptor. (See Figure 5.2(b).) As discussed in Chapter 4, the substitution pattern on the thiophene units is another "handle" by which optoelectronic properties can be manipulated.

The second approach involves designing π-purine-π monomers (instead of the purine-π-purine monomers described in this dissertation) to couple with conjugated building blocks (such as BDT, Th, or BT) in Stille or Suzuki cross-coupling polymerizations.

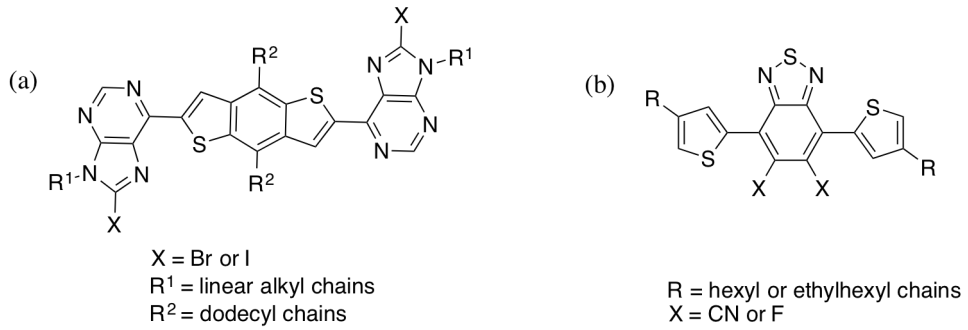

Figure 5.2. (a) Variations on the PBDTP building block and (b) variations of the benzothiadiazole acceptor monomer that are known to affect optoelectronic properties and active layer morphology.

The most facile approach stems from the initial studies of Stille cross-couplings with 2,6-dichloropurine. As shown in Figure 5.3, this would involve synthesizing a 2,6-dithienylpurine monomer that can be either halogenated or stannylated and used as a coupling partner in Stille cross-coupling polymerizations. As highlighted above, it will be necessary to investigate the role of solubilizing chains on solid-state morphology and optoelectronic properties. This idea of using π-purine-π building blocks extends findings from my dissertation work and allows additional insights of how the substitution pattern around the purine chromophore affects polymerizability, polymer characteristics, and the thermal and photophysical properties.

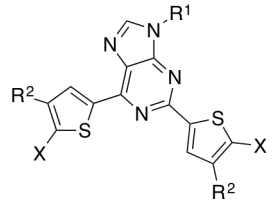

X = Br or $SnMe_3$
R^1 = linear or branched alkyl chains
R^2 = liner or branched alkyl chains

Figure 5.3. A representative 2,6-dithienylpurine monomer that can offer halogenation or stannylation functionality for cross-coupling polymerizations, as well as solubilizing chains on the thiophene heterocycles or at the N-9 position of the purine.

5.2.2 Purines in Small-Molecule π-Conjugated Systems

Through the research efforts described in my dissertation, I have highlighted the ability to manipulate the optoelectronic properties of small-molecule purine-based chromophores. The structure-property relationships motivate efforts to expand the library of donor-acceptor chromophores. These materials may be used to more fully understand how purines can be incorporated into functional small-molecule materials. Figure 5.4 highlights various donor and acceptor building blocks that can be used to more broadly investigate structure-property relationships of purine-based chromophores.

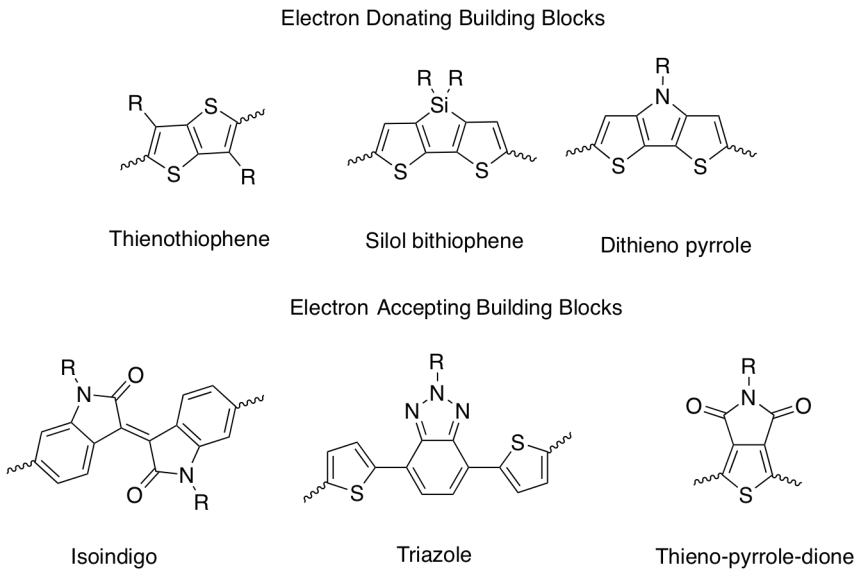

Figure 5.4. Various electron-donating and electron-accepting building blocks commonly found in conjugated polymers used for optoelectronic devices. These may be useful for developing structure-property relationships of purine-based chromophores.

From this set of materials, a library of structure-property relationships can be established. Ultimately, these will provide guidance for synthesizing purine-based conjugated materials with targeted properties suitable for optoelectronic applications.

As an approach to "fine-tune" the optoelectronic properties of the purine-based donor-acceptor chromophores, electron-donating and electron-accepting can be incorporated at multiple positions around the purine-heterocycle. (See Figure 5.1.) Investigating the effects of varying the electron-donating or electron-accepting substitution on the purine heterocycle while varying either the donor or the acceptor bridging units would yield a library of purine-based donor-acceptor chromophores with optoelectronic tunability. Having access to a synthetically diverse purine-based chromophore library and understanding the subsequent structure-property relationships will allow realization of the usefulness of purines in optoelectronic applications.

Finally, motivated by the integral role of purines in daily life as a building block of the DNA helix, hydrogen-bonding motifs of purine-based chromophores can be exploited as a means to control self-assembly of π-conjugated systems. As highlighted in Figure 5.1, purines have multiple positions that participate in H-bonding or that allow motifs to be added around the heterocyclic system. Many previous studies have found that adding H-bonding motifs to purines is a useful way to manipulate self-assembly processes in functional polymers and molecules. Studying purine-based chromophores with H-bonding motifs built into the chromophore would provide insight into how H-bonding functionalities are beneficial for optoelectronic applications. Using nucleobase chromophores with H-bonding motifs could provide a new "handle" by which issues of

morphology facing applications of conjugated polymers in organic electronic devices can be addressed.

5.3. Conclusion

Overall, this work has built the foundation for structure-property relationships of purine-based copolymers and chromophores that is necessary for continuing to study purines as building blocks for polymeric materials. Through the research described in my dissertation, I have demonstrated the ability to introduce diverse functionalities to the purine scaffold that led to distinct changes in thermal, photophysical, and electrochemical properties. My initial hypothesis was confirmed, specifically, that the tailorability provided by the purine scaffold leads to diverse polymeric and molecular properties of purine-based polymers and chromophores. My work has opened the doorway for further investigations of purine design-structure-property relationships for advanced functional materials.

REFERENCES

(1) Legraverend, M.; Grierson, D. S. The Purines: Potent and Versatile Small Molecule Inhibitors and Modulators of Key Biological Targets. *Bioorg. Med. Chem.* **2006**, *14*, 3987-4006.

(2) Rosemeyer, H. The Chemodiversity of Purine as a Constituent of Natural Products. *Chem. Biodivers.* **2004**, *1*, 361-401.

(3) Montgomery, J. A.; Hewson, K. Analogs of 6-methyl-9.beta.-D-ribofuranosylpurine. *J. Med. Chem.* **1968**, *11*, 48-52.

(4) Sagi, G.; Otvos, L.; Ikeda, S.; Andrei, G.; Snoeck, R.; De Clercq, E. Synthesis and Antiviral Activities of 8-Alkynyl-, 8-Alkenyl-, and 8-Alkyl-2'-deoxyadenosine Analogs. *J. Med. Chem.* **1994**, *37*, 1307-1311.

(5) Anderson, T. R.; Frihart, C. R.; Leonard, N. J.; Schmitz, R. Y.; Skoog, F. Cytokinins with Different Connecting Links Between Purine and Isopentenyl or Benzyl Groups. *Phytochemistry* **1975**, *14*, 1687-1690.

(6) Legraverend, M. Recent Advances in the Synthesis of Purine Derivatives and Their Precursors. *Tetrahedron* **2008**, *64*, 8585-8603.

(7) Venkatesh, V.; Shukla, A.; Sivakumar, S.; Verma, S. Purine-Stabilized Green Fluorescent Gold Nanoclusters for Cell Nuclei Imaging Applications. *ACS App. Mater. Interfaces* **2014**, *6*, 2185-2191.

(8) Yang, Y.; Cohn, P.; Eom, S.-H.; Abboud, K. A.; Castellano, R. K.; Xue, J. Ultraviolet-Violet Electroluminescence from Highly Fluorescent Purines. *J. Mater. Chem. C* **2013**, *1*, 2867-2874.

(9) Yang, Y.; Cohn, P.; Dyer, A. L.; Eom, S.-H.; Reynolds, J. R.; Castellano, R. K.; Xue, J. Blue-Violet Electroluminescence from a Highly Fluorescent Purine. *Chem. Mater.* **2010**, *22*, 3580-3582.

(10) Berti, L.; Burley, G. A. Nucleic Acid and Nucleotide-Mediated Synthesis of Inorganic Nanoparticles. *Nat. Nano.* **2008**, *3*, 81-87.

(11) Kumar, A.; Kumar, V. Biotemplated Inorganic Nanostructures: Supramolecular Directed Nanosystems of Semiconductor(s)/Metal(s) Mediated by Nucleic Acids and Their Properties. *Chem. Rev.* **2014**, *114*, 7044-7078.

(12) McHale, R.; O'Reilly, R. K. Nucleobase Containing Synthetic Polymers: Advancing Biomimicry via Controlled Synthesis and Self-Assembly. *Macromolecules* **2012**, *45*, 7665-7675.

(13) Sivakova, S.; Rowan, S. J. Nucleobases as Supramolecular Motifs. *Chem. Soc. Rev.* **2005**, *34*, 9-21.

(14) Fathalla, M.; Lawrence, C. M.; Zhang, N.; Sessler, J. L.; Jayawickramarajah, J. Base-Pairing Mediated Non-Covalent Polymers. *Chem. Soc. Rev.* **2009**, *38*, 1608-1620.

(15) Sessler, J. L.; Lawrence, C. M.; Jayawickramarajah, J. Molecular Recognition via Base-Pairing. *Chem. Soc. Rev.* **2007**, *36*, 314-325.

(16) Sessler, J. L.; Sathiosatham, M.; Brown, C. T.; Rhodes, T. A.; Wiederrecht, G. Hydrogen-Bond-Mediated Photoinduced Electron-Transfer: Novel Dimethylaniline−Anthracene Ensembles Formed via Watson−Crick Base-Pairing. *J. Am. Chem. Soc.* **2001**, *123*, 3655-3660.

(17) Lo, P. K.; Sleiman, H. F. Nucleobase-Templated Polymerization: Copying the Chain Length and Polydispersity of Living Polymers into Conjugated Polymers. *J. Am. Chem. Soc.* **2009**, *131*, 4182-4183.

(18) Kang, Y.; Lu, A.; Ellington, A.; Jewett, M. C.; O'Reilly, R. K. Effect of Complementary Nucleobase Interactions on the Copolymer Composition of RAFT Copolymerizations. *ACS Macro Lett.* **2013**, *2*, 581-586.

(19) Cheng, S.; Zhang, M.; Dixit, N.; Moore, R. B.; Long, T. E. Nucleobase Self-Assembly in Supramolecular Adhesives. *Macromolecules* **2012**, *45*, 805-812.

(20) Spijker, H. J.; Dirks, A. J.; van Hest, J. C. M. Synthesis and Assembly Behavior of Nucleobase-Functionalized Block Copolymers. *J. Polym. Sci. A Polym. Chem.* **2006**, *44*, 4242-4250.

(21) Lutz, J.-F.; Thünemann, A. F.; Nehring, R. Preparation by Controlled Radical Polymerization and Self-Assembly via Base-Recognition of Synthetic Polymers Bearing Complementary Nucleobases. *J. Polym. Sci. A Polym. Chem.* **2005**, *43*, 4805-4818.

(22) Spijker, H. J.; van Delft, F. L.; van Hest, J. C. M. Atom Transfer Radical Polymerization of Adenine, Thymine, Cytosine, and Guanine Nucleobase Monomers. *Macromolecules* **2007**, *40*, 12-18.

(23) Bazzi, H. S.; Sleiman, H. F. Adenine-Containing Block Copolymers via Ring-Opening Metathesis Polymerization: Synthesis and Self-Assembly into Rod Morphologies. *Macromolecules* **2002**, *35*, 9617-9620.

(24) Cheng, C.-C.; Chang, F.-C.; Ko, F.-H.; Yu, F.-C.; Lin, Y.-T.; Shieh, Y.-T.; Chen, J.-K.; Lee, D.-J. Supramolecular Polymeric Micelles as High Performance Electrochemical Materials. *J. Mater. Chem. C* **2015**, *3*, 9528-9533.

(25) Cheng, C.-C.; Chu, Y.-L.; Chang, F.-C.; Lee, D.-J.; Yen, Y.-C.; Chen, J.-K.; Chu, C.-W.; Xin, Z. New Bioinspired Hole Injection/Transport Materials for Highly Efficient Solution-Processed Phosphorescent Organic Light-Emitting Diodes. *Nano Energy* **2015**, *13*, 1-8.

(26) Zhang, K.; Aiba, M.; Fahs, G. B.; Hudson, A. G.; Chiang, W. D.; Moore, R. B.; Ueda, M.; Long, T. E. Nucleobase-Functionalized Acrylic ABA Triblock Copolymers and Supramolecular Blends. *Polym. Chem.* **2015**, *6*, 2434-2444.

(27) Agrofoglio, L. A.; Gillaizeau, I.; Saito, Y. Palladium-Assisted Routes to Nucleosides. *Chem. Rev.* **2003**, *103*, 1875-1916.

(28) Slagt, V. F.; de Vries, A. H. M.; de Vries, J. G.; Kellogg, R. M. Practical Aspects of Carbon−Carbon Cross-Coupling Reactions Using Heteroarenes. *Org. Process. Res. Dev.* **2009**, *14*, 30-47.

(29) Langli, G.; Gundersen, L.-L.; Rise, F. Regiochemistry in Stille Couplings of 2,6-Dihalopurines. *Tetrahedron* **1996**, *52*, 5625-5638.

(30) Jens. M J. Nolsoe; Lise-Lotte Gunderson; Rise, F. Regiochemistry in the Pd-Mediated Coupling between 6,8-Dihalopurines and Organometallic Reagents. *Acta. Chemica. Scand.* **1999**, *53*, 366-372.

(31) Hocek, M. Syntheses of Purines Bearing Carbon Substituents in Positions 2, 6, or 8 by Metal- or Organometal-Mediated C−C Bond-Forming Reactions. *Eur. J. Org. Chem.* **2003**, 245-254.

(32) Gundersen, L.-L. 6-Chloropurines and Organostannanes in Palladium Catalyzed Cross Coupling Reactions. *Tetrahedron Lett.* **1994**, *35*, 3155-3158.

(33) Gundersen, L.-L.; Kristin Bakkestuen, A.; Jørgen Aasen, A.; Øver»s, H.; Rise, F. 6-Halopurines in Palladium-Catalyzed Coupling with Organotin and Organozinc Reagents. *Tetrahedron* **1994**, *50*, 9743-9756.

(34) Havelková, M.; Dvořák, D.; Hocek, M. The Suzuki-Miyaura Cross-Coupling Reactions of 2-, 6- or 8-Halopurines with Boronic Acids Leading to 2-, 6- or 8-Aryl- and -Alkenylpurine Derivatives. *Synthesis* **2001**, 1704-1710.

(35) Bou Zerdan, R.; Cohn, P.; Puodziukynaite, E.; Baker, M. B.; Voisin, M.; Sarun, C.; Castellano, R. K. Synthesis, Optical Properties, and Electronic Structures of Nucleobase-Containing π-Conjugated Oligomers. *J. Org. Chem.* **2015**, *80*, 1828-1840.

(36) Lu, L.; Zheng, T.; Wu, Q.; Schneider, A. M.; Zhao, D.; Yu, L. Recent Advances in Bulk Heterojunction Polymer Solar Cells. *Chem. Rev.* **2015**, *115*, 12666-12731.

(37) Facchetti, A. π-Conjugated Polymers for Organic Electronics and Photovoltaic Cell Applications. *Chem. Mater.* **2011**, *23*, 733-758.

(38) Carsten, B.; He, F.; Son, H. J.; Xu, T.; Yu, L. Stille Polycondensation for Synthesis of Functional Materials. *Chem. Rev.* **2011**, *111*, 1493-1528.

(39) Bao, Z.; Chan, W. K.; Yu, L. Exploration of the Stille Coupling Reaction for the Synthesis of Functional Polymers. *J. Am. Chem. Soc.* **1995**, *117*, 12426-12435.

(40) Bao, Z.; Chan, W.; Yu, L. Synthesis of Conjugated Polymer by the Stille Coupling Reaction. *Chem. Mater.* **1993**, *5*, 2-3.

(41) Liang, Y.; Yu, L. A New Class of Semiconducting Polymers for Bulk Heterojunction Solar Cells with Exceptionally High Performance. *Acc. Chem. Res.* **2010**, *43*, 1227-1236.

(42) Li, W.; You, W.: CHAPTER 15 Donor-Acceptor Alternating Copolymers. In *Conjugated Polymers: A Practical Guide to Synthesis*; The Royal Society of Chemistry, 2014; pp 319-342.

(43) Miyaura, N.; Suzuki, A. Palladium-Catalyzed Cross-Coupling Reactions of Organoboron Compounds. *Chem. Rev.* **1995**, *95*, 2457-2483.

(44) Stille, J. K. Step-growth polymerization. *J. Chem. Educ.* **1981**, *58*, 862.

(45) Odian, G.: *Principles of Polymerization*; 4th ed.; Wiley, 2004.

(46) Galbrecht, F.; Bünnagel, T. W.; Scherf, U.; Farrell, T. Microwave-Assisted Preparation of Semiconducting Polymers. *Macromol. Rapid. Commun.* **2007**, *28*, 387-394.

(47) Tierney, S.; Heeney, M.; McCulloch, I. Microwave-Assisted Synthesis of Polythiophenes via the Stille Coupling. *Synthetic Metals* **2005**, *148*, 195-198.

(48) Nehls, B. S.; Asawapirom, U.; Füldner, S.; Preis, E.; Farrell, T.; Scherf, U. Semiconducting Polymers via Microwave-Assisted Suzuki and Stille Cross-Coupling Reactions. *Adv. Funct. Mater.* **2004**, *14*, 352-356.

(49) Coffin, R. C.; Peet, J.; Rogers, J.; Bazan, G. C. Streamlined Microwave-Assisted Preparation of Narrow-Bandgap Conjugated Polymers for High-Performance Bulk Heterojunction Solar Cells. *Nat. Chem.* **2009**, *1*, 657-661.

(50) Li, W.; Yang, L.; Tumbleston, J. R.; Yan, L.; Ade, H.; You, W. Controlling Molecular Weight of a High Efficiency Donor-Acceptor Conjugated Polymer and Understanding Its Significant Impact on Photovoltaic Properties. *Adv. Mater.* **2014**, *26*, 4456-4462.

(51) Lu, W.; Sengupta, S.; Petersen, J. L.; Akhmedov, N. G.; Shi, X. Mitsunobu Coupling of Nucleobases and Alcohols: An Efficient, Practical Synthesis for Novel Nonsugar Carbon Nucleosides. *J. Org. Chem.* **2007**, *72*, 5012-5015.

(52) Gray, N. S.; Kwon, S.; Schultz, P. G. Combinatorial Synthesis of 2,9-Substituted Purines. *Tetrahedron Lett.* **1997**, *38*, 1161-1164.

(53) Zhou, H.; Yang, L.; You, W. Rational Design of High Performance Conjugated Polymers for Organic Solar Cells. *Macromolecules* **2012**, *45*, 607-632.

(54) Heeger, A. J. 25th Anniversary Article: Bulk Heterojunction Solar Cells: Understanding the Mechanism of Operation. *Adv. Mater.* **2014**, *26*, 10-28.

(55) Mazzio, K. A.; Luscombe, C. K. The Future of Organic Photovoltaics. *Chem. Soc. Rev.* **2015**, *44*, 78-90.

(56) Thejo Kalyani, N.; Dhoble, S. J. Organic Light Emitting Diodes: Energy Saving Lighting Technology—A Review. *Renew. Sust. Energ. Rev.* **2012**, *16*, 2696-2723.

(57) Sirringhaus, H. 25th Anniversary Article: Organic Field-Effect Transistors: The Path Beyond Amorphous Silicon. *Adv. Mater.* **2014**, *26*, 1319-1335.

(58) Carsten, B.; Szarko, J. M.; Son, H. J.; Wang, W.; Lu, L.; He, F.; Rolczynski, B. S.; Lou, S. J.; Chen, L. X.; Yu, L. Examining the Effect of the Dipole Moment on Charge Separation in Donor–Acceptor Polymers for Organic Photovoltaic Applications. *J. Am. Chem. Soc.* **2011**, *133*, 20468-20475.

(59) Carsten, B.; Szarko, J. M.; Lu, L.; Son, H. J.; He, F.; Botros, Y. Y.; Chen, L. X.; Yu, L. Mediating Solar Cell Performance by Controlling the Internal Dipole Change in Organic Photovoltaic Polymers. *Macromolecules* **2012**, *45*, 6390-6395.

(60) Ha, J. S.; Kim, K. H.; Choi, D. H. 2,5-Bis(2-octyldodecyl)pyrrolo[3,4-c]pyrrole-1,4-(2H,5H)-dione-Based Donor–Acceptor Alternating Copolymer Bearing 5,5′-Di(thiophen-2-yl)-2,2′-biselenophene Exhibiting 1.5 cm2·V–1·s–1 Hole Mobility in Thin-Film Transistors. *J. Am. Chem. Soc.* **2011**, *133*, 10364-10367.

(61) Tsao, H. N.; Cho, D. M.; Park, I.; Hansen, M. R.; Mavrinskiy, A.; Yoon, D. Y.; Graf, R.; Pisula, W.; Spiess, H. W.; Müllen, K. Ultrahigh Mobility in Polymer Field-Effect Transistors by Design. *J. Am. Chem. Soc.* **2011**, *133*, 2605-2612.

(62) Li, Y.; Singh, S. P.; Sonar, P. A High Mobility P-Type DPP-Thieno[3,2-b]thiophene Copolymer for Organic Thin-Film Transistors. *Adv. Mater.* **2010**, *22*, 4862-4866.

(63) Zhou, H.; Yang, L.; Stoneking, S.; You, W. A Weak Donor−Strong Acceptor Strategy to Design Ideal Polymers for Organic Solar Cells. *ACS App. Mater. & Interfaces* **2010**, *2*, 1377-1383.

(64) Clarke, T. M.; Durrant, J. R. Charge Photogeneration in Organic Solar Cells. *Chem. Rev.* **2010**, *110*, 6736-6767.

(65) Lakowicz, J. R.: *Principles of Fluorescence Spectroscopy*; 3rd ed.; Springer US, 2006.

(66) Dimitrov, S.; Schroeder, B.; Nielsen, C.; Bronstein, H.; Fei, Z.; McCulloch, I.; Heeney, M.; Durrant, J. Singlet Exciton Lifetimes in Conjugated Polymer Films for Organic Solar Cells. *Polymers* **2016**, *8*, 14.

(67) Osaheni, J. A.; Jenekhe, S. A. Electroactive and Photoactive Rod-Coil Copolymers: Design, Synthesis, and Supramolecular Regulation of Photophysical Properties. *J. Am. Chem. Soc.* **1995**, *117*, 7389-7398.

(68) Dang, M. T.; Hirsch, L.; Wantz, G. P3HT:PCBM, Best Seller in Polymer Photovoltaic Research. *Adv. Mater.* **2011**, *23*, 3597-3602.

(69) Son, S. Y.; Kim, Y.; Lee, J.; Lee, G.-Y.; Park, W.-T.; Noh, Y.-Y.; Park, C. E.; Park, T. High-Field-Effect Mobility of Low-Crystallinity Conjugated Polymers with Localized Aggregates. *J. Am. Chem. Soc.* **2016**, *138*, 8096-8103.

(70) Spano, F. C.; Silva, C. H- and J-Aggregate Behavior in Polymeric Semiconductors. *Annu. Rev. Phys. Chem.* **2014**, *65*, 477-500.

(71) Yang, J.-S.; Swager, T. M. Porous Shape Persistent Fluorescent Polymer Films: An Approach to TNT Sensory Materials. *J. Am. Chem. Soc.* **1998**, *120*, 5321-5322.

(72) Butler, R. S.; Myers, A. K.; Bellarmine, P.; Abboud, K. A.; Castellano, R. K. Highly Fluorescent Donor-Acceptor Purines. *J. Mater. Chem.* **2007**, *17*, 1863-1865.

(73) Butler, R. S.; Cohn, P.; Tenzel, P.; Abboud, K. A.; Castellano, R. K. Synthesis, Photophysical Behavior, and Electronic Structure of Push−Pull Purines. *J. Am. Chem. Soc.* **2009**, *131*, 623-633.

(74) Li, J.-P.; Wang, H.-X.; Wang, H.-X.; Xie, M.-S.; Qu, G.-R.; Niu, H.-Y.; Guo, H.-M. Push–Pull-Type Purine Nucleoside-Based Fluorescent Sensors for the Selective Detection of Pd2+ in Aqueous Buffer. *Eur. J. Org. Chem.* **2014**, 2225-2230.

(75) Zhang, K.; Fahs, G. B.; Aiba, M.; Moore, R. B.; Long, T. E. Nucleobase-Functionalized ABC Triblock Copolymers: Self-Assembly of Supramolecular Architectures. *Chem. Commun.* **2014**, *50*, 9145-9148.

(76) Garcia, M.; Beecham, M. P.; Kempe, K.; Haddleton, D. M.; Khan, A.; Marsh, A. Water Soluble Triblock and Pentablock Poly(methacryloyl nucleosides) from Copper-Mediated Living Radical Polymerisation using PEG Macroinitiators. *Eur. Polym. J.* **2015**, *66*, 444-451.

(77) Kang, Y.; Pitto-Barry, A.; Willcock, H.; Quan, W.-D.; Kirby, N.; Sanchez, A. M.; O'Reilly, R. K. Exploiting Nucleobase-Containing Materials - from Monomers to Complex Morphologies using RAFT Dispersion Polymerization. *Polym. Chem.* **2015**, *6*, 106-117.

(78) Garcia, M.; Kempe, K.; Haddleton, D. M.; Khan, A.; Marsh, A. Templated Polymerizations on Solid Supports Mediated by Complementary Nucleoside Interactions. *Polym. Chem.* **2015**, *6*, 1944-1951.

(79) Čerňa, I.; Pohl, R.; Klepetářová, B.; Hocek, M. Synthesis of 6,8,9-Tri- and 2,6,8,9-Tetrasubstituted Purines by a Combination of the Suzuki Cross-coupling, N-Arylation, and Direct C−H Arylation Reactions. *J. Org. Chem.* **2008**, *73*, 9048-9054.

(80) Gu, Z.; Tang, P.; Zhao, B.; Luo, H.; Guo, X.; Chen, H.; Yu, G.; Liu, X.; Shen, P.; Tan, S. Synthesis and Photovoltaic Properties of Copolymers Based on Benzo[1,2-b:4,5-b

′]dithiophene and Thiophene with Different Conjugated Side Groups. *Macromolecules* **2012**, *45*, 2359-2366.

(81) Yang, M.; Peng, B.; Liu, B.; Zou, Y.; Zhou, K.; He, Y.; Pan, C.; Li, Y. Synthesis and Photovoltaic Properties of Copolymers from Benzodithiophene and Thiazole. *J. Phys. Chem. C.* **2010**, *114*, 17989-17994.

(82) Cao, J.; Zhang, W.; Xiao, Z.; Liao, L.; Zhu, W.; Zuo, Q.; Ding, L. Synthesis and Photovoltaic Properties of Low Band Gap Polymers Containing Benzo[1,2-b:4,5-c′]dithiophene-4,8-dione. *Macromolecules* **2012**, *45*, 1710-1714.

(83) Liu, B.; Chen, X.; Zou, Y.; Xiao, L.; Xu, X.; He, Y.; Li, L.; Li, Y. Benzo[1,2-b:4,5-b′]difuran-Based Donor–Acceptor Copolymers for Polymer Solar Cells. *Macromolecules* **2012**, *45*, 6898-6905.

(84) Hoang, Q. V.; Song, C. E.; Moon, S. J.; Lee, S. K.; Lee, J. C.; Kim, B. J.; Shin, W. S. Asymmetric Electron-Donating 4-Alkyl-8-alkoxybenzo[1,2-b:4,5-b ']dithiophene Unit for Use in High-Efficiency Bulk Heterojunction Polymer Solar Cells. *Macromolecules* **2015**, *48*, 3918-3927.

(85) Liao, X.; Wu, F.; Zhang, L.; Chen, L.; Chen, Y. Solution-Processed Small Molecules Based on Benzodithiophene and Difluorobenzothiadiazole for Inverted Organic Solar Cells. *Polym. Chem.* **2015**, *6*, 7726-7736.

(86) Jia, M.; Ma, X.; Yan, L.; Wang, H.; Guo, Q.; Wang, X.; Wang, Y.; Zhan, X.; Xia, A. Photophysical Properties of Intramolecular Charge Transfer in Two Newly Synthesized Tribranched Donor−π−Acceptor Chromophores. *J. Phys. Chem. C.* **2010**, *114*, 7345-7352.

(87) Beaujuge, P. M.; Amb, C. M.; Reynolds, J. R. Spectral Engineering in π-Conjugated Polymers with Intramolecular Donor−Acceptor Interactions. *Acc. Chem. Res.* **2010**, *43*, 1396-1407.

(88) Wen, L.; Heth, C. L.; Rasmussen, S. C. Thieno[3,4-b]pyrazine-based Oligothiophenes: Simple Models of Donor-Acceptor Polymeric Materials. *Phys. Chem. Chem. Phys.* **2014**, *16*, 7231-7240.

(89) Wang, Y.; Parkin, S. R.; Watson, M. D. Benzodichalcogenophenes with Perfluoroarene Termini. *Org. Lett.* **2008**, *10*, 4421-4424.

(90) Bilkay, T.; Schulze, K.; Egorov-Brening, T.; Fink, K.; Janietz, S. Solution Processable TIPS-Benzodithiophene Small Molecules with Improved Semiconducting Properties in Organic Field Effect Transistors. *Org. Electron.* **2013**, *14*, 344-353.

(91) Elangovan, A.; Kao, K.-M.; Yang, S.-W.; Chen, Y.-L.; Ho, T.-I.; Su, Y. O. Synthesis, Electronic Properties, and Electrochemiluminescence of Donor-Substituted Phenylethynylanthronitriles. *J. Org. Chem.* **2005**, *70*, 4460-4469.

(92) Haid, S.; Marszalek, M.; Mishra, A.; Wielopolski, M.; Teuscher, J.; Moser, J.-E.; Humphry-Baker, R.; Zakeeruddin, S. M.; Grätzel, M.; Bäuerle, P. Significant Improvement of Dye-Sensitized Solar Cell Performance by Small Structural Modification in π-Conjugated Donor–Acceptor Dyes. *Adv. Funct. Mater.* **2012**, *22*, 1291-1302.

(93) Lin, Y.; Li, Y.; Zhan, X. Small Molecule Semiconductors for High-Efficiency Organic Photovoltaics. *Chem. Soc. Rev.* **2012**, *41*, 4245-4272.

(94) Beaujuge, P. M.; Reynolds, J. R. Color Control in π-Conjugated Organic Polymers for Use in Electrochromic Devices. *Chem. Rev.* **2010**, *110*, 268-320.

(95) McQuade, D. T.; Pullen, A. E.; Swager, T. M. Conjugated Polymer-Based Chemical Sensors. *Chem. Rev.* **2000**, *100*, 2537-2574.

(96) Gunathilake, S. S.; Magurudeniya, H. D.; Huang, P.; Nguyen, H.; Rainbolt, E. A.; Stefan, M. C.; Biewer, M. C. Synthesis and Characterization of Novel Semiconducting Polymers Containing Pyrimidine. *Polym. Chem.* **2013**, *4*, 5216-5219.

(97) Collier, G. S.; Brown, L. A.; Boone, E. S.; Long, B. K.; Kilbey, S. M. Synthesis of Main Chain Purine-Based Copolymers and Effects of Monomer Design on Thermal and Optical Properties. *ACS Macro Letters* **2016**, *5*, 682-687.

(98) Šponer, J.; Leszczynski, J.; Hobza, P. Electronic Properties, Hydrogen Bonding, Stacking, and Cation Binding of DNA and RNA Bases. *Biopolymers* **2001**, *61*, 3-31.

(99) Hou, Q.; Xu, Y.; Yang, W.; Yuan, M.; Peng, J.; Cao, Y. Novel Red-Emitting Fluorene-Based Copolymers. *J. Mater. Chem.* **2002**, *12*, 2887-2892.

(100) Havelková, M.; Hocek, M.; esnek, M.; Dvoák, D. The Suzuki-Miyaura Cross-Coupling Reactions of 6-Halopurines with Boronic Acids Leading to 6-Aryl- and 6-Alkenylpurines. *Synlett* **1999**, 1145-1147.

(101) Wang, Y.; Michinobu, T. Benzothiadiazole and Its pi-extended, Heteroannulated Derivatives: Useful Acceptor Building Blocks for High-Performance Donor-Acceptor Polymers in Organic Electronics. *J. Mater. Chem. C* **2016**, *4*, 6200-6214.

(102) Marin, D. M.; Payerpaj, S.; Collier, G. S.; Ortiz, A. L.; Singh, G.; Jones, M.; Walter, M. G. Efficient Intersystem Crossing Using Singly Halogenated Carbomethoxyphenyl Porphyrins Measured Using Delayed Fluorescence, Chemical

Quenching, and Singlet Oxygen Emission. *Phys. Chem. Chem. Phys.* **2015**, *17*, 29090-29096.

(103) Dias, F. B.; Pollock, S.; Hedley, G.; Pålsson, L.-O.; Monkman, A.; Perepichka, I. I.; Perepichka, I. F.; Tavasli, M.; Bryce, M. R. Intramolecular Charge Transfer Assisted by Conformational Changes in the Excited State of Fluorene-dibenzothiophene-S,S-dioxide Co-oligomers. *J. Phys. Chem. B* **2006**, *110*, 19329-19339.

(104) Patel, D. G.; Feng, F.; Ohnishi, Y.-y.; Abboud, K. A.; Hirata, S.; Schanze, K. S.; Reynolds, J. R. It Takes More Than an Imine: The Role of the Central Atom on the Electron-Accepting Ability of Benzotriazole and Benzothiadiazole Oligomers. *J. Am. Chem. Soc.* **2012**, *134*, 2599-2612.

(105) Kato, S.-i.; Furuya, T.; Kobayashi, A.; Nitani, M.; Ie, Y.; Aso, Y.; Yoshihara, T.; Tobita, S.; Nakamura, Y. π-Extended Thiadiazoles Fused with Thienopyrrole or Indole Moieties: Synthesis, Structures, and Properties. *J. Org. Chem.* **2012**, *77*, 7595-7606.

(106) Thompson, B. C.; Kim, Y.-G.; McCarley, T. D.; Reynolds, J. R. Soluble Narrow Band Gap and Blue Propylenedioxythiophene-Cyanovinylene Polymers as Multifunctional Materials for Photovoltaic and Electrochromic Applications. *J. Am. Chem. Soc.* **2006**, *128*, 12714-12725.

(107) Mei, J.; Bao, Z. Side Chain Engineering in Solution-Processable Conjugated Polymers. *Chem. Mater.* **2014**, *26*, 604-615.

(108) Gamadeku, T.; Gundersen, L.-L. Synthesis of 8-Bromo-N-benzylpurines via 8-Lithiated Purines: Scope and Limitations. *Synthetic Commun.* **2010**, *40*, 2723-2735.

(109) Lee, D.; Hubijar, E.; Kalaw, G. J. D.; Ferraris, J. P. Enhanced and Tunable Open-Circuit Voltage using Dialkylthio Benzo[1,2-b:4,5-b′]dithiophene in Polymer Solar Cells. *Chem. Mater.* **2012**, *24*, 2534-2540.

(110) Hou, J.; Chen, H.-Y.; Zhang, S.; Yang, Y. Synthesis and Photovoltaic Properties of Two Benzo[1,2-b:3,4-b′]dithiophene-Based Conjugated Polymers. *J. Phys. Chem. C.* **2009**, *113*, 21202-21207.

(111) Deng, P.; Yu, J.; Yin, X.; Geng, Y.; Zhou, B.; Zhang, F.; Tang, W. Effect of Bisalkylthio Side Chains on Benzo[1,2-b:4,5-b′]dithiophene-Based Polymers for Organic Solar Cells. *Dyes and Pigments* **2017**, *138*, 47-55.

(112) Kim, J.-H.; Song, C. E.; Kim, B.; Kang, I.-N.; Shin, W. S.; Hwang, D.-H. Thieno[3,2-b]thiophene-Substituted Benzo[1,2-b:4,5-b′]dithiophene as a Promising Building Block for Low Bandgap Semiconducting Polymers for High-Performance Single and Tandem Organic Photovoltaic Cells. *Chem. Mater.* **2014**, *26*, 1234-1242.

(113) Yao, H.; Ye, L.; Zhang, H.; Li, S.; Zhang, S.; Hou, J. Molecular Design of Benzodithiophene-Based Organic Photovoltaic Materials. *Chem. Rev.* **2016**, *116*, 7397-7457.

(114) Hou, J.; Park, M.-H.; Zhang, S.; Yao, Y.; Chen, L.-M.; Li, J.-H.; Yang, Y. Bandgap and Molecular Energy Level Control of Conjugated Polymer Photovoltaic Materials Based on Benzo[1,2-b:4,5-b′]dithiophene. *Macromolecules* **2008**, *41*, 6012-6018.

(115) Nguyen, T. L.; Song, S.; Ko, S.-J.; Choi, H.; Jeong, J.-E.; Kim, T.; Hwang, S.; Kim, J. Y.; Woo, H. Y. Benzodithiophene-thiophene-based photovoltaic polymers with different side-chains. *J. Polym. Sci. A Polym. Chem.* **2015**, *53*, 854-862.

(116) Huang, Y.; Liu, F.; Guo, X.; Zhang, W.; Gu, Y.; Zhang, J.; Han, C. C.; Russell, T. P.; Hou, J. Manipulating Backbone Structure to Enhance Low Band Gap Polymer Photovoltaic Performance. *Adv. Energy Mater.* **2013**, *3*, 930-937.

(117) Zhan, X.; Zhu, D. Conjugated polymers for high-efficiency organic photovoltaics. *Polym. Chem.* **2010**, *1*, 409-419.

(118) Alonzo, J.; Kochemba, W. M.; Pickel, D. L.; Ramanathan, M.; Sun, Z.; Li, D.; Chen, J.; Sumpter, B. G.; Heller, W. T.; Kilbey II, S. M. Assembly and Organization of Poly(3-hexylthiophene) Brushes and Their Potential use as Novel Anode Buffer Layers for Organic Photovoltaics. *Nanoscale* **2013**, *5*, 9357-9364.

(119) Brown, P. J.; Thomas, D. S.; Köhler, A.; Wilson, J. S.; Kim, J.-S.; Ramsdale, C. M.; Sirringhaus, H.; Friend, R. H. Effect of interchain interactions on the absorption and emission of poly(3-hexylthiophene). *Phys. Rev. B* **2003**, *67*, 064203.

(120) Satrijo, A. Controlling the Architectures and Optical Properties of Conjugated Polymer Aggregates and Films. Massachusetts Institute of Technology, 2007.

(121) Schwartz, B. J. Conjugated Polymers as Molecular Materials: How Chain Conformation and Film Morphology Influence Energy Transfer and Interchain Interactions. *Annu. Rev. Phys. Chem.* **2003**, *54*, 141-172.

(122) Scharber, M. C.; Mühlbacher, D.; Koppe, M.; Denk, P.; Waldauf, C.; Heeger, A. J.; Brabec, C. J. Design Rules for Donors in Bulk-Heterojunction Solar Cells—Towards 10 % Energy-Conversion Efficiency. *Adv. Mater.* **2006**, *18*, 789-794.

APPENDICES

Appendix A-Chapter 2: Synthesis of Main Chain Purine-Based Copolymers and Effects of Monomer Design on Thermal and Optical Properties

NMR Spectroscopy

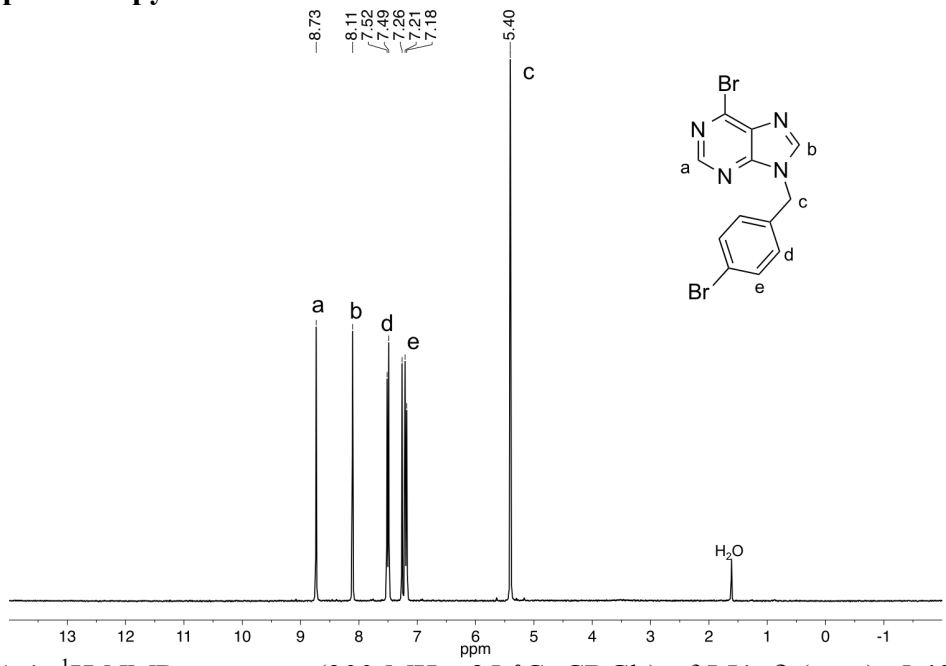

Figure A.1. ^{1}H NMR spectrum (300 MHz, 25 ˚C, $CDCl_3$) of **M1**; δ (ppm): 5.40 (s, 2H, CH_2), 7.20 (d, 2H, J = 9 Hz, Ph), 7.50 (d, 2H, J = 6 Hz, Ph), 8.11 (s, 1H, purine H), 8.73 (s, 1H, purine H).

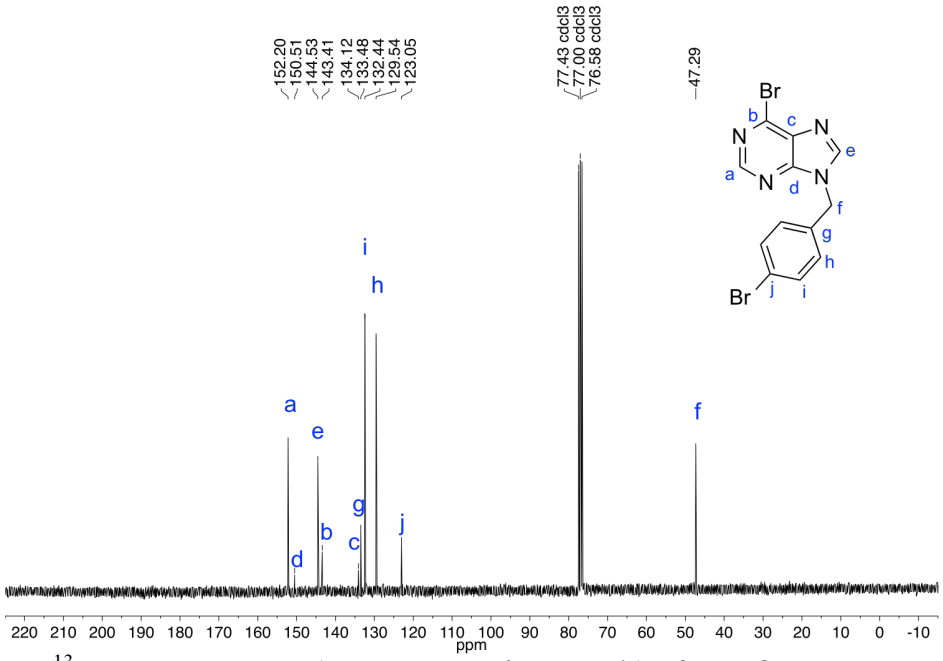

Figure A.2. ^{13}C NMR spectrum (300 MHz, 25 ˚C, $CDCl_3$) of **M1**; δ, ppm: 47.29, 123.05, 129.54 (×2), 132.44 (×2), 133.48, 134.12, 143.41, 144.53, 150.51, 152.20.

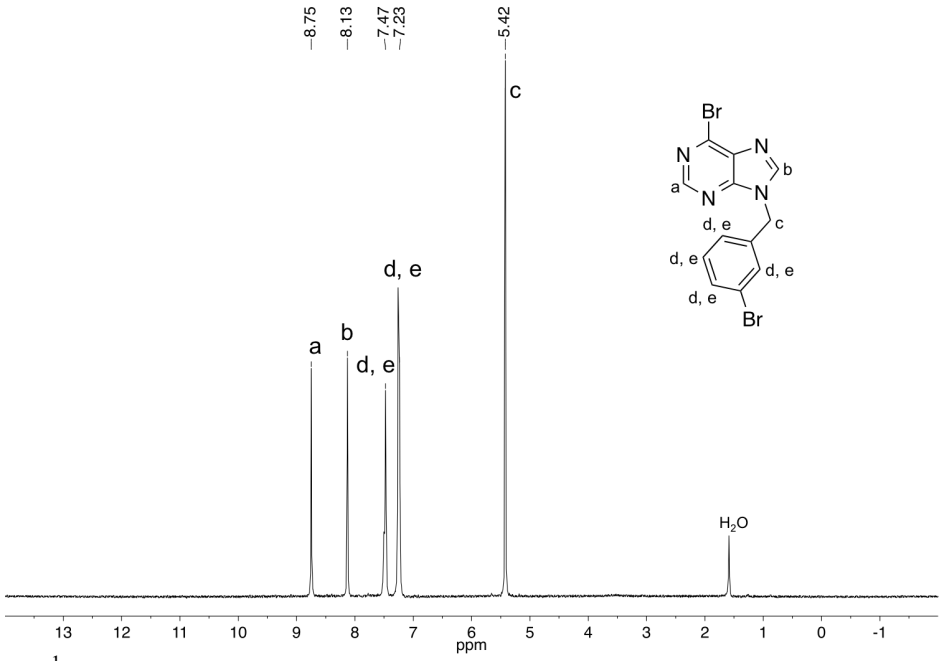

Figure A.3. ^{1}H NMR spectrum (300 MHz, 25 ˚C, $CDCl_3$) of **M2**; δ, ppm: 5.42 (s, 2H), 7.23 (m, 2H, PhH), 7.47 (m, 2H, PhH), 8.13 (s, 1H, purine H), 8.75 (s, 1H, purine H).

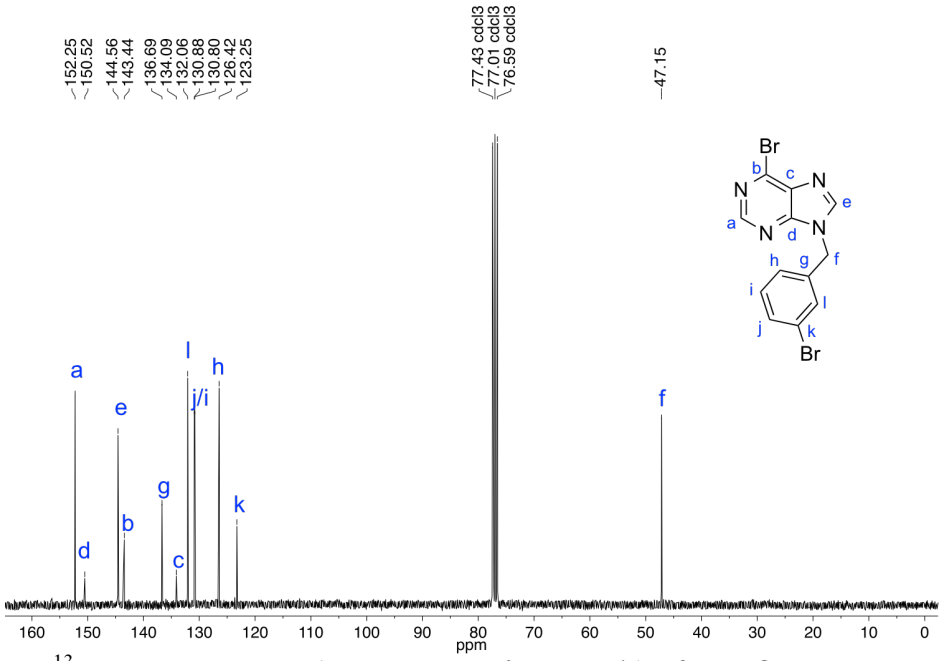

Figure A.4. ^{13}C NMR spectrum (300 MHz, 25 ˚C, $CDCl_3$) of **M2**; δ, ppm: 47.15, 123.25, 126.42, 130.80, 130.88, 132.06, 134.09, 136.69, 143.44, 144.56, 150.52, 152.25.

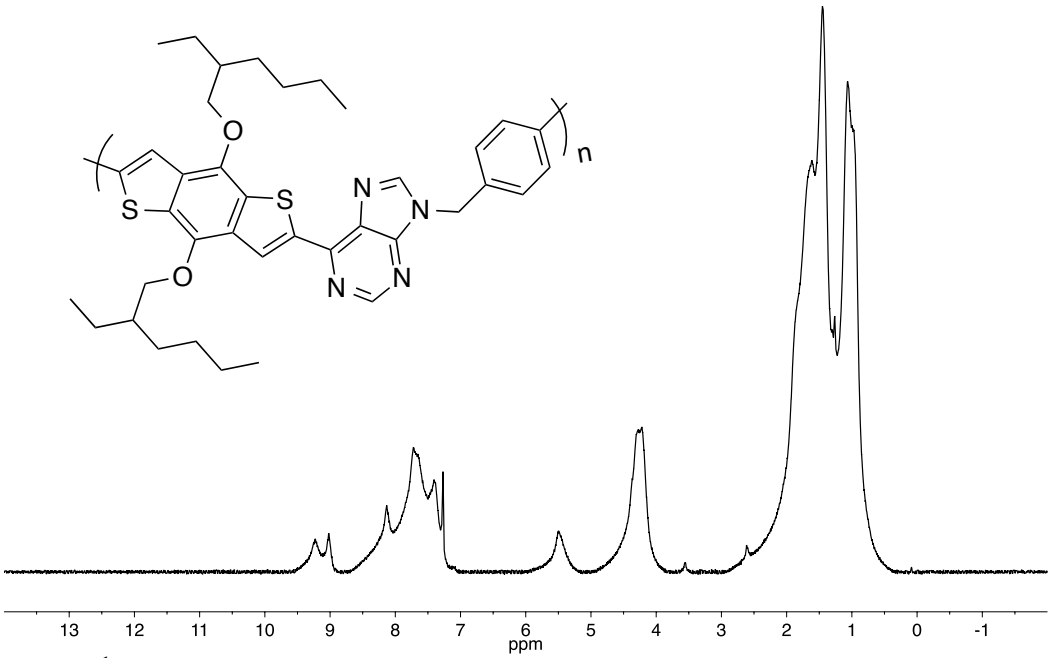

Figure A.5. ^{1}H NMR spectrum (300 MHz, 25 ˚C, $CDCl_3$) of **P1** (depicted in inset).

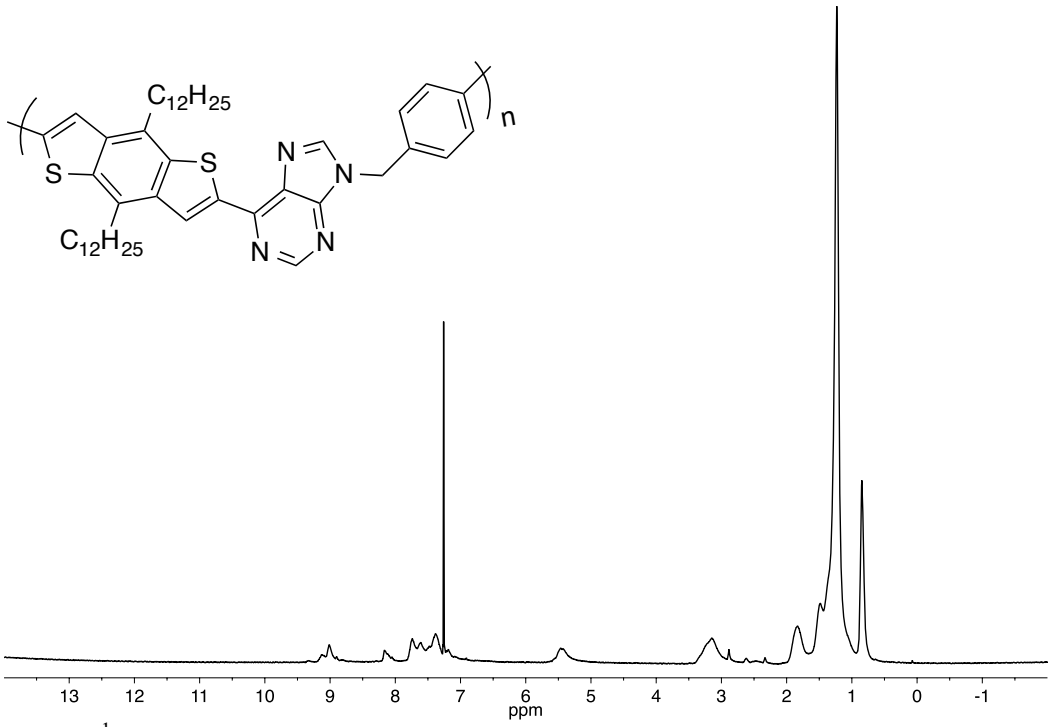

Figure A.6. ^{1}H NMR spectrum (300 MHz, 25 ˚C, $CDCl_3$) of **P2** (depicted in inset).

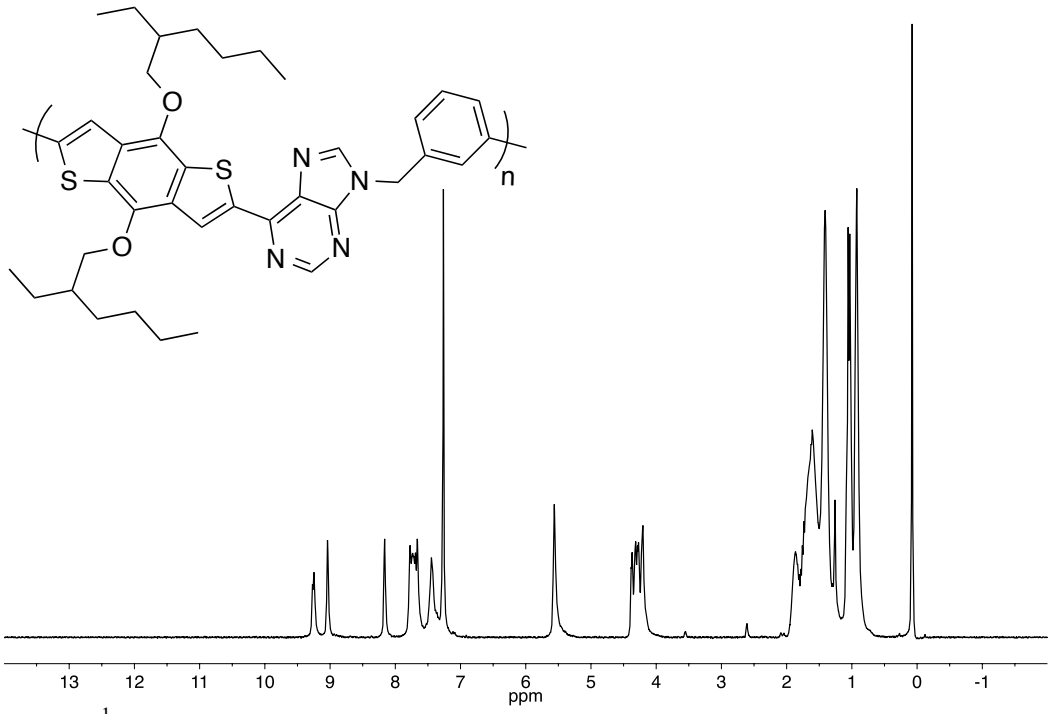

Figure A.7. ^{1}H NMR spectrum (300 MHz, 25 ˚C, $CDCl_3$) of **P3** (depicted in inset).

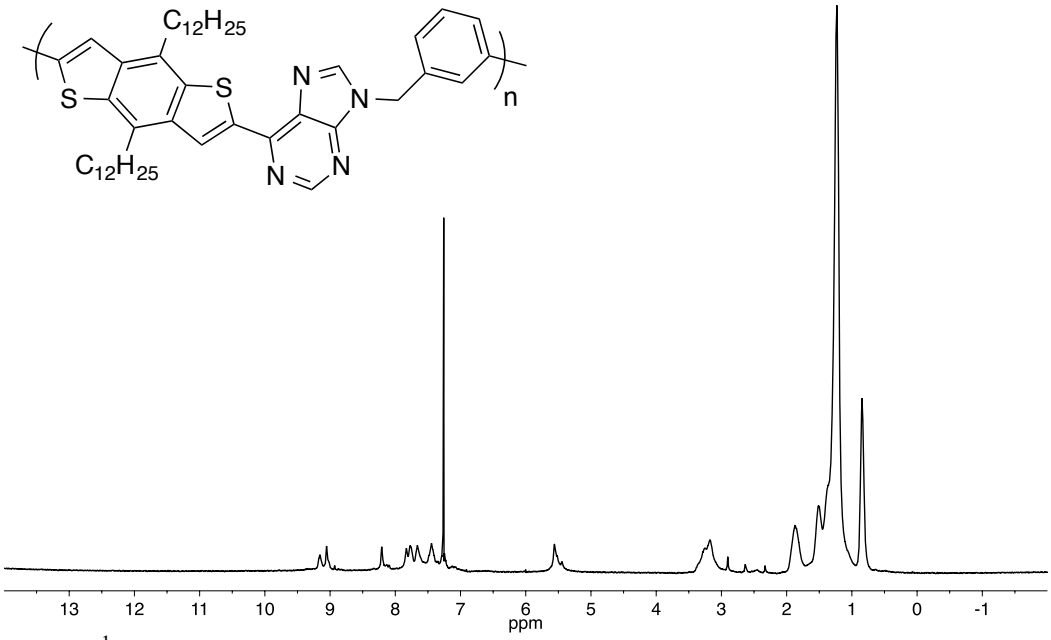

Figure A.8. ^{1}H NMR spectrum (300 MHz, 25 ˚C, $CDCl_3$) of **P4** (depicted in inset).

Table A.1. Molecular weight characterization of poly(purine)s synthesized using microwave-assisted polymerizations.

Entry	Polymer[a]	Solvent	Catalyst	Temp. (°C)	M_n (g/mol)	M_w (g/mol)	PDI	yield (%)
1	**P1**	Toluene	$Pd(PPh_3)_4$	110	5,500	9,900	1.80	76
2	**P1**	Toluene	$Pd(PPh_3)_2Cl_2$	110	6,500	11,900	1.83	62
3[b]	**P1**	Toluene	$Pd(dba)_2/P(o\text{-tol})_3$	110	-	-	-	-
4[b]	**P1**	Toluene	$PdCl_2(P(o\text{-tol})_3)_2$	110	-	-	-	-
5[b]	**P1**	Toluene	$Pd(dppf)Cl_2$	110	-	-	-	-
6[b]	**P1**	Toluene	PEPPSI	110	-	-	-	-
7[c]	**P1**	*o*-xylene	$Pd(PPh_3)_4$	110	5,000	6,400	1.28	64
8	**P1**	*o*-xylene	$PdCl_2(P(o\text{-tol})_3)_2$	150	8,100	14,300	1.76	80
9	**P1**	*o*-xylene	$Pd(t\text{-}Bu_3P)_2$	110	6,100	8,300	1.36	78
10	**P1**	*o*-xylene	$Pd(dba)_2/P(o\text{-tol})_3$	110	5,800	7,700	1.32	71
11	**P1**	DMF	$Pd(PPh_3)_2Cl_2$	90	6,700	10,000	1.49	79
12[c]	**P1**	DMF	$Pd(PPh_3)_4$	110	5,300	6,100	1.15	70
13	**P1**	NMP	$Pd(PPh_3)_4$	110	4,700	5,500	1.17	65
14[c]	**P1**	PhCl	$Pd(PPh_3)_4$	110	5,000	6,200	1.24	70
15	**P1**	PhCl	$PdCl_2(P(o\text{-tol})_3)_2$	150	6,100	7,800	1.37	73
16	**P2**	PhCl	$PdCl_2(P(o\text{-tol})_3)_2$	150	5,200	8,600	1.65	70
17	**P3**	PhCl	$PdCl_2(P(o\text{-tol})_3)_2$	150	5,400	8,400	1.56	69
18	**P4**	PhCl	$PdCl_2(P(o\text{-tol})_3)_2$	150	4,700	6,900	1.46	64

[a]Corresponds to the polymers labeled in Scheme 2.6. [b]Reaction conditions did not generate polymeric material. [c]Corresponds to reaction conditions that led to insoluble material that could not be dissolved in chloroform following the Soxhlet extractions. Data reported is from sparingly soluble material.

Size-exclusion Chromatography

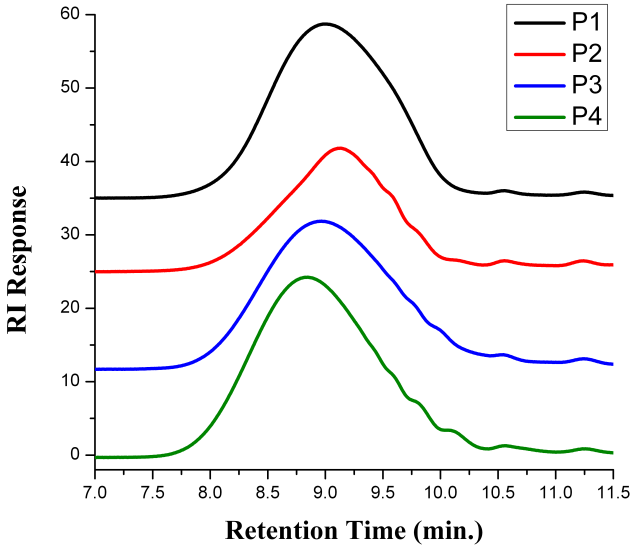

Figure A.9. SEC traces poly(purine)s **P1-P4** synthesized using conventional heating.

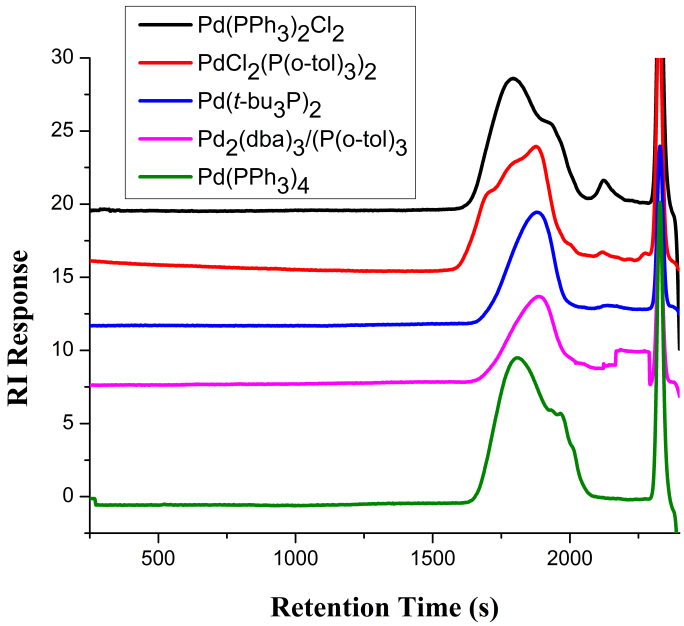

Figure A.10. SEC traces of polymer **P1** that was synthesized using different palladium catalysts (identified in legend).

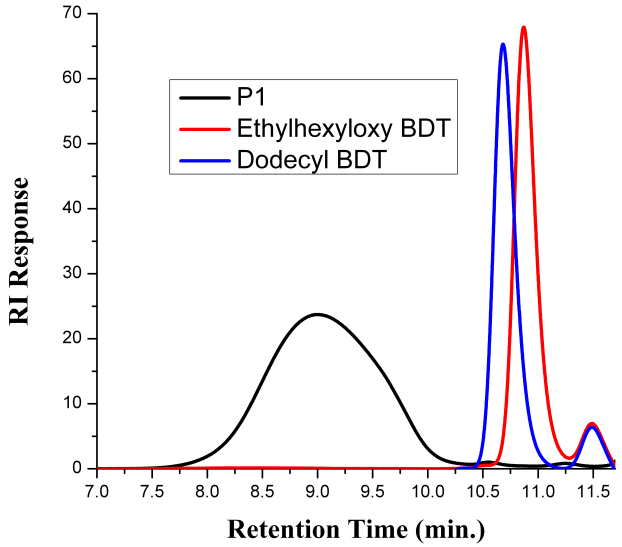

Figure A.11. SEC traces showing the comparison of **P1** to BDT stannyl comonomers to demonstrate successful coupling between the purine and BDT comonomers.

Differential Scanning Calorimetry

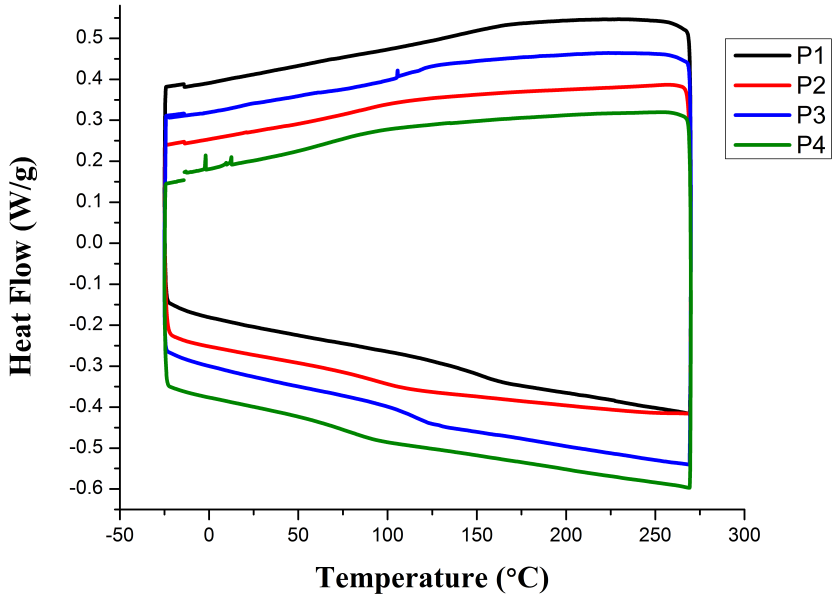

Figure A.12. DSC traces for polymers **P1-P4** on the second heat-cycle.

Appendix B-Chapter 3: Synthesis of Donor-Acceptor Purine-Based Chromophores and an Investigation of Thermal, Photophysical, and Electrochemical Properties

NMR Spectroscopy

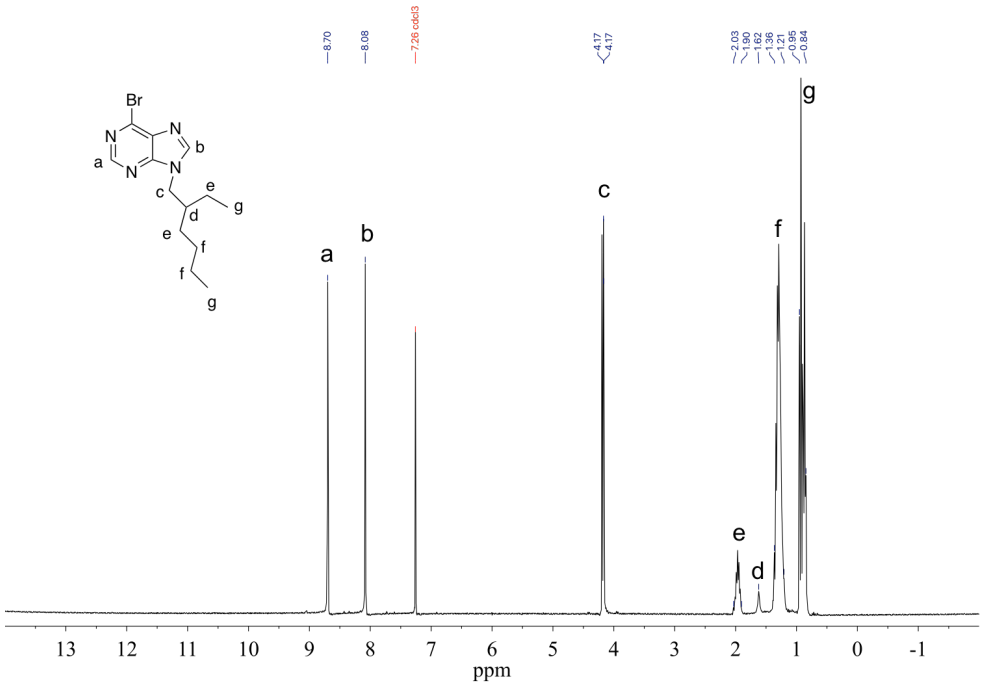

Figure B.1. ^{1}H NMR spectrum (500 MHz, 25 °C, $CDCl_3$) of 9-ethylhexylpurine; δ (ppm): 0.85-0.95 (m) 1.20-1.36 (m), 1.62 (br singlet), 1.91-2.03 (m), 4.18 (d, 2H, CH_2), 8.08 (s, 1H, purine H), 8.70 (s, 1H, purine H).

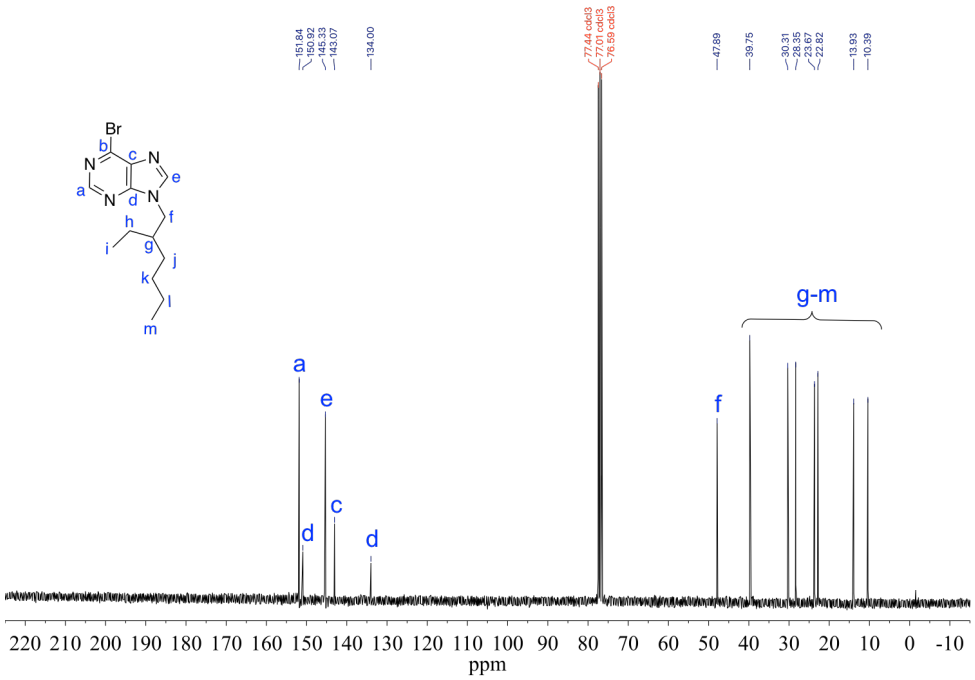

Figure B.2. ^{13}C NMR spectrum (500 MHz, 25 °C, $CDCl_3$) of 9-ethylhexylpurine; δ (ppm): 10.39, 13.93, 22.82, 23.67, 28.35, 30.31, 39.75, 47.89, 134.00, 143.07, 145.33, 150.92, 151.84.

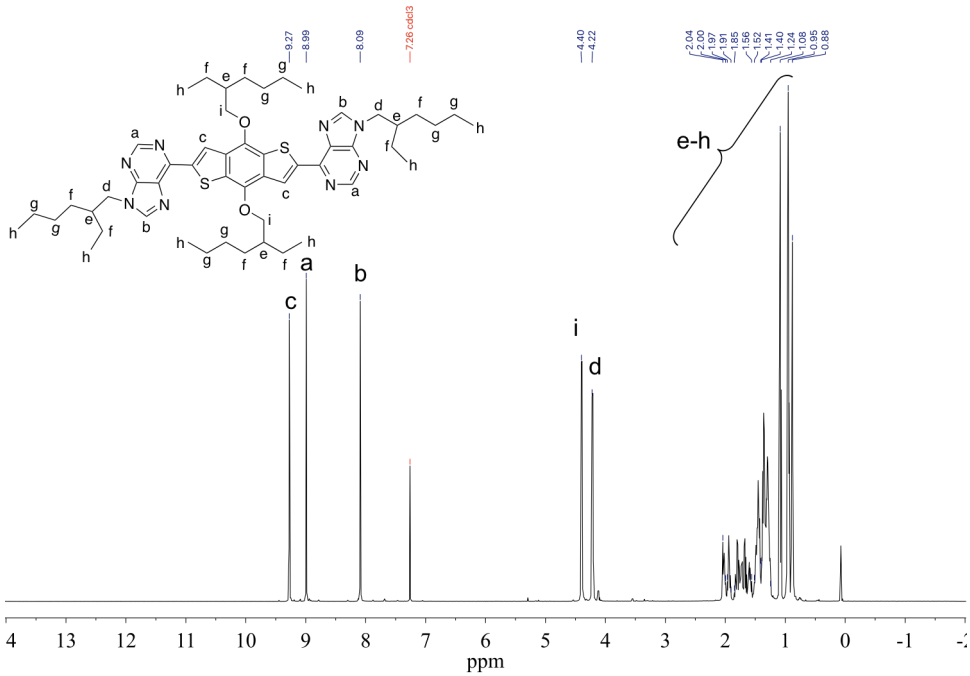

Figure B.3. ^{1}H NMR spectrum (500 MHz, 25 °C, $CDCl_3$) of **P-BDT-P**; δ (ppm): 0.88 (t), 0.94-0.98 (m), 1.08 (t), 1.24-1.40 (m), 1.41-1.52 (m), 1.55-1.84 (m), 1.91-1.97 (m), 2.00-2.05 (m), 4.21 (d), 4.40 (d) ,8.09 (s, 1H,), 8.99 (s, 1H, purine H), 9.27 (s, 1H, purine H).

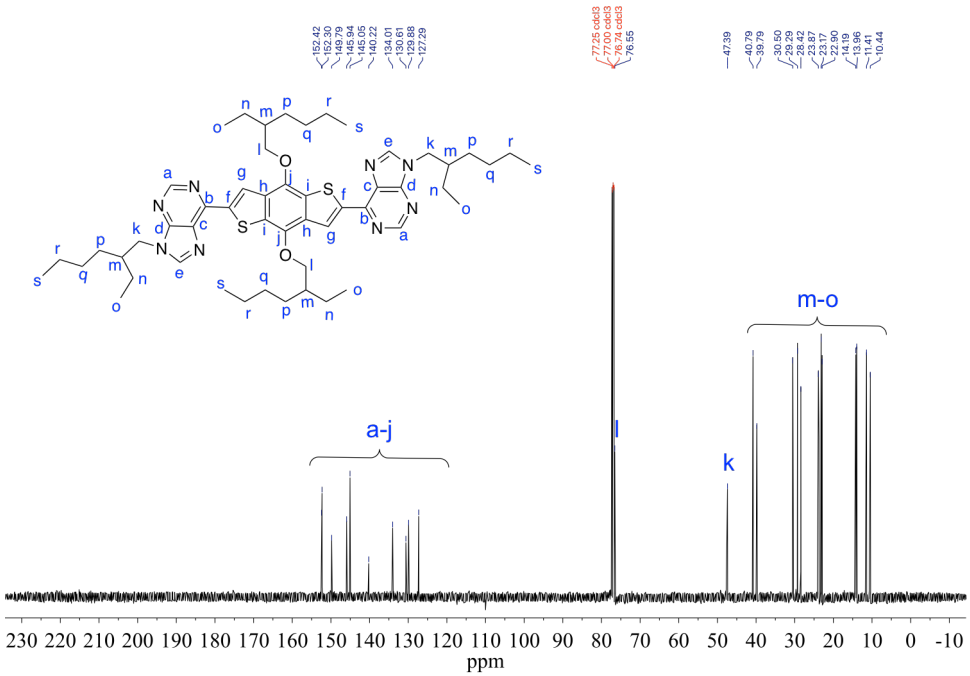

Figure B.4. ^{13}C NMR spectrum (500 MHz, 25 °C, $CDCl_3$) of **P-BDT-P**; δ (ppm): 10.44, 11.41, 13.96, 14.19, 22.90, 23.17, 23.72, 23.87, 28.42, 29.29, 30.39, 30.50, 39.79, 40.79, 47.39, 75.55, 127.29, 129.88, 130.61, 134.01, 140.22, 145.05, 145.94, 149.79, 152.30, 152.42.

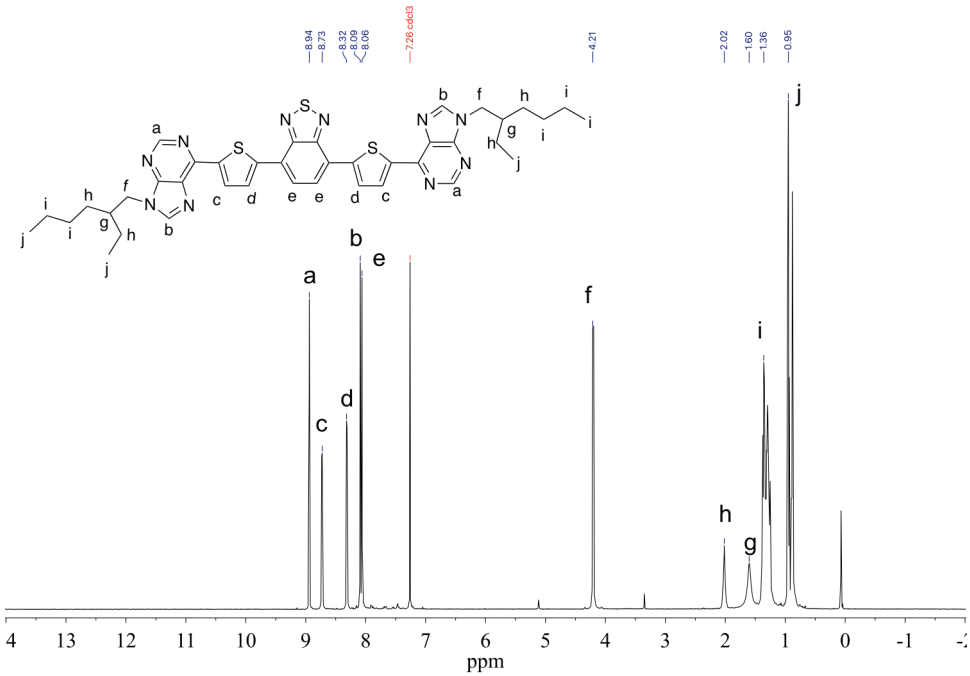

Figure B.5. ^{1}H NMR spectrum (500 MHz, 25 °C, $CDCl_3$) of **P-TBTT-P**; δ (ppm): 0.88 (t), 0.95 (t), 1.24-1.40 (m), 1.60 (s, br), 2.01 (m), 4.22 (d), 8.06 (s, 2H, purine H), 8.09 (s, 2H, purine H), 8.31 (d, 2 H, thiophene H) 8.73 (d, 2H, thiophene H), 8.94 (s, 2H, BT H).

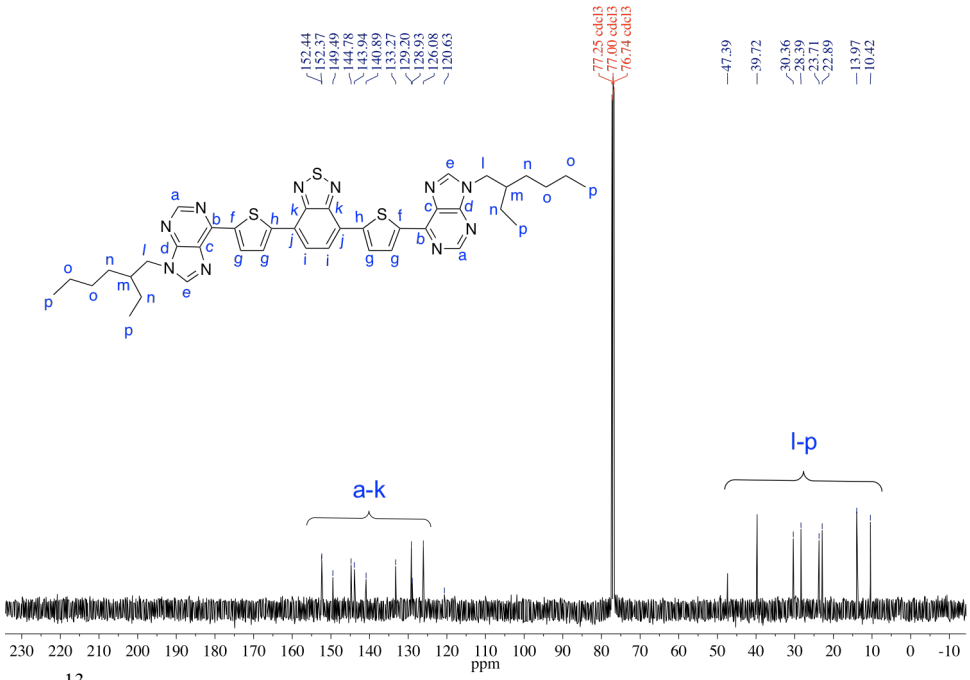

Figure B.6. ^{13}C NMR spectrum (500 MHz, 25 °C, $CDCl_3$) of **P-TBTT-P**; δ (ppm): 10.42, 13.97, 22.89, 23.71, 28.39, 30.36, 39.72, 47.39, 120.63, 126.08, 128.93, 129.20, 133.27, 140.89, 143.94 144.78, 149.49, 152.37, 152.44.

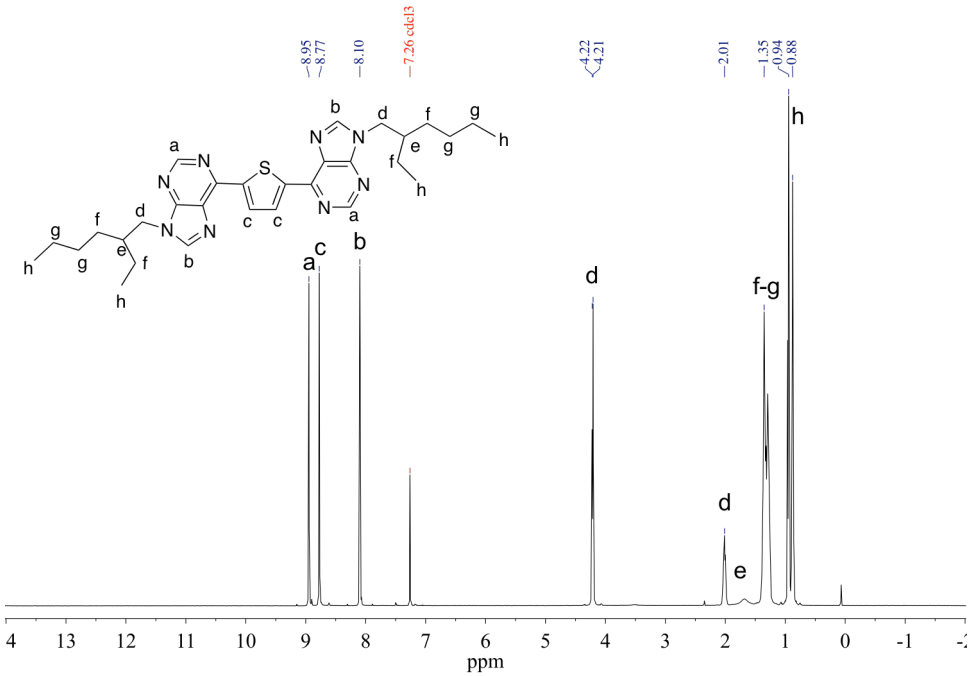

Figure B.7. ^{1}H NMR spectrum (500 MHz, 25 °C, $CDCl_3$) of **P-Th-P**; δ (ppm): 0.88 (t), 0.94 (t), 1.24-1.39 (m), 2.01 (m), 4.21 (d), 8.10 (s), 8.77 (s, 1H, purine H), 8.94 (s, 1H, purine H).

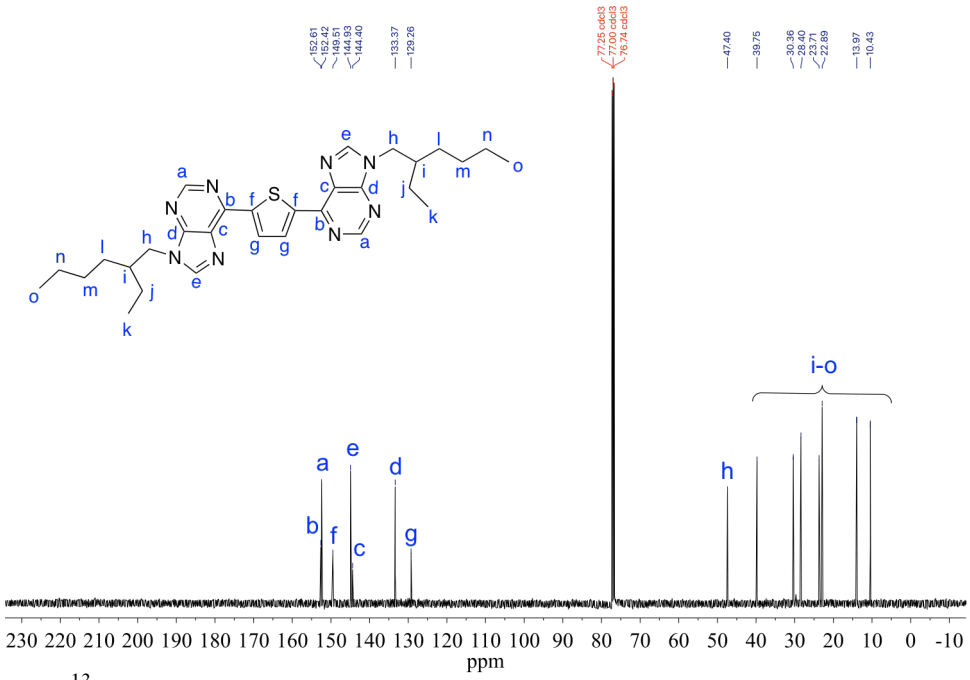

Figure B.8. ^{13}C NMR spectrum (500 MHz, 25 °C, $CDCl_3$) of **P-Th-P**; δ (ppm): 10.43, 13.97, 22.89, 23.71, 28.40, 30.36, 39.75, 47.40, 129.26, 133.37, 144.40, 144.93, 149.51, 152.42, 152.61.

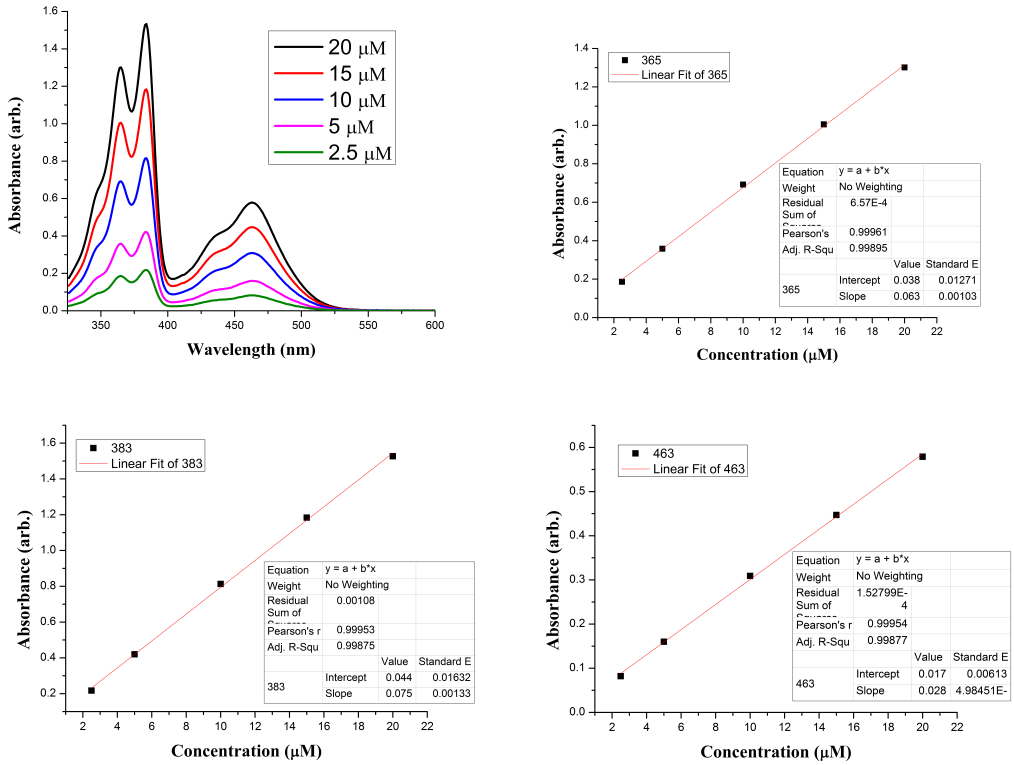

Figure B.9. UV-Vis spectra of varying concentrations (2.5-20 μM) of **P-BDT-P** in chloroform scanning from 325-600 nm and the corresponding Beer's Law plots at the absorbance maximums.

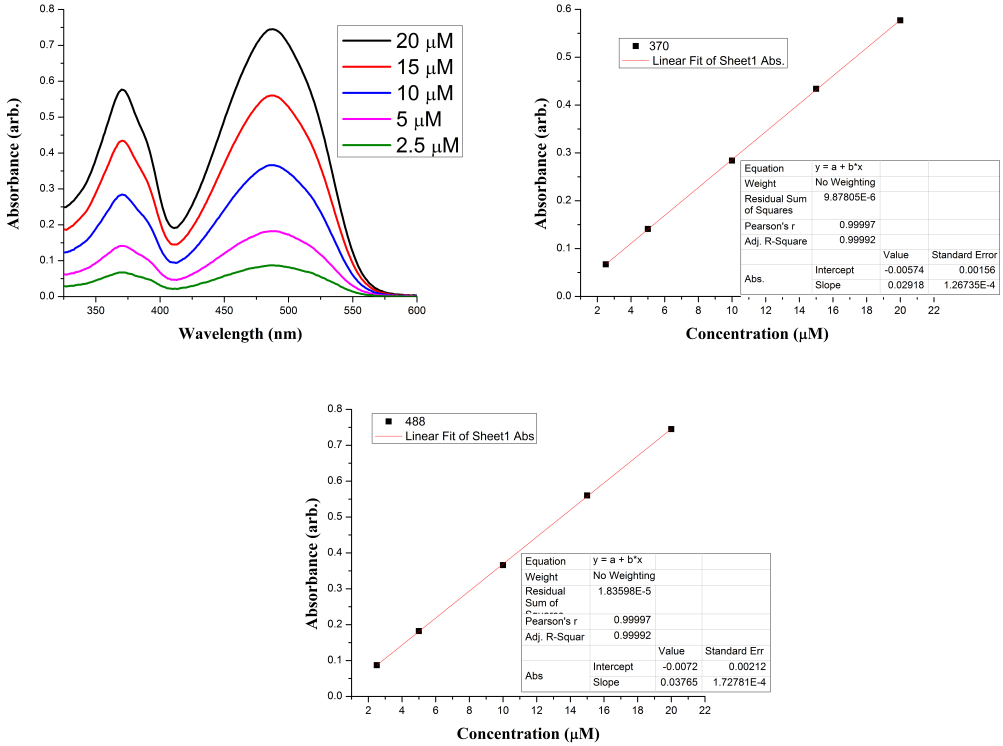

Figure B.10. UV-Vis spectra of varying concentrations (2.5-20 μM) of **P-TBTT-P** in chloroform scanning from 325-600 nm and the corresponding Beer's Law plots at the absorbance maximums.

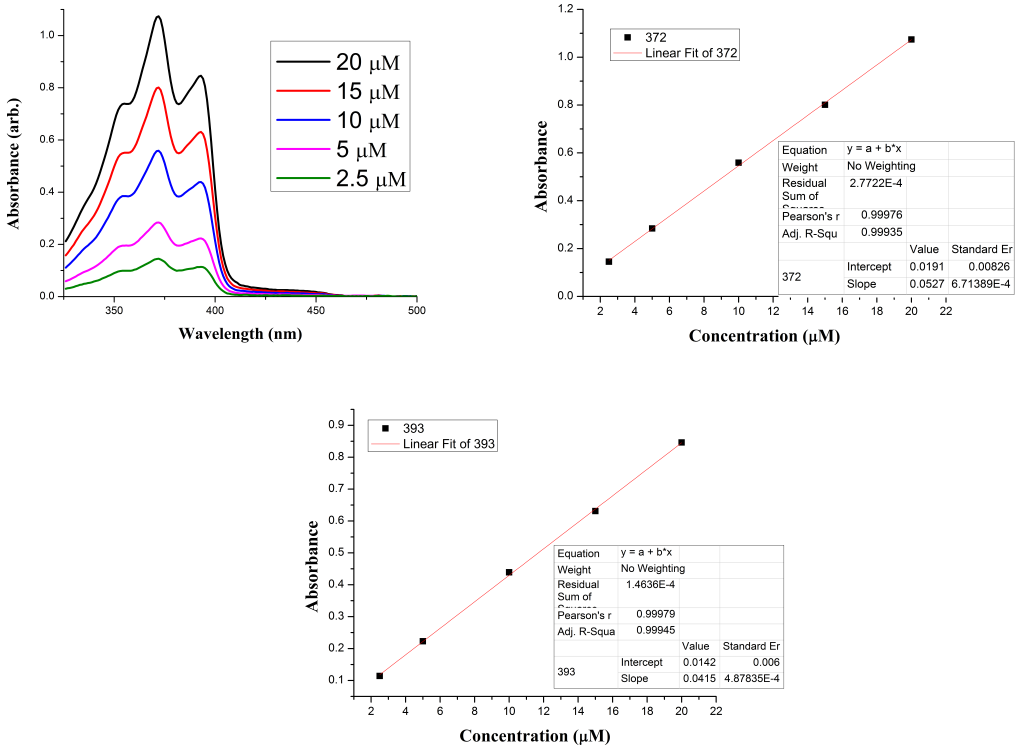

Figure B.11. UV-Vis spectra of varying concentrations (2.5-20 μM) of **P-Th-P** in chloroform scanning from 325-600 nm and the corresponding Beer's Law plots at the absorbance maximums.

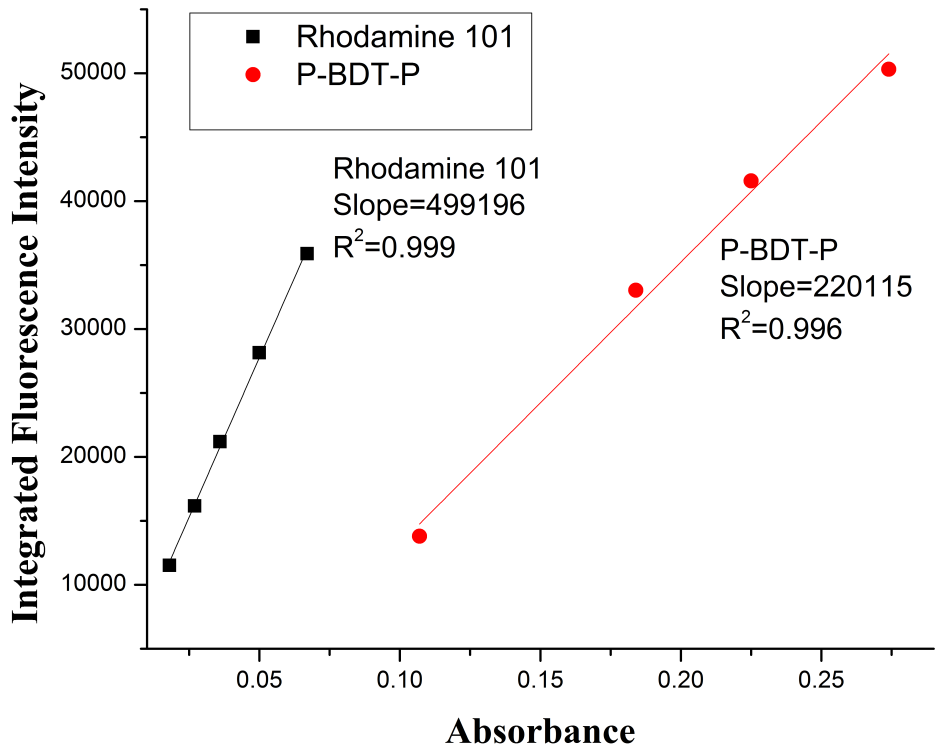

Figure B.12. Absorbance versus integrated fluorescence intensity plots used for calculating the quantum yield for **P-BDT-P**.

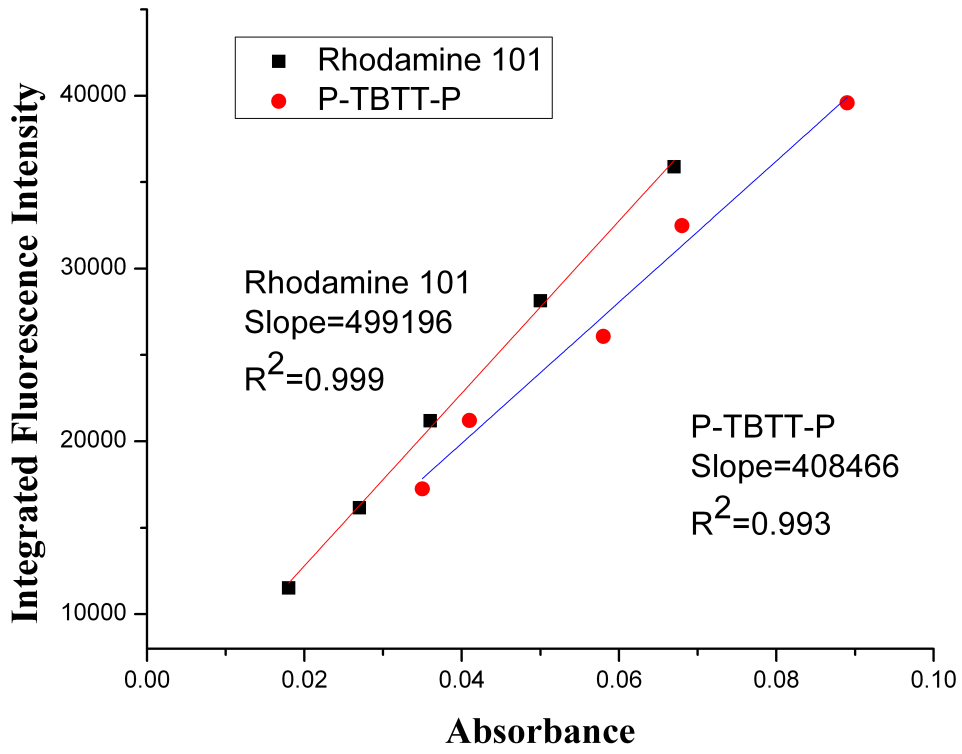

Figure B.13. Absorbance versus integrated fluorescence intensity plots used for calculating the quantum yield for **P-TBTT-P**.

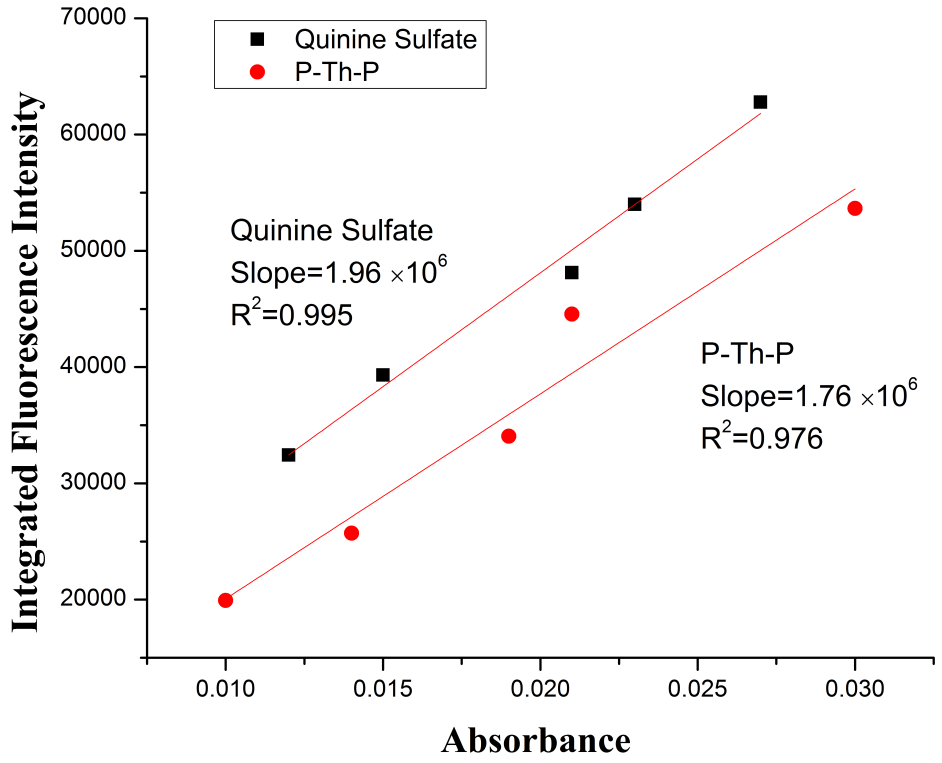

Figure B.14. Absorbance versus integrated fluorescence intensity plots used for calculating the quantum yield for **P-Th-P**.

Appendix C- Synthesis of Purine-Based Donor-Acceptor Conjugated Polymers and the Effect of Incorporating Purines on Photophysical Properties

NMR Spectroscopy

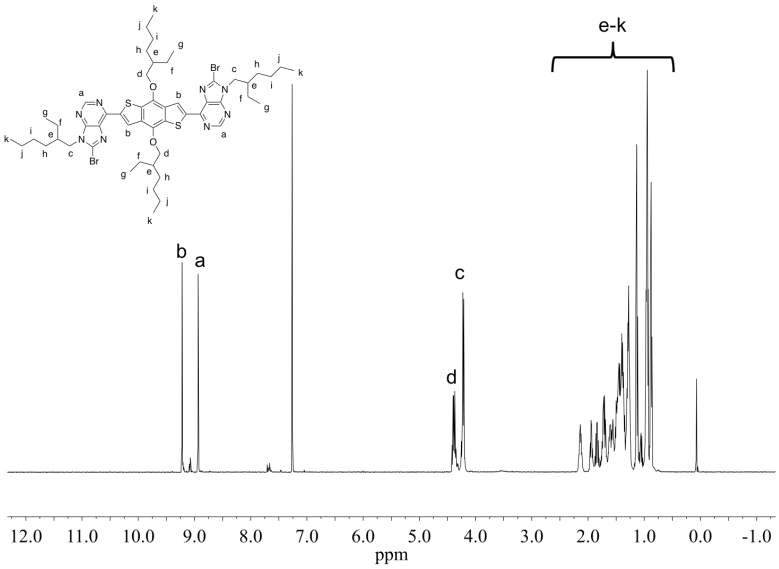

Figure C.1. ^{1}H NMR spectrum (500 MHz, 25 °C, $CDCl_3$) of **Br_2PBDTP**; δ (ppm): 0.85-0.95 (m) 1.20-1.36 (m), 1.62 (br singlet), 1.91-2.03 (m), 4.18 (d, 2H, CH_2), 8.08 (s, 1H, purine H), 8.70 (s, 1H, purine H).

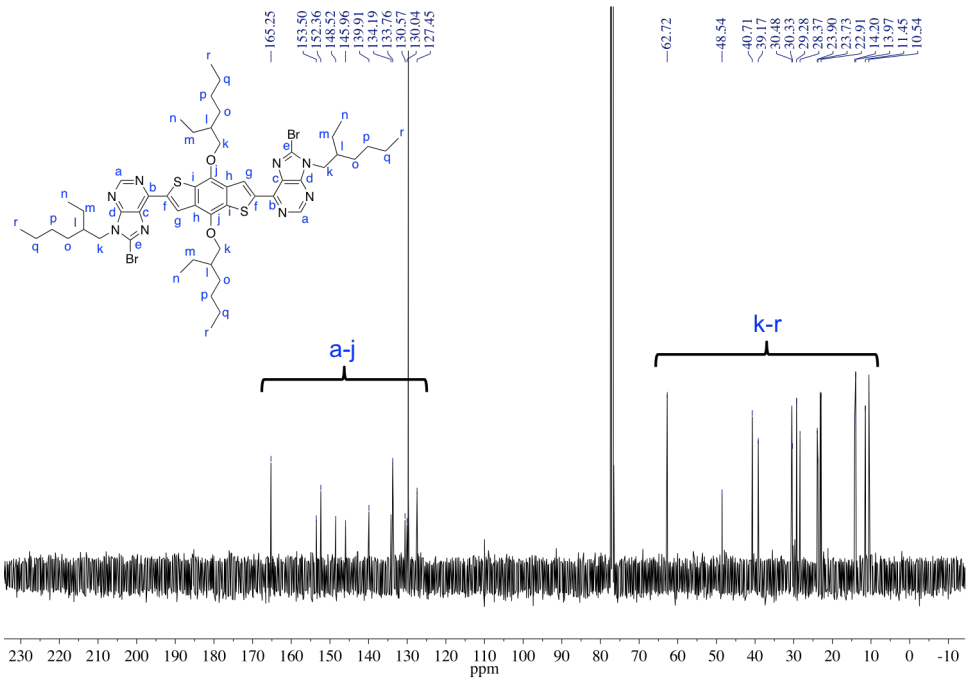

Figure C.2. ^{13}C NMR spectrum (500 MHz, 25 °C, $CDCl_3$) of **Br_2PBDTP**; δ (ppm): 10.54, 11.45, 13.97, 14.20, 22.91, 23.73, 23.90, 28.37, 29.28, 30.33, 30.48, 39.17, 40.71, 48.54, 62.72, 127.45, 130.04, 130.57, 133.76, 134.19, 139.91, 145.96, 148.52, 152.36, 153.50, 165.25.

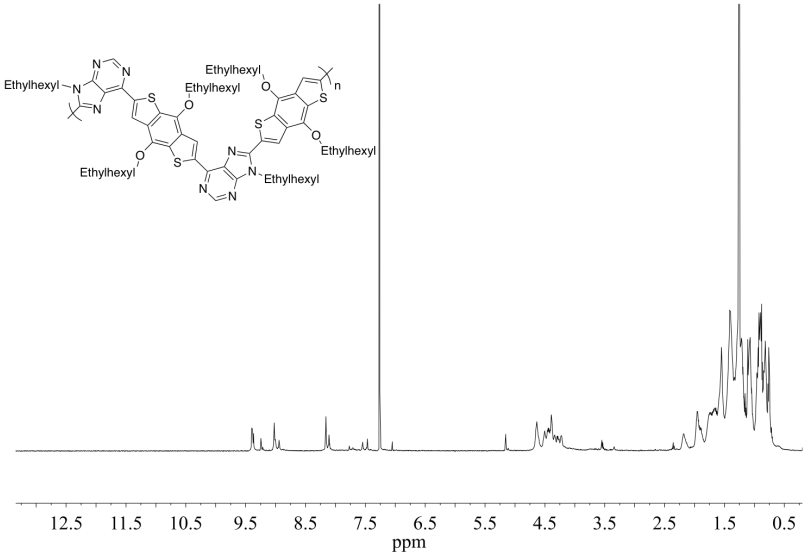

Figure C.3. ^{1}H NMR spectrum (500 MHz, 25 °C, $CDCl_3$) of PPBDTPBDT; δ (ppm): 0.85-0.95 (m) 1.20-1.36 (m), 1.62 (br singlet), 1.91-2.03 (m), 4.18 (d, 2H, CH_2), 8.08 (s, 1H, purine H), 8.70 (s, 1H, purine H).

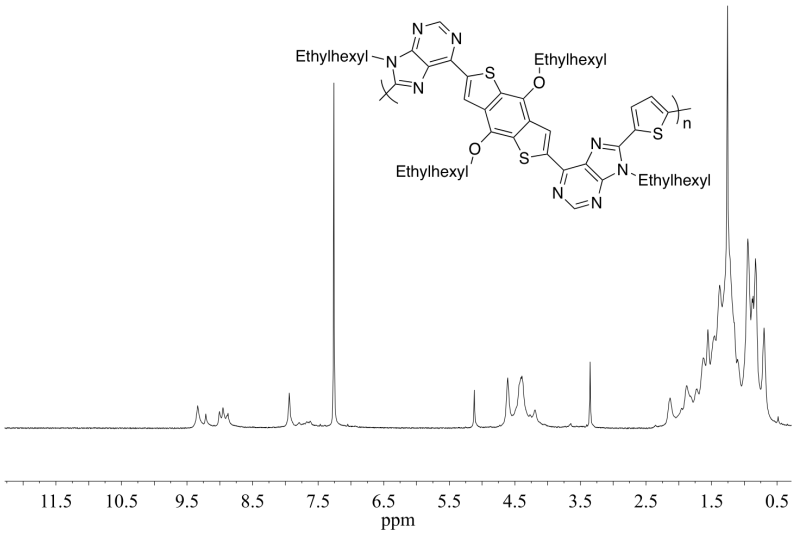

Figure C.4. ^{1}H NMR spectrum (500 MHz, 25 °C, $CDCl_3$) of PPBDTPTh; δ (ppm): 0.85-0.95 (m) 1.20-1.36 (m), 1.62 (br singlet), 1.91-2.03 (m), 4.18 (d, 2H, CH_2), 8.08 (s, 1H, purine H), 8.70 (s, 1H, purine H).

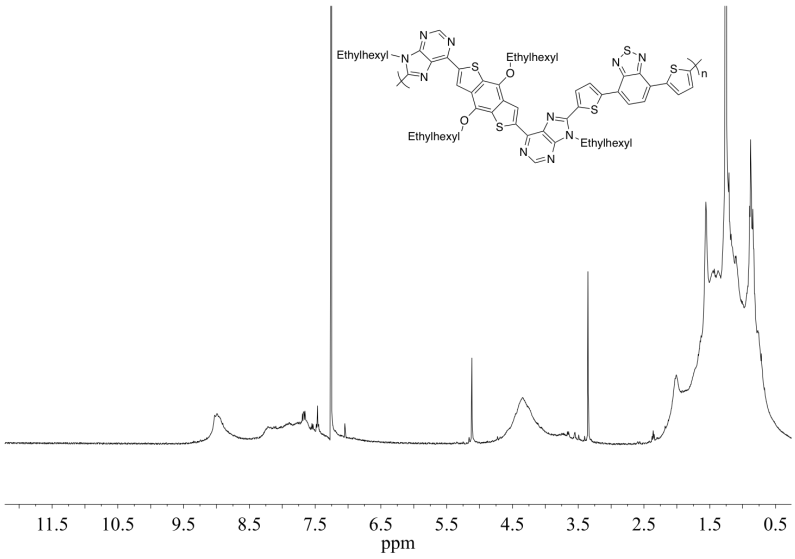

Figure C.5. ^{1}H NMR spectrum (500 MHz, 25 °C, $CDCl_3$) of PPBDTPBT; δ (ppm): 0.85-0.95 (m) 1.20-1.36 (m), 1.62 (br singlet), 1.91-2.03 (m), 4.18 (d, 2H, CH_2), 8.08 (s, 1H, purine H), 8.70 (s, 1H, purine H).

Size-Exclusion Chromatography

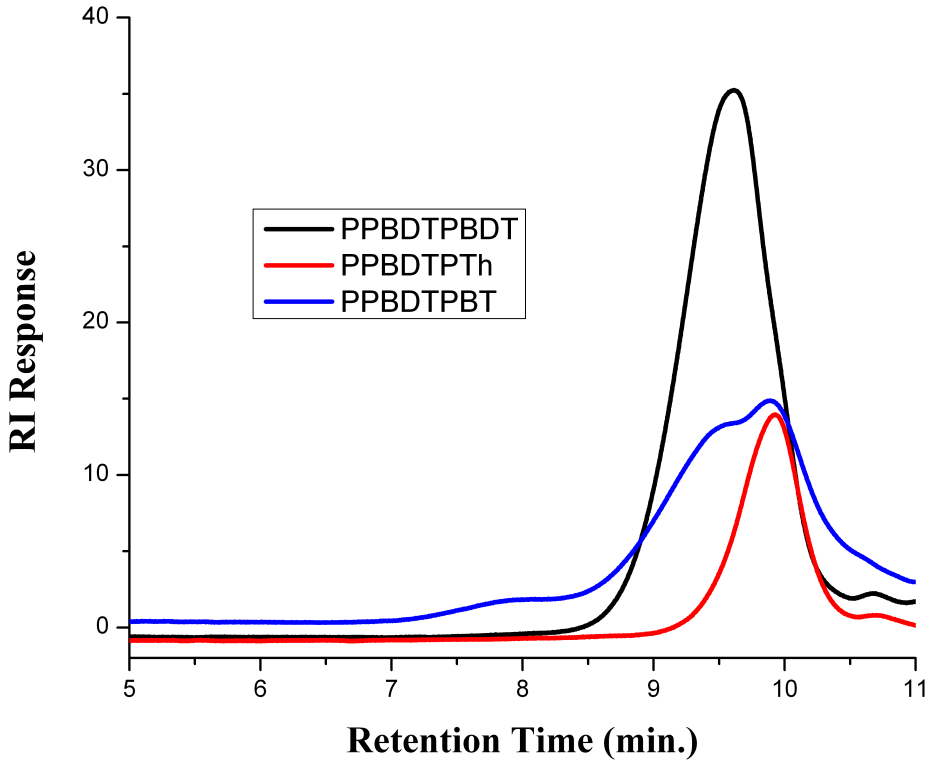

Figure C.6. SEC traces for **PPBDTPBDT**, **PPBDTPTh**, and **PPBDTPBT** synthesized by Stille cross-coupling polymerizations.

Appendix D-Synthesis of Various Purine Building Blocks and Chromophores

General Alkylation Procedure

A solution of 6-bromopurine (1 equiv.) and potassium carbonate (3 equiv.) in DMF was prepared in a 250 mL 3-neck round-bottom flask equipped with a Teflon stir bar and the resulting mixture was stirred for 20 min. The corresponding alkyl-halide (2 equiv.) was then added and the reaction mixture was stirred for 24 h. After 24 h, the reaction mixture was poured into DCM, washed with H_2O, and the combined organic layers were dried with $MgSO_4$ and filtered. The crude product was purified by flash chromatography on silica gel using hexanes and ethyl acetate.

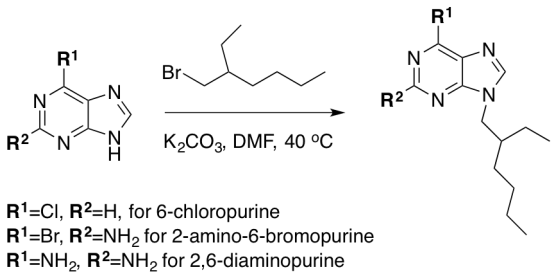

Scheme D.1. Synthesis of N-9 functionalized purines by alkylation.

NMR Spectroscopy

6-chloro-9-ethylhexylpurine

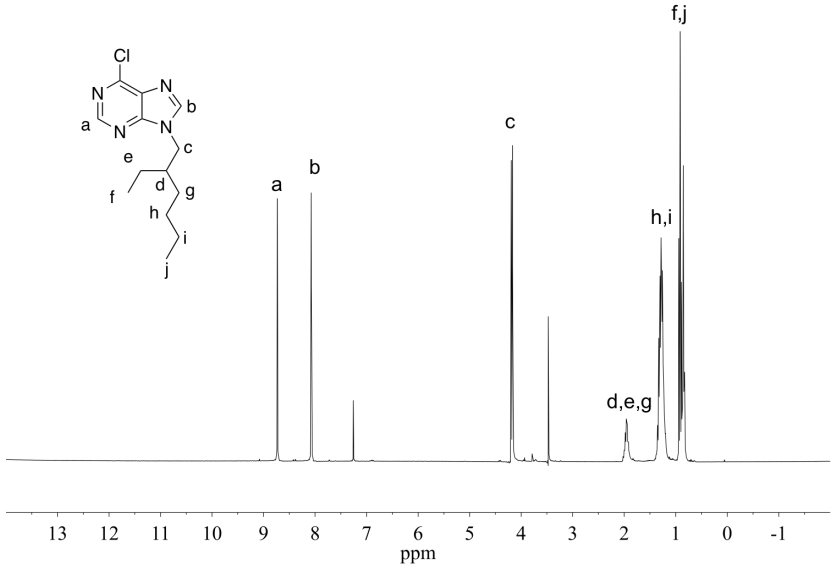

Figure D.1. ^{1}H NMR spectrum (500 MHz, 25 °C, $CDCl_3$) of 6-chloro9-ethylhexylpurine; δ (ppm): 0.81-0.95 (m) 1.18-1.36 (m), 1.90-2.01 (m), 4.18 (d, 2H, CH_2), 8.07 (s, 1H, purine H), 8.73 (s, 1H, purine H).

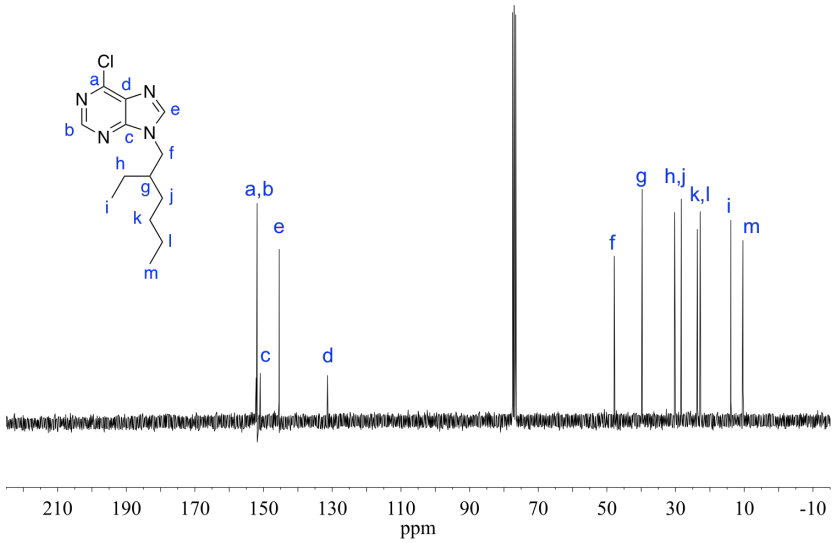

Figure D.2. ^{13}C NMR spectrum (500 MHz, 25 °C, $CDCl_3$) of 6-chloro-9-ethylhexylpurine; δ (ppm): 10.38, 13.92, 22.81, 23.67, 28.35, 30.31, 39.75, 47.86, 131.38, 145.46, 150.95, 151.89, 152.15.

2-amino-6-bromo-9-ethylhexylpurine

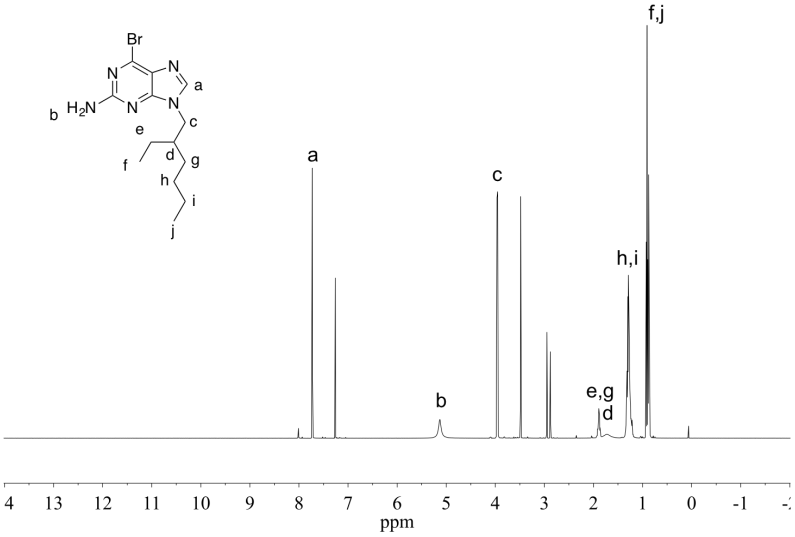

Figure D.3. ^{1}H NMR spectrum (500 MHz, 25 °C, $CDCl_3$) of 2-amino-6-bromo-9-ethylhexylpurine; δ (ppm): 0.84-0.93 (m) 1.19-1.34 (m), 1.72 (br singlet), 1.84-2.93 (m), 3.95 (d, 2H, CH_2), 5.13 (s, br, $-NH_2$), 7.73 (s, 1H, purine H).

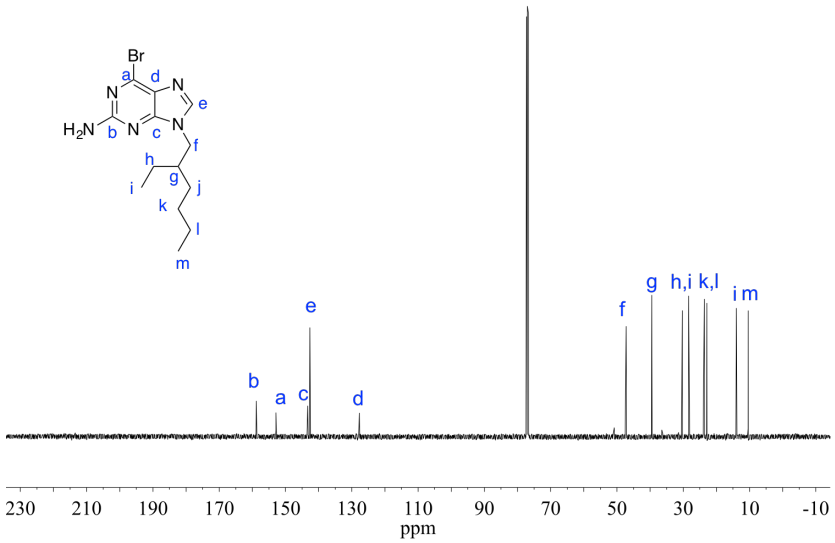

Figure D.4. ^{13}C NMR spectrum (500 MHz, 25 °C, $CDCl_3$) of 2-amino-6-bromo-9-ethylhexylpurine; δ (ppm): 10.42, 13.98, 22.87, 23.65, 28.38, 30.29, 39.49, 47.24, 127.71, 142.63, 143.29, 152.79, 158.79

2,6-diamino-9-ethylhexylpurine

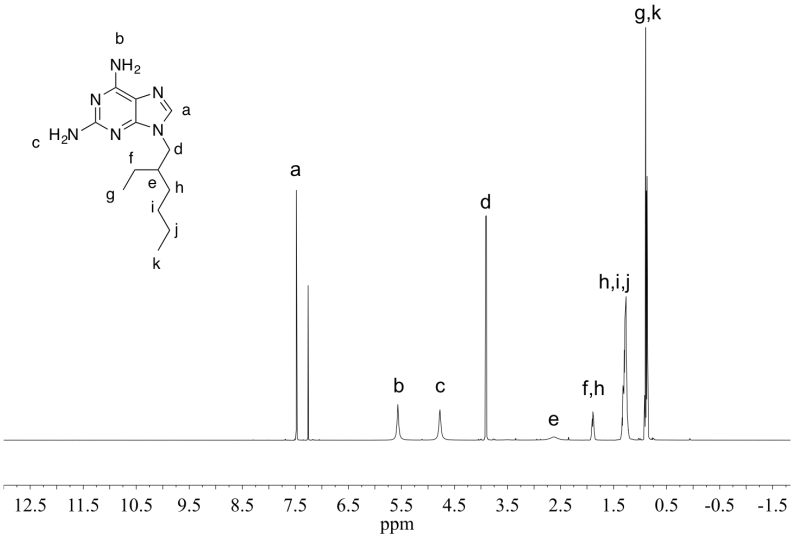

Figure D.5. ^{1}H NMR spectrum (500 MHz, 25 °C, $CDCl_3$) of 2,6-diamino-9-ethylhexylpurine; δ (ppm): 0.84-0.92 (m) 1.21-1.35 (m), 1.85-1.92 (m), 2.62 (br singlet), 3.91 (d, 2H, CH_2), 4.77 (s, br, $-NH_2$), 5.57 (s, br, $-NH_2$), 7.48 (s, 1H, purine H).

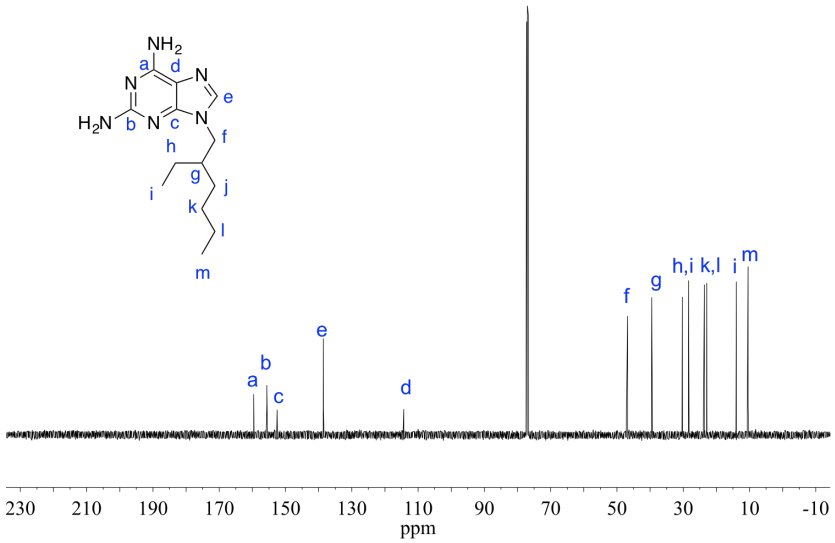

Figure D.6. ^{13}C NMR spectrum (500 MHz, 25 °C, $CDCl_3$) of 2,6-diamino-9-ethylhexylpurine; δ (ppm): 10.44, 14.00, 22.91, 23.64, 28.41, 30.29, 39.52, 46.81, 114.31, 138.55, 152.51, 155.63, 159.58.

Synthesis of $(NH_2)_2$P-BDT-P by Stille Cross-Coupling Reaction

6-bromo-9-ethylhexyl-purine (2 mol. equiv.), the distannyl monomer (1 mol. equiv.), and $Pd(PPh_3)_4$ (5 mol. %) were added to a single-neck 15 mL round bottom flask equipped with a Teflon stir bar and the flask was sealed with a rubber stopper. The atmosphere was rendered inert via three evacuation and refill cycles with argon. Degassed toluene was then added via syringe under an argon atmosphere and the reaction flask was placed in an oil bath set to 100 °C and the mixture was stirred for 18-24 h. After the allotted stirring time, the toluene was removed and the crude mixture was dissolved in DCM. The crude mixture was then passed through a pad of celite to remove the palladium catalyst. The filtrate was then concentrated in *vacuo* and the desired product was purified via column chromatography.

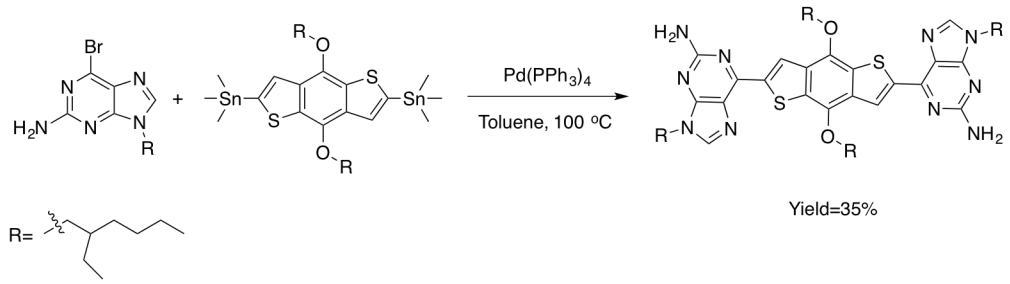

Scheme D.2. Synthesis of **$(NH_2)_2$P-BDT-P** via Stille cross-coupling.

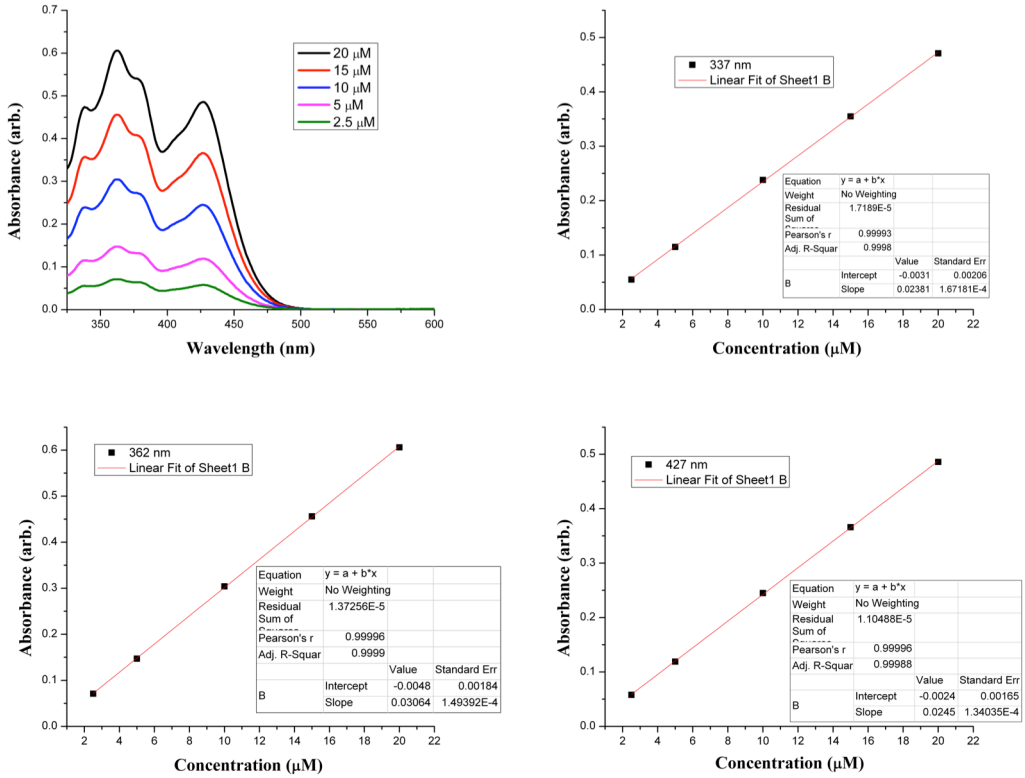

Figure D.7. UV-Vis spectra of varying concentrations (2.5-20 μM) of **$(NH_2)_2$P-BDT-P** in chloroform scanning from 325-600 nm and the corresponding Beer's Law plots at the absorbance maximums.

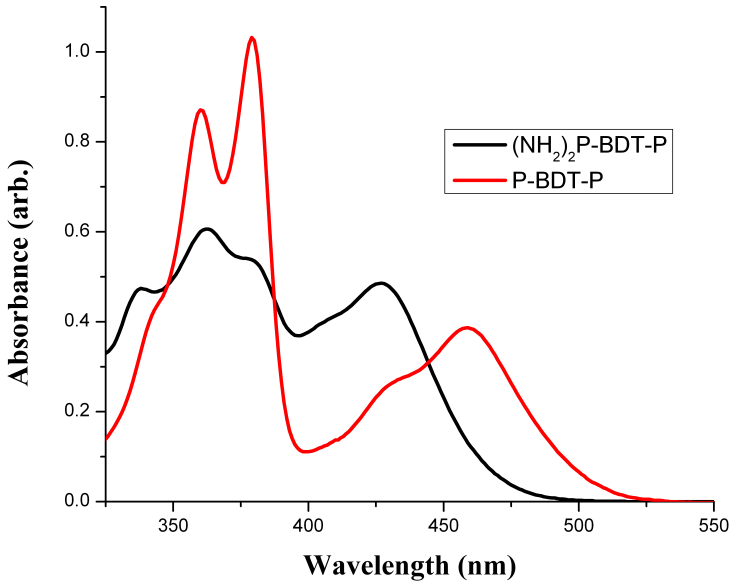

Figure D.8. UV-Vis spectra comparing the absorbance of **P-BDT-P** (red) and **$(NH_2)_2$P-BDT-P** (black) in chloroform.

VITA

Graham Smith Collier was born in Sanford, North Carolina and raised in Fayetteville, North Carolina. Graham attended Pine Forest High School where he was an All-Conference selection in both football and baseball. In 2006, Graham represented Cumberland County at the American Legion Tar Heel Boys' State, an experience he is appreciative of to this day. Upon graduation in 2007, Graham enrolled at the University of North Carolina at Wilmington in Wilmington, NC, where he earned a B.S. in Chemistry. In 2011, Graham enrolled in the Master of Science program at the University of North Carolina at Charlotte, where his thesis research efforts focused on porphyrin light absorbers for organic photovoltaics. Upon completion of his Masters of Science degree in 2013, Graham enrolled at the University of Tennessee-Knoxville to major in polymer chemistry. He joined the research group of Prof. S. Michael Kilbey II, where his research involved the synthesis and development of structure-property relationships for novel purine-based copolymers.